
Article:
Caillol, P. (2017) A singular vortex Rossby wave packet within a rapidly rotating vortex. Physics of Fluids, 29 (4). 046601. ISSN 1070-6631

https://doi.org/10.1063/1.4979489

A singular vortex Rossby wave packet within a rapidly rotating vortex

Philippe Caillol

Citation: Physics of Fluids **29**, 046601 (2017); doi: 10.1063/1.4979489
View online: https://doi.org/10.1063/1.4979489
View Table of Contents: http://aip.scitation.org/toc/phf/29/4
Published by the American Institute of Physics

A singular vortex Rossby wave packet within a rapidly rotating vortex

Philippe Caillol[a)]
Department of Fundamental Sciences, University of Bío-Bío, Chillán, Chile

(Received 27 September 2016; accepted 17 March 2017; published online 17 April 2017)

This paper describes the quasi-steady régime attained by a rapidly rotating vortex after a wave packet has interacted with it. We consider singular, nonlinear, helical, and shear asymmetric modes within a linearly stable, columnar, axisymmetric, and dry vortex in the f-plane. The normal modes enter resonance with the vortex at a certain radius r_c, where the phase angular speed is equal to the rotation frequency. The related singularity in the modal equation at r_c strongly modifies the flow in the 3D helical critical layer, the region where the wave/vortex interaction occurs. This interaction induces a secondary mean flow of higher amplitude than the wave packet and that diffuses at either side of the critical layer inside two spiral diffusion boundary layers. We derive the leading-order equations of the system of nonlinear coupled partial differential equations that govern the slowly evolving amplitudes of the wave packet and induced mean flow a long time after this interaction started. We show that the critical layer imposes its proper scalings and evolution equations; in particular, two slow times are involved, the faster being secular. This system leads to a more complex dynamics with respect to the previous studies on wave packets where this coupling was omitted and where, for instance, a nonlinear Schrödinger equation was derived [D. J. Benney and S. A. Maslowe, "The evolution in space and time of nonlinear waves in parallel shear flows," Stud. Appl. Math. **54**, 181 (1975)]. Matched asymptotic expansion method lets appear that the neutral modes are distorted. The main outcome is that a stronger wave/vortex interaction takes place when a wave packet is considered with respect to the case of a single mode. Numerical simulations of the leading-order inviscid Burgers-like equations of the derived system show that the wave packet rapidly breaks and that the vortex, after intensifying in the transition stage, is substantially weakened before the breaking onset. This breaking could give a dynamical explanation of the formation of an inner spiral band through the prism of the critical layer theory. *Published by AIP Publishing.* [http://dx.doi.org/10.1063/1.4979489]

I. INTRODUCTION

Large-scale rapidly rotating vortices frequently occur in nature. Understanding their complex dynamics and forecasting their intensity are true challenges. The intensity evolution of such vortices can be accurately predicted only after a good knowledge of their internal structure and their environment. The presence of asymmetric disturbances inside a vortex, for instance, may lead to its intensification. Asymmetries are sheared by the differentially rotating flow, causing upgradient eddy fluxes of angular momentum, intensifying the vortex. Most of tropical cyclones (TCs), for example, exhibit a set of spiral rainbands that spiral toward the TC center and whose evolution is related to intensity changes.[1] Convection is frequently observed in the TC neighborhood; it releases latent heat that generates potential vorticity (PV) asymmetrical bands. Then, the vortex tends to return to axisymmetry through an adjustment process consisting of mainly radiating gravity-inertia waves and vorticity waves, the so-called Vortex Rossby (VR) waves. Wave activity analysis in rainbands following numerical simulations of a hurricane-like vortex shows that the vortex only interacts with vorticity waves and that the related modes are continuous.[2] This interaction is thus strong in a localized zone around a critical radius r_c, the so-called critical layer (CL) where wave activity is absorbed.[3,4]

When PV asymmetric disturbances are introduced in a vortex, they induce inner-core vorticity anomalies, at radii where the gradient of basic-state vorticity is large, which then emit VR wave packets. These waves possess characteristic features: if the PV gradient is locally negative, the VR wavepacket propagates radially outward and the waves are retrograde with respect to the azimuthal wind.[5,6] The resulting eddy angular-momentum flux is orientated in the opposite way with respect to the packet propagation. These waves can transport energy out of the vortex core whereas mean radial eddy fluxes cause an inward transport of angular momentum, intensifying or weakening the symmetric vortex,[1,7] according to whether the momentum is deposited in the eyewall or in the eye.[8] Inner spiral rainbands are thought to be formed inside the surf zone through VR wave breaking.[2,4] They are indeed observed to travel outside the vortex core at an angular speed that is less than that of the mean azimuthal wind, such as dispersive VR waves.[5] This breaking can explain the rainband filamentation through the rapid and irreversible deformation of PV contours.

Our paper wishes to improve the understanding of the complex dynamics of nonlinear VR waves embedded in a rapidly rotating vortex. To do so, it analytically examines the

a)Electronic mail: pcaillol@ubiobio.cl

critical layer-like interaction between such a vortex and a VR wave packet. Our study builds on the use of the nonlinear CL theory, which is attractive for the modeling of VR wave breaking because it implies an analysis of two coupled regions: an inner flow where nonlinear dynamics is prevailing and an outer flow where wave-like motions are dominating.[9,10] This coupling is technically realized through matched asymptotic expansions and multiple time scales. Here, we will focus on an outer flow described by a VR wave packet. The critical layer is the narrow surf zone[11] where VR waves overturn and form recirculating zones. An analytical study is of interest here, as the numerical and observational data are often erroneous owing to an insufficient resolution; the nonlinear CL that can be considered as a thin transition layer is usually not resolved by numerical codes[5,12–14] and is not detected by observational devices. Carrying out an analytical study nevertheless implies a lot of simplifying assumptions.[15,16] The vortex is taken axisymmetric, columnar, dry, and linearly stable. This simple model is thus very far from taking into account the complex physics of a hurricane or even a tornado, but as a first step, we wish to examine the dry dynamics that may be overshadowed in a more realistic model. We will not study the very unsteady transition stage of the interaction, but we will only consider the asymptotic quasi-steady stage, a long time after the vortex has been perturbed by a singular-mode packet, which is easier to describe mathematically because the vortex evolution has become slow.

Caillol[15] (2014) described a free, steady, continuous, helical, and shear asymmetric mode in the same simplified vortex model through the nonlinear CL theory. This previous paper will be referred to as C14. The considered mode is neutral and singular in the nonlinear theory while it is stable in the linear theory provided certain conditions be satisfied in the basic-vorticity profile.[15,17] We here extend the theory by considering a packet of such modes and we shall examine the changes that result in the dynamics. When a marginally stable asymmetric mode is superimposed onto the basic vortex, provided the resonance condition of the modal angular speed with the basic-vortex rotation frequency be verified at the radius r_c, a first linear stage starts characterized by the CL formation and the beginning of the wave/mean-flow interaction (WMFI). The critical layer is assumed to form in the vortex outer core where the mean absolute axial vorticity is smaller than the absolute inertial frequency.[16] A strong interaction occurs between the VR wave and the mean flow in the vicinity of r_c. There, the resonant-wave amplitude grows so much that linear inviscid theory then fails and needs to be replaced by a theory in which nonlinearity and/or diffusion terms are invoked.[10] Inside intense atmospheric vortices, the Reynolds number is very large. Nonlinearity is thus the dominant effect, so the nonlinear CL theory is prevailing. The nonlinear CL settles down in a transition stage where the vortex/wave interaction continues in an unsteady way. The interaction strength depends on the amount of the absolute axial vorticity at r_c. Owing to the vorticity erosion that occurs in the critical layer, the WMFI is gradually decelerating. This permits to assume the appearance of a quasi-steady state when the wave has become weakly singular provided the basic-wave phase tilt $\varpi = kr_c/m$ (ratio of axial wavenumber times critical radius over azimuthal wavenumber) be small;[15,16] it continues interacting with the vortex but in a more slow way. The emergence of a quasi-steady state is related to the smoothness of the radial eigenfunction. The weakly singular mode radial structure is indeed sufficiently smooth to enable it to resist shear and store part of the basic-vortex angular momentum and subsequently to weaken the vortex in this asymptotic stage. The vorticity that is removed from the nonlinear CL[15] diffuses in two thick spiral layers at either side of the CL, the (DBLs) diffusion boundary layers. Far from r_c, these layers gradually become thin and produce filaments that are associated with the high-vorticity inner spiral bands. This first study[15] showed that the presence of such a steady asymmetric mode within a rapidly rotating vortex could explain the existence of small-vorticity secondary coherent vortices rotating with respect to the basic-vortex axis roughly at a distance r_c. It also showed that the transition stage WMFI resulted in a vortex intensification.

Monochromatic waves are in fact sparse in nature; observations show the existence of groups of waves that generally span a certain frequency band. When their frequency is peaked, the resulting wave packet takes the form of an amplitude-modulated wave. The neutral mode we will study here, hence, has an amplitude that is slowly evolving in time and height. The objective is the derivation of the evolution equation of the wave envelope. Through the CL coupling, we assume the same slow space-time scales for the CL induced mean flow around the critical radius. This CL induced vertical shear is however too weak in the present study for dispersion to appear in the leading-order evolution equations. This work nevertheless emphasizes the nonlinear interplay between the mean flow and the wave packet that has been omitted in the nonlinear CL dynamics until now. We will notice that the leading-order CL induced mean flow is of higher amplitude than the wave packet, so ignoring this mean flow constitutes a serious mistake. Most of the past studies of quasi-steady CLs aimed to follow the evolution of a slightly supercritical instability in the presence of a viscous or nonlinear CL, created by the interaction of a nearly neutral mode with a background shear flow. Those studies did not take the CL induced mean flow into account.[18–21] In the absence of the latter, various scenarios are possible: a stabilization, a chaotic regime, or an explosive growth within the CL can occur. For instance, the saturation of the weak instability of a zonal flow can yield soliton-like Rossby waves.[21] However, as supercriticality increases, the evolution of the amplitude of a Rossby wave packet can become chaotic.[22,23] Until now, the induced mean flow was only included in a few analytical steady-CL studies[24,25] and remained steady; for example, 2D solitary waves were encountered[26–28] in the presence of both a nonlinear CL and an induced mean flow. Troitskaya and Reznik (1996)[29] considered a quasi-steady nonlinear dissipative internal wave CL. They derived the mean inner flow equations but did not study their evolution over time. Internal gravity wave packets approaching a CL were however numerically studied jointly with the induced mean flow, in the case of free waves[30] or forced waves.[31] A similar analysis was undertaken for forced Rossby wave packets.[32]

In the CL absence, the nonlinear asymmetric wave equation is derived from the orthogonality conditions on the

perturbation non-homogeneous linear equations. Here, that would imply a derivation at the fourth order of the outer-flow expansion, which would lead to a considerable calculation. If a CL emerges in the flow, one difficulty lies in the determination of the equation coefficients. Applying the Fredholm alternative on the outer-flow perturbation non-homogeneous equations is more delicate as the involved integrals are generally singular at r_c.[33] Fortunately, matchings within the CL on the separatrices generally impose strong conditions on the outer flow to lower orders: for instance, generating the mean-flow and perturbation distortions at either side of the CL, or leading to the derivation of the nonlinear wave evolution equation, as was done for 2D solitary waves.[26–28] Two amplitude equations are in fact derived here more simply through the phase-averaged outer equations of the distortions of the leading-order mean axial and azimuthal vorticities. The related distortions are determined by the first nontrivial-order inner flow analysis. This dynamics is hence described by a system of coupled nonlinear partial differential equations (PDEs) that deal with the wave packet amplitude A and with the CL induced mean flow generated at the critical radius r_c. The whole system is derived via the phase-averaged outer equations and is constrained by matching conditions within the CL.

Our paper is hence organized as follows. Section II displays the general perturbation and phase-averaged outer equations. Section III gives the low-order outer flow solutions through Frobenius series. Section IV describes the first nontrivial-order inner flow, modified by the wave packet assumption with respect to C14. The mean-flow equations that form the first-order set of the infinite system characterizing the wave packet/vortex CL-type interaction are displayed in Section V. Section VI explores inner-flow higher orders in order to attempt to close this subsystem by determining the unknown terms in the PDEs. Section VII numerically solves the first-order set of equations and qualitatively examines the quasi-steady WMFI and the wave packet breaking process. Section VIII examines the mean-flow evolution inside the diffusion boundary layers and the CL/DBL coupling. Finally, Section IX offers our conclusion.

II. FORMULATION AND MAIN ASSUMPTIONS

A rapidly rotating vortex can be assimilated in the high swirl ratio approximation to a barotropic vortex. Therefore we consider the motion of an axisymmetric and columnar vortex in the rotating earth's slightly viscous, incompressible, and dry atmosphere. We use the cylindrical coordinates (r, θ, z), where the variable z being related to the height of the vortex along its rotation axis and (u, v, w) being the velocity vector in these coordinates. Quantities have been made dimensionless through characteristic velocity and length scales: the maximum azimuthal wind of the vortex V_{mw} and the radius of maximum wind R_{mw}. The related Reynolds number is $Re = V_{mw}R_{mw}/\nu$, where ν is the kinematic viscosity. The inertial force $\mathbf{f}_i$ due to the rotating framework is $\mathbf{f}_i = v/r\,(v\,\mathbf{e}_r - u\,\mathbf{e}_\theta)$. The geopotential (centrifugal force due to earth's rotation and gravity) with kinematic pressure p is inserted into the gradient force to form the variable Γ defined by $\Gamma = p + gz - Co^2/8r^2$ and erroneously called geopotential. The body force $\mathbf{F}$ balances the basic-vortex viscous diffusion. We use the so-called f-plane approximation; a constant value of the Coriolis parameter $Co = (fR_{mw})/V_{mw}$ is used throughout the study. The dimensionless equations governing this motion are the momentum and mass conservation equations in the ground-based frame of reference

$$\partial_t \mathbf{u} + \mathbf{u}\boldsymbol{\nabla}\mathbf{u} + Co\,\mathbf{z}\times\mathbf{u} = \mathbf{f}_i - \boldsymbol{\nabla}\Gamma + \frac{1}{Re}\Delta\mathbf{u} + \mathbf{F}, \tag{1}$$

$$\mathrm{D}^* u + \frac{1}{r}\partial_\theta v + \partial_z w = 0\,, \quad \text{with} \quad \mathrm{D}^*\bullet = \partial_r \bullet + \frac{1}{r}\bullet. \tag{2}$$

The velocity and geopotential are decomposed into the wave phase-averaged flow and the asymmetric perturbations in the following form:

$$\begin{aligned} u &= \overline{U}(r,\Phi) + \epsilon\, U_r(\xi, r, \Phi)\,, \quad v = \overline{V}(r,\Phi) + \epsilon\, U_\theta(\xi, r, \Phi)\,, \\ w &= \overline{W}(r,\Phi) + \epsilon\, U_z(\xi, r, \Phi)\,, \quad \Gamma = \overline{\Gamma}(r,\Phi) + \epsilon\, P(\xi, r, \Phi), \end{aligned} \tag{3}$$

where the helical coordinate ξ is the wave phase $\xi = kz + m\theta - \omega t$ with k and m, respectively, the axial and azimuthal wavenumbers. We introduce the overbar notation to define the phase-averaged flow. The average of the quantity q over ξ is thus $\overline{q}(r) = 1/(2\pi)\int_0^{2\pi} q(r,\xi)\,d\xi$. The first-order perturbation is an amplitude-modulated neutral VR wave whose small dimensionless amplitude is ϵ and whose real frequency is ω. We assume a quasi-steady asymptotic state so that the fast time t only appears in the phase ξ, the wave/vortex interaction evolving at slow time scales that are omitted in the notation.

Spiral rainbands vertically extend from the surface boundary layer up to the middle troposphere. The VR wave coupling with the boundary layer is in fact a possible explanation for the formation of spiral rainbands.[4] The boundary layer alters rainband dynamics and[34] it imposes, for example, an upward motion to the band via Ekman pumping. We will however study the wave/vortex interaction above the boundary layer for simplicity sake, in order to neglect the effects of the latter on the interaction; in particular, we will neglect the mean radial flow of the inflow layer and viscosity.[35] Although large vertical and radial velocities may occur in tropical cyclones, these are always one order less than the rotational velocities above the inflow layer,[36] we will then assume that the basic vortex only contains a field of azimuthal velocity. The WMFI will nevertheless yield induced mean vertical and radial velocity fields.

The amplitude modulation space and time scales are taken

$$\Phi = \epsilon\frac{m}{r_c}z, \quad \text{and} \quad \tau_3 \equiv \epsilon^{3/2}t.$$

The vertical derivative in this multiple scaling approach is then computed in this way

$$\partial_z \bullet = k\partial_\xi \bullet + \epsilon\frac{m}{r_c}\partial_\Phi \bullet.$$

The wave envelope vertical scale is thus $O(\epsilon^{-1})$, and the chosen régime is not the wave packet linear CL but the

nonlinear critical layer:[32,37] the nonlinear effects are prevailing on the wave packet linear effects. The system of Equation (1) after the decomposition (3) yields two systems of equations: the first, Eq. (4), describing the evolution of the perturbations, and the second, Eq. (5), the evolution of the mean flow,

$$\frac{DU_r}{Dt} = \varrho(r)U_\theta - D[\overline{U}U_r + P] - \epsilon\frac{m}{r_c}\partial_\Phi\overline{U}\,U_z + \epsilon D^*[\overline{U_r^2}] + \frac{\epsilon}{r}(U_\theta^2 - \overline{U_\theta^2}) + \epsilon^2\frac{m}{r_c}\partial_\Phi\overline{U_rU_z} + \frac{1}{Re}\Big[\Big(\Delta_r + \frac{\partial_\xi^2}{S(r)}\Big)U_r - \frac{2m}{r^2}\partial_\xi U_\theta\Big], \tag{4a}$$

$$\frac{DU_\theta}{Dt} = -Q_z(r)U_r - \overline{U}D^*[U_\theta] - \frac{m}{r}\partial_\xi P - \epsilon\frac{m}{r_c}\partial_\Phi\overline{V}\,U_z + \frac{\epsilon}{r^2}D[r^2\overline{U_rU_\theta}] - \epsilon\,\frac{U_\theta}{r}U_r + \epsilon^2\frac{m}{r_c}\partial_\Phi\overline{U_zU_\theta} + \frac{1}{Re}\Big[\Big(\Delta_r + \frac{\partial_\xi^2}{S(r)}\Big)U_\theta + \frac{2m}{r^2}\partial_\xi U_r\Big], \tag{4b}$$

$$\frac{DU_z}{Dt} = Q_\theta(r)U_r - \overline{U}D[U_z] - k\partial_\xi P - \epsilon\frac{m}{r_c}\partial_\Phi\overline{W}\,U_z + \epsilon D^*[\overline{U_rU_z}] - \epsilon\frac{m}{r_c}\partial_\Phi P + \epsilon^2\frac{m}{r_c}\partial_\Phi\overline{U_z^2} + \frac{1}{Re}\Big(\Delta_z + \frac{\partial_\xi^2}{S(r)}\Big)U_z, \tag{4c}$$

$$D^*U_r + \frac{m}{r}\partial_\xi U_\theta + k\partial_\xi U_z + \epsilon\frac{m}{r_c}\partial_\Phi U_z = 0\,. \tag{4d}$$

This first system is coupled with the following boundary conditions:

$$r\to\infty,\quad (U_r,\,U_\theta,\,U_z,\,P)\to(0,0,0,0),\qquad r\to 0,\quad U_\theta\to 0,\quad \text{and}\quad \text{if } |m|\neq 1,\quad U_r\to 0.$$

As for the mean flow, we have the set of equations

$$\frac{\mathcal{D}\overline{U}}{Dt} = \overline{V}(Co+\Omega) - D[\overline{\Gamma} + \frac{1}{2}\overline{U}^2] - \epsilon^2 D^*[\overline{U_r^2}] + \frac{\epsilon^2}{r}\overline{U_\theta^2} - \epsilon^3\frac{m}{r_c}\partial_\Phi\overline{U_rU_z} + \frac{1}{Re}\Delta_r\overline{U}, \tag{5a}$$

$$\frac{\mathcal{D}\overline{V}}{Dt} = -Q_z\overline{U} - \frac{\epsilon^2}{r^2}D[r^2\overline{U_rU_\theta}] - \epsilon^3\frac{m}{r_c}\partial_\Phi\overline{U_zU_\theta} + \frac{1}{Re}\Delta_r\overline{V} + F(r), \tag{5b}$$

$$\frac{\mathcal{D}\overline{W}}{Dt} = Q_\theta\overline{U} - \epsilon\frac{m}{r_c}\partial_\Phi[\overline{\Gamma} + \epsilon^2\overline{U_z^2}] - \epsilon^2 D^*[\overline{U_rU_z}] + \frac{1}{Re}\Delta_z\overline{W}(r), \tag{5c}$$

$$D^*\overline{U} + \epsilon\frac{m}{r_c}\partial_\Phi\overline{W} = 0. \tag{5d}$$

The mean flow expands in the two diffusion boundary layers at either side of the CL and does not have any boundary conditions at $r = 0$. At infinity, the mean flow asymptotes the basic-state vortex. The circular vortex is characterized by the mean angular rotation $\Omega(r) = \overline{V}(r)/r$, the absolute mean axial vorticity $Q_z(r) = 1/rD[r\overline{V}(r)] + Co$, the mean azimuthal vorticity $Q_\theta(r) = -\overline{W}'(r)$, and the absolute inertial frequency $\varrho(r) = 2\Omega(r) + Co$. The prime denotes the radial derivative of the phase-averaged quantities and D denotes the radial differential operator. We also have the following notation:

$$\omega^D(r) = \omega - m\Omega(r) - k\overline{W}(r)\,,\quad S(r) = \frac{r^2}{m^2+k^2r^2}\,,\quad F(r) = -\frac{1}{Re}\,Q'_{z,0}(r),\qquad \frac{1}{Re} = \lambda\,\epsilon^{\frac{3}{2}},$$

$$\frac{D}{Dt}\bullet = \partial_t\bullet + \epsilon\,[U_r\partial r + (\frac{m}{r}U_\theta + kU_z)\partial_\xi + \frac{m}{r_c}(\overline{W} + \epsilon\,U_z)\partial_\Phi]\bullet - (\omega^D + \omega_t\,t)\partial_\xi\bullet,$$

$$\frac{\mathcal{D}}{Dt}\bullet = \partial_t\bullet + \epsilon\,\frac{m}{r_c}\overline{W}\partial_\Phi\bullet,\quad \Delta_r\bullet = D[D^*[\bullet]] + \epsilon^2\frac{m^2}{r_c^2}\partial_\Phi^2\bullet,\quad \Delta_z\bullet = D^*[D[\bullet]] + \epsilon^2\frac{m^2}{r_c^2}\partial_\Phi^2\bullet,$$

and

$$\partial_t\bullet = \epsilon^{1/2}\partial_{\tau_1}\bullet + \epsilon\,\partial_{\tau_2}\bullet + \epsilon^{3/2}\,\partial_{\tau_3}\bullet,\quad \tau_i \equiv \epsilon^{i/2}\,t,\ i = 1,2,3.$$

The rationale for employing these time scales will be explained in Sections IV and VIII.

Here, we shall use the nonlinear CL theory, so we will assume the Haberman parameter λ, i.e., the cubic ratio of the viscous CL thickness to the nonlinear CL thickness is small, which allows for a λ-expansion of the flow, dividing it into an inviscid part and a smaller viscous part, e.g., for the radial velocity $U = U_{r,i} + \lambda U_{r,v} + \mathrm{o}(\lambda)$. The perturbations of velocity, geopotential, and vorticity are expanded according to the square root of the wave packet amplitude, for instance, for the radial velocity

$$U_r = U_r^{(0)} + \epsilon^{1/2}\,U_r^{(1)} + \epsilon\ln\epsilon\,U_r^{(2a)} + \epsilon\,U_r^{(2)} + \cdots \tag{6}$$

with the zeroth order characterizing the amplitude-modulated normal VR mode. The presence of a logarithmic order will be explained later on. The mean radial, azimuthal, and axial shear flows are also $\epsilon^{1/2}$-expanded in the same way

$$\overline{U}(r,\Phi) = \epsilon^{\frac{3}{2}}\,\overline{U}_3(r,\Phi) + \epsilon^2\,\overline{U}_4(r,\Phi) + \cdots, \tag{7a}$$

$$\overline{V}(r,\Phi) = \overline{V}_0(r) + \epsilon^{\frac{1}{2}}\overline{V}_1(r,\Phi) + \epsilon\,\overline{V}_2(r,\Phi) + \cdots,$$

$$\overline{W}(r,\Phi) = \epsilon^{\frac{1}{2}}\overline{W}_1(r,\Phi) + \cdots, \tag{7b}$$

$$Q_z(r,\Phi) = Q_0(r) + \epsilon^{\frac{1}{2}}Q_{z,1}(r,\Phi) + \epsilon\,Q_{z,2}(r,\Phi) + \cdots,$$

$$Q_\theta(r,\Phi) = \epsilon^{\frac{1}{2}}Q_{\theta,1}(r,\Phi) + \cdots. \tag{7c}$$

The subscript 0 characterizes the $O(1)$ phase-averaged swirling flow, which results from the interaction between the basic vortex and the wave packet at the end of the transition stage. Note the appearance of a small mean radial velocity in the quasi-steady régime. We also assume that Co expansion is restricted to $Co = Co_0 + \epsilon^{1/2}Co_1$. To the first orders, the mean geopotential is defined by the gradient-wind balance according to Eq. (5a),

$$\overline{\Gamma}_0(r) = \frac{1}{4}(\varrho_{0,c}^2 - Co_0^2)r_c^2 + \frac{1}{4}\int_{r_c}^{r} \varrho_0^2(r) - Co_0^2\, r\mathrm{d}r, \tag{8a}$$

$$\overline{\Gamma}_1(r,\Phi) = \overline{\Gamma}_1(r_c,\Phi) + \frac{1}{2}\int_{r_c}^{r} \varrho_0(r)\varrho_1(r,\Phi) - Co_0Co_1\, r\mathrm{d}r, \tag{8b}$$

$$\overline{\Gamma}_2(r,\Phi) = \overline{\Gamma}_2(r_c,\Phi) + \frac{1}{4}\int_{r_c}^{r} 2\varrho_0(r)\varrho_2(r,\Phi) + \varrho_1^2(r,\Phi) - Co_1^2\, r\mathrm{d}r. \tag{8c}$$

III. THE OUTER FLOW

In this section, we give the outer-flow solution valid near r_c to the first orders, which will enable us to determine the inner flow by matching both flows.

A. The singular wave packet

The eigenmode satisfies a single differential equation obtained from the linearized, inviscid, and stationary system (4). When the latter is related to the VR mode radial velocity $U_r^{(0)}$, it is the Howard-Gupta modal equation generalized to the f-plane and expressed as $\mathcal{L}_0(U_r^{(0)}) = 0$, namely,

$$D[S(r)D^*U_r^{(0)}] + \partial_\xi^2 U_r^{(0)} + \frac{m\,U_r^{(0)}}{\omega_0^D(r)r^2}\left((rD-2)[S(r)Q_0(r)] + \frac{k^2r^2\varrho_0(r)}{m\omega_0^D(r)}S(r)Q_0(r)\right) = 0. \tag{9}$$

Equation (9) is singular at the critical radius r_c such that the Doppler-shifted frequency vanishes, that is, $\omega_0^D(r_c) = 0$ ($\omega_0 = m\Omega_{0,c}$) but admits a weakly singular solution around r_c in the function of two Frobenius series of the variable $\eta = r - r_c$, when the local equivalent Richardson number at r_c, $J_c = \varpi^2\,\varrho_{0,c}Q_{0,c}/(Q_{0,c} - \varrho_{0,c})^2$, is small, i.e., at the end of the vortex/wave packet interaction as the zeroth-order mean axial vorticity has become small around r_c. The subscript c characterizes the critical radius. This number is related to the linear stability of a swirling sheared flow and is analogous to the Richardson number of a parallel stratified sheared flow. For more details on the neutral VR mode and the equivalent Richardson number, see Subsection 3.1 of C14. Both Frobenius series are

$$\phi_a(\eta) = \eta + \sum_{n=2}^{\infty} a_{0,n}\eta^n, \quad \phi_b(\eta) = 1 + \sum_{n=2}^{\infty} b_{0,n}\eta^n + b_0\phi_a(\eta)\ln\eta^*. \tag{10}$$

The cross-stream coordinate η is normalized inside the logarithm with $\eta^* = \eta/\eta_0$, where $\eta_0 = r_c/\sqrt{2}$. Finally, the neutral-mode radial velocity is written around the critical radius

$$U_r^{(0)}(r,\Phi,\tau_3) = [\frac{a^\pm}{r_c}\phi_a(\eta) + \phi_b(\eta)]\,U_0(\Phi,\tau_3)\,\sin\xi + b_0C\phi_a(\eta)U_0(\Phi,\tau_3)\,\cos\xi. \tag{11}$$

The complex logarithmic function in (10) induces an additional and in phase quadrature term in (11) caused by the logarithmic phase shift ϕ as $r < r_c$, so C is defined by

$$r > r_c, \qquad C^+ = 0 \qquad \text{and } r < r_c, \quad C^- = \phi(\lambda). \tag{12}$$

Haberman (1972) showed that the phase shift ϕ was a function of the so-called Haberman parameter λ for any CL régime, from the viscous CL ($\lambda \gg 1$) up to the nonlinear CL[24] ($\lambda \ll 1$). This quadrature term then allows for small $O(\phi\,\epsilon^{7/2})$ viscous mean radial eddy fluxes of azimuthal and axial momenta that generate a small deceleration of the vortex. We choose to use the superscript $-$ to characterize the vortex core flow where $r < r_c$ and the superscript $+$ for $r > r_c$.

B. Order $\epsilon^{\frac{3}{2}}$

The inviscid radial velocity $U_{r,i}^{(1)}$ satisfies the following non-homogeneous equation:

$$\mathcal{L}_0(U_{r,i}^{(1)}) = -\mathcal{L}_1(U_{r,i}^{(0)}) \tag{13}$$

with the operator $\mathcal{L}_1$ defined by

$$\mathcal{L}_1(U) = \left\{(r\mathrm{D}-2)\left[S(r)\left(Q_{z,1}(r) - \frac{kr}{m}Q_{\theta,1}(r)\right)\right] + kr\frac{S(r)\varrho_0(r)}{\omega_0^D(r)}\left(\frac{kr}{m}Q_{z,1}(r) + Q_{\theta,1}(r)\right) - \frac{\hat{\omega}_1^D(r)}{\omega_0^D(r)}(r\mathrm{D}-2)[S(r)Q_{z,0}(r)] + \frac{k^2r^2}{m}\frac{S(r)\varrho_0(r)}{\omega_0^D(r)} \times \left[\frac{\varrho_1(r)}{\varrho_0(r)} - 2\frac{\hat{\omega}_1^D(r)}{\omega_0^D(r)}\right]Q_{z,0}(r)\right\}\frac{mU}{\omega_0^D(r)r^2}, \tag{14}$$

where $\hat{\omega}_1^D(r) = \omega_1^D(r) + \omega_{1,\tau_2}\tau_2$. The Frobenius series related to the first-order radial velocity is

$$U_{r,i}^{(1)} = \left[\sum_{n=0}^{\infty}(c_{l,1,n}\ln|\eta^*| + d_{l,1,n})\,\eta^n + \alpha_{l,1}\phi_a + \beta_{l,1}\phi_b\right] \times U_0(\Phi,\tau_3)\,\sin\xi. \tag{15}$$

The first-order equivalent Richardson number is derived from (14) and is expressed by

$$J_{1,c} = \frac{\varpi}{\varrho_{0,c}}(Q_{z,1,c} + \varpi Q_{\theta,1,c}) - (1+2\varpi^2)\hat{\omega}^D_{1,c}\frac{r_c Q'_{z,0,c}}{m\varrho^2_{0,c}}. \quad (16)$$

The quasi-steady stage is characterized by $Q_0(r_c) = 0$, so the local equivalent Richardson number expansion starts by $J_c = \epsilon^{1/2}J_{c,1} + \epsilon J_{2,c} + \dots$.

C. Order ϵ^2

The second-order inviscid outer flow is decomposed between four terms,

$$U^{(2)}_{r,i} = \ln\epsilon\, U^{(2a)}_{r,l} + U^{(2)}_{r,l} + U^{(2)}_{r,d} + U^{(2)}_{r,n},$$

where two linear terms with respect to U_0, one of which is amplified by $\ln\epsilon$, a term induced by the mode vertical shear that will introduce dispersion into the next-order evolution equations, and a quadratic term, namely,

$$U^{(2)}_{r,i} = [\ln\epsilon\,\phi^{(2a)}_l(\eta) + \phi^{(2)}_l(\eta)]\,U_0(\Phi,\tau_3)\,\sin\xi + \phi^{(2)}_d(\eta)\,U_{0,\Phi}(\Phi,\tau_3)\cos\xi + \frac{1}{2}\phi^{(2)}_n(\eta)\,U^2_0(\Phi,\tau_3)\sin 2\xi.$$

The logarithmic-order radial velocity obeys the homogeneous equation $\mathcal{L}_0(\phi^{(2a)}_l\sin\xi) = 0$, which yields the solution

$$\phi^{(2a)}_l(\eta) = \alpha_{l,2a}\phi_a(\eta) + \beta_{l,2a}\phi_b(\eta). \quad (17)$$

The outer flow induced by the vertical shear is given by

$$\mathcal{L}_0(U^{(2)}_{r,d}) = \frac{2}{r_c}\Big[\frac{m}{r}\frac{Q_{z,0}(r)}{\omega^D_0(r)} - D\Big][S(r)\,U^{(0)}_{z,\Phi}(r)].$$

The related Frobenius series is

$$\phi^{(2)}_d(\eta) = \Big(\sum_{n=0}^{\infty}[b_{d,2,n}\ln|\eta^*| + c_{d,2,n}]\,\eta^n + \alpha_{d,2}\phi_a(\eta) + \beta_{d,2}\phi_b(\eta)\Big).$$

The last flow is in phase quadrature with the mode but allows for $O(\epsilon^3)$ inviscid mean radial eddy fluxes of azimuthal and axial momenta that are too small as well to accelerate the vortex. The long equations and related Frobenius series for the velocities $U^{(2)}_{r,l}$ and $U^{(2)}_{r,n}$ are given in Appendix A 2.

IV. THE NONLINEAR CRITICAL LAYER

A. Rescaling and low-order inner flow

When the mean absolute axial vorticity is smaller than the absolute inertial frequency at the radius r_c, i.e., when the equivalent Richardson number J_c is small, the critical-layer width is $O(\epsilon^{1/2})$. The relevant inner cross-stream variable R is thus $R = \epsilon^{-\frac{1}{2}}\eta$. The expansion of the outer flow following R gives the way with which the inner expansion must proceed

$$U = \epsilon^{\frac{3}{2}}\overline{U}_{3,c} + \epsilon\left\{U^{(0)} + \epsilon^{\frac{1}{2}}\ln\epsilon\,U^{(1)} + \epsilon^{\frac{1}{2}}U^{(2)} + \epsilon\ln^2\epsilon\,U^{(3)} + \epsilon\ln\epsilon\,U^{(4)} + \epsilon\ln\epsilon\,U^{(5)} + \cdots\right\},$$
$$V = \Omega_{0,c}r + \epsilon^{\frac{1}{2}}\Omega_{1,c}r + \epsilon^{\frac{1}{2}}\left\{V^{(0)} + \epsilon^{\frac{1}{2}}\ln\epsilon\,V^{(1)} + \cdots\right\},\quad W = \epsilon^{\frac{1}{2}}\overline{W}_{1,c} + \left\{\epsilon^{\frac{1}{2}}\ln\epsilon\,W^{(1)} + \cdots\right\},$$
$$\mathcal{P} = \frac{1}{2}\Omega_{0,c}(\Omega_{0,c} + Co_0)r^2 + \epsilon\left\{\mathcal{P}^{(0)} + \epsilon^{\frac{1}{2}}\ln\epsilon\,\mathcal{P}^{(1)} + \epsilon^{\frac{1}{2}}\mathcal{P}^{(2)} + \cdots\right\}.$$

In order to get simplified coefficients in the inner equations, let us make the following rescaling using the zeroth-order mean flow evaluated at r_c:

$$X = \xi + \frac{\pi}{2}(1-s_i),\qquad R = s_i r_c\mathcal{R},\qquad \tau_i = m\varrho_{0,c}\,\epsilon^{i/2}t,\qquad s_i = -\mathrm{sgn}[m\varrho_{0,c}U_0],$$
$$V^{(i)} = \varrho_{0,c}r_c\,\hat{V}^{(i)},\quad W^{(i)} = \varpi\varrho_{0,c}r_c\hat{W}^{(i)},\quad U^{(i)} = s_i m\varrho_{0,c}r_c\hat{U}^{(i)},\quad \mathcal{P}^{(i)} = s_i\varrho^2_{0,c}r^2_c\hat{\mathcal{P}}^{(i)},$$
$$\mathcal{V}_i = \overline{V}_{i,c}/\varrho_{0,c}r_c,\quad \mathcal{W}_i = \overline{W}_{i,c}/(\varpi\varrho_{0,c}r_c),\quad \mathcal{U}_i = \overline{U}_{i,c}/(m\varrho_{0,c}r_c),\quad \mathfrak{P}_i = \overline{\Gamma}_{i,c}/(\varrho^2_{0,c}r^2_c),$$
$$\mathfrak{P}'_i = \overline{\Gamma}'_{i,c}/(\varrho^2_{0,c}r_c),\quad \mathfrak{V}_i = \omega_i/(m\varrho_{0,c}),\quad \mathcal{C}_i = Co_i/\varrho_{0,c},\quad \mathcal{S}_i = \varrho_{i,c}/\varrho_{0,c},$$
$$\mathcal{Q}_{z,1} = Q_{z,1,c}/\varrho_{0,c},\quad \mathcal{Q}_{\theta,1} = -\overline{W}'_{1,c}/\varrho_{0,c},\quad \zeta = r_c Q'_{z,0,c}/\varrho_{0,c},\quad \zeta_{z,1} = r_c Q'_{z,1,c}/\varrho_{0,c},$$
$$\zeta_{\theta,1} = r_c Q'_{\theta,1,c}/\varrho_{0,c},\quad \zeta' = r^2_c Q''_{z,0,c}/\varrho_{0,c},\quad \zeta'_{z,1} = r^2_c Q''_{z,1,c}/\varrho_{0,c},\quad \zeta'_{\theta,1} = r^2_c Q''_{\theta,1,c}/\varrho_{0,c},$$
$$\lambda' = \frac{\lambda}{U_0 r_c},\qquad A(\Phi,\tau_3) = \Big|\frac{U_0(\Phi,\tau_3)}{m\varrho_{0,c}r_c}\Big|.$$

In the following analysis, we drop the hat with the understanding that we are dealing with the new variables. The rescaled wave packet amplitude $A(\Phi,\tau_3)$ is the solution of two nonlinear space-time evolution equations that we will derive later on, relevant to the asymptotic régime, a long time after the CL formation when the VR wave packet is slowly exchanging momentum and kinetic energy with the basic vortex.

The leading-order inner equations lead to the simple solutions as follows:

$$U^{(0)} = -s_i A\sin X,\qquad V^{(0)} = -s_i\mathcal{R},$$
$$\mathcal{P}^{(0)} = s_i\mathfrak{P}_2 + \frac{1}{2}(\mathcal{S}_1 - \mathcal{C}_0\mathcal{C}_1 - s_i\mathcal{R})\mathcal{R}.$$

The first-order flow is deduced straightforwardly from the singular Frobenius solution

$$U^{(1)} = [\frac{\zeta}{2}(1+\varpi^2)\mathcal{R} - \frac{s_i}{2}J_{1,c}]\,A\sin X\,,$$
$$W^{(1)} = V^{(1)} = \frac{\zeta}{2}A\,\cos X, \quad \mathcal{P}^{(1)} = \frac{\zeta}{2}A\mathcal{R}\,\cos X.$$

We denote the quantities inside the cat's eye by the superscript $\odot$. We, respectively, denote the jump and the average of a quantity q at either side of the critical radius as $[q]^+_- = q^+ - q^-$ and $\{q\}^+_- = (q^+ + q^-)/2$. Both inner flows are identical inside and outside the separatrices, so $U^{(j,\odot)} = U^{(j)}$, $V^{(j,\odot)} = V^{(j)}, \ldots, j = 1, 2$. Solving first-order inner equations leads to $\hat{\omega}^D_{1,c} = 0$. The matchings of $\mathcal{P}^{(0)}$ and $U^{(1)}$ on the separatrices also imply $[\mathfrak{P}_2]^+_- = 0$ and

$$[J_{1,c}]^+_- = 0. \tag{18}$$

B. $O(\epsilon^{3/2})$ mean-flow equations

Evaluating the phase-averaged Equation (5) at the critical radius yields the time evolution equations of the CL induced mean flow: $\overline{V}_1$, $\overline{W}_1$, $\mathcal{Q}_{z,1}$, $\mathcal{Q}_{\theta,1}$, and $\overline{V}_2 \ldots$ at r_c. It is possible to straightforwardly derive the inviscid equations to the lowest orders for the mean inviscid flow is regular there. It is no longer the case to higher orders, for instance, for the fourth-order rotational velocity. Note that the vertical gradient of geopotential in (5c) generates a vertical wind at r_c. This motion is not however relevant at low orders to the wave packet dynamics. We therefore assume that the two first orders of the mean geopotential (8b) and (8c) are zero at r_c, so $\mathfrak{P}_1 = \mathfrak{P}_2 = 0$. From ((5b) and (5c)), we deduce the absence of the τ_2-evolution of the leading-order induced inviscid mean velocity at r_c

$$\mathcal{V}_{1,\tau_2} = 0, \qquad \mathcal{W}_{1,\tau_2} = 0. \tag{19}$$

After r-differentiating Equations (5b) and (5c) and by using (8b), we obtain the vorticity evolution equations. The induced mean vorticities do evolve over τ_2 in the following way:

$$\mathcal{Q}_{z,1,\tau_2} = -\zeta\,\mathcal{U}_3, \qquad \mathcal{Q}_{\theta,1,\tau_2} = \mathcal{V}_{1,\Phi}. \tag{20}$$

The time variation of the mean axial vorticity is provided by the divergence of the mean radial flux of the zeroth-order axial vorticity. The time variation of the mean azimuthal vorticity is related to the crossed radial and axial gradients of the first-order mean pressure, i.e., the vertical shear of the mean azimuthal velocity $\mathcal{V}_1$. Note that, in the presence of a small viscosity, the mean velocities $\overline{V}_1$ and $\overline{W}_1$ are slowly evolving with τ_2 around r_c due to the diffusion of the normal mode. Indeed, Equations (5b) and (5c) yield that these velocities are driven, respectively, by the divergences of the radial eddy fluxes of the angular and axial momenta

$$\overline{V}_{1,t}(r) = -\lambda\frac{\epsilon^3}{r^2}\frac{\partial}{\partial r}[r^2\overline{U^{(0)}_{r,i}U^{(3)}_{\theta,v}}],$$
$$\overline{W}_{1,t}(r) = -\lambda\frac{\epsilon^3}{r}\frac{\partial}{\partial r}[r\overline{U^{(0)}_{r,i}U^{(3)}_{z,v}}], \tag{21}$$

which comes down, at the leading order, while approximating $U^{(0)}_{r,i}$,$U^{(3)}_{\theta,v}$ and $U^{(3)}_{z,v}$ by the first terms of their Frobenius series, to

$$\overline{V}_{1,t}(\eta) = -\lambda\epsilon^3\frac{\zeta r_c^3}{\eta^4}A^2\,\varrho_{0,c}, \qquad \overline{W}_{1,t}(\eta) = -\lambda\varpi\epsilon^3\frac{\zeta r_c^3}{\eta^4}A^2\,\varrho_{0,c}. \tag{22}$$

The r.h.s. of these equations is $O(\lambda\epsilon)$ near the CL since $\eta = O(\epsilon^{1/2})$. The mean-flow equations are in fact singular at r_c as soon as the first order when viscosity is considered. Indeed, viscous diffusion makes the velocities $\overline{V}_1$ and $\overline{W}_1$ and the vorticities $\mathcal{Q}_{z,1}$ and $\mathcal{Q}_{\theta,1}$ not only singular at r_c but also, furthermore, enhances distortion. So, $\mathcal{V}_1$, $\mathcal{W}_1$, $\mathcal{Q}_{z,1}$, and $\mathcal{Q}_{\theta,1}$ do no longer exist in the presence of viscosity. To rigorously study the induced mean flow, it would be then necessary to consider the evolution of the inner velocities, vorticities, ... averaged over a CL half-width. For instance, for the rotational velocity, we would have a leading-order mean velocity $\mathcal{V}_1$ defined by $(r_{B2} - r_c)r_c\mathcal{V}_1^+ \equiv \int_{r_c}^{r_{B2}}\overline{V^{(0)}}r\,d\mathcal{R}$. The CL width is limited by two boundaries r_{B1} and r_{B2}. The growth rate of the mean angular momentum inside the critical layer is related to the jump of the mean radial eddy flux of this momentum across the CL: $[\overline{uv}]^{r_{B1}}_{r_{B2}}$, an approximate value is given by the outer-flow Frobenius series

$$\int_{r_{B1}}^{r_{B2}}\partial_t\overline{V}_1\,r\,\mathrm{d}r = \frac{16}{3}\lambda\zeta\frac{\varrho_{0,c}r_c^4}{\delta_{cl}^3}A^2\epsilon^{3/2} \tag{23}$$

with $r_{B1} = r_c - \delta_{cl}/2 + \cdots$ and $r_{B2} = r_c + \delta_{cl}/2 + \cdots$. The CL thickness δ_{cl} is not constant but evolves with time following the wave packet amplitude: it scales like $\delta_{cl} = 4\sigma\,(A\,\epsilon)^{1/2}r_c$ with $1 < \sigma \ll \epsilon^{-1/2}$; σ is the ratio of the CL thickness over the cat's eye thickness. It follows a deceleration over the viscous homogenization time scale $\tau = \epsilon\lambda t/r_c^2$ in the quasi-steady régime since $\zeta < 0$ for stable basic-vorticity profiles:

$$\mathcal{V}_{1,\tau} = \frac{\zeta}{48\sigma^4}.$$

The radial vorticity gradient ζ can be $O(1)$ near the maximum-wind radius but is usually small in the outer core and around r_c.[38] As $\sigma > 1$, the τ-evolution remains weak; it is negligible in the steady-state assumption.[16] We will neglect it here with respect to the τ_3-evolution.

C. The third-order inner flow

This section gives the analytical expressions of the first nontrivial inviscid flow in the critical layer. The procedure is identical to this in C14, so we only give details for specific results related to the wave packet assumption. The azimuthal velocity $V^{(2)}$ is defined through the streamfunction-like function $\psi^{(2)}$,

$$V^{(2)} = \frac{1}{2}\mathcal{R}^2 - s_i\mathcal{S}_1\mathcal{R} + \mathcal{V}_2(\Phi,\tau_2,\tau_3) + \psi^{(2)}_{\mathcal{R}},$$

which is the solution of the azimuthal-momentum of equation (24); the vertical-momentum equation is as follows:

$$\sin X\psi^{(2)}_{\mathcal{R}\mathcal{R}} + \frac{1}{A}(\mathcal{R}\,\psi^{(2)}_{X\mathcal{R}} - \psi^{(2)}_X) = \lambda'(\psi^{(2)}_{\mathcal{R}\mathcal{R}\mathcal{R},i} - \zeta), \tag{24}$$
$$\sin X W^{(2)}_{\mathcal{R}} + \frac{1}{A}(\mathcal{R}\,W^{(2)}_X - \psi^{(2)}_X) = \lambda' W^{(2)}_{\mathcal{R}\mathcal{R},i}\,. \tag{25}$$

The geopotential $\mathcal{P}^{(2)}$ and the radial velocity $U^{(2)}$ are expressed as functions of $\psi^{(2)}$ and $W^{(2)}$ via the radial momentum and mass conservation equations

$$\mathcal{P}^{(2)} = \frac{1}{2}\mathcal{R}^3 - \frac{1}{4}s_i(3\mathcal{S}_1+\mathcal{C}_0\mathcal{C}_1)\mathcal{R}^2 + [\mathcal{V}_2 + \frac{1}{4}(\mathcal{S}_1^2 - \mathcal{C}_1^2)]\mathcal{R} + \psi^{(2)} + s_i\mathfrak{P}_3(\Phi,\tau_2,\tau_3)\,, \quad (26)$$

$$U_{\mathcal{R}}^{(2)} = A\,\sin X - \psi_{\mathcal{R}X}^{(2)} - \varpi^2 W_X^{(2)}. \quad (27)$$

Equations (24)–(27) yield distinct solutions inside and outside the separatrices.

1. Outside the separatrices

The inviscid general solution of (24) is

$$\psi_{i,\mathcal{R}\mathcal{R}}^{(2)} = \mathcal{F}_2(Z,\Phi,\tau_2,\tau_3),$$

where

$$Z = \frac{1}{2}\mathcal{R}^2 + A\cos X. \quad (28)$$

The variable Z characterizes the classic cat's eye CL pattern. Two helical separatrices divide the inner flow in three domains: two outside the separatrices: one, on the outer edge of the CL, and the other in the vortex core, where all streamlines span the whole 2π θ-range, and the third one, where streamlines draw m recirculation zones and only span a part of the $2\pi/m$ θ-range, the cat's eyes. Streamlines are defined by only one value of Z; for instance, the separatrices are characterized by $Z = A$, see in Figure 1 the helical sheet and the location of the outer separatrices for a $m = 2$ CL. In order to better pose the problem, we therefore perform the change of variables: $(\mathcal{R}, X) \to (Z, x = X)$. We can define $\mathcal{R}$ as a function of Z and x such as $\mathcal{R} = Z_{\mathcal{R}} = s\sqrt{2}(Z - A\cos x)^{1/2}$ with the sign s of $\mathcal{R}$ being $s = s_i$ for $r > r_c$ and $s = -s_i$ for $r < r_c$. The magnitude of $\mathcal{R}$ on the separatrix is denoted as $\mathcal{R}^X = 2|\sin(x/2)|\,A^{1/2}$. Owing to the distortions of the inner flow, the cat's eye is not strictly symmetric with respect to the level $\mathcal{R} = 0$. As a result, the independent variable Z only gives a first approximation to the location of the dividing streamlines. A better variable, the stressed coordinate $\tilde{Z}$, is needed in order to correctly describe the deformed trajectory of the streamlines inside the critical layer. Thus, it is necessary to ensure that the tangential and axial velocities are linked in the frame moving with the linear VR wave speed, at the core of the cat's eye and at the crossing point of the separatrices, by the relationship (E2), topological property which has previously been overlooked, see, for instance, Refs. 9 and 10. The variable Z does not allow satisfying (E2) as soon as the first order of the inner expansion. In this way, we rescale Z in an asymptotic expansion following $\tilde{Z}$; the method is explained in Appendix E. The new fields, denoted by a tilde, are thus expanded in the following way, for instance, for the radial velocity

$$\tilde{U}(\tilde{Z},x) = \epsilon\,[\,\tilde{U}^{(0)} + \epsilon^{\frac{1}{2}}\ln\epsilon\,\tilde{U}^{(1)} + \epsilon^{\frac{1}{2}}\,\tilde{U}^{(2)} + \cdots\,].$$

In the quasi-steady state, the radial velocities at the saddle points and at the center point are not zero like in C14. Using these analytical expressions of the 3D velocity field, we were able to analytically compute the streamlines inside the critical layer (cf. Appendix C in C14). For instance, a nonlinear vortex Rossby wave packet is shown in Figures 2 and 3, at constant height Φ and in a vertical constant-θ plane, for the azimuthal wavenumber $m = 2$, revealing a tripolar vortex whose satellites spiral along the vortex axis and are asymmetric with respect to the critical radius. Figure 2 displays the CL around the height $\Phi = 0$ where it is the thickest and Figure 3 displays the CL around $\Phi = \Pi$ where it is the thinnest. The contours in these figures are not the trajectories of air particles but their envelopes, the surfaces on which particles slide but cannot cross. These streamlines are drawn in the local referential moving with the linear wave speed $v = (\Omega_{0,c}+\epsilon^{1/2}\Omega_{1,c})r$ and $w = \epsilon^{1/2}\overline{W}_{1,c}$ plus

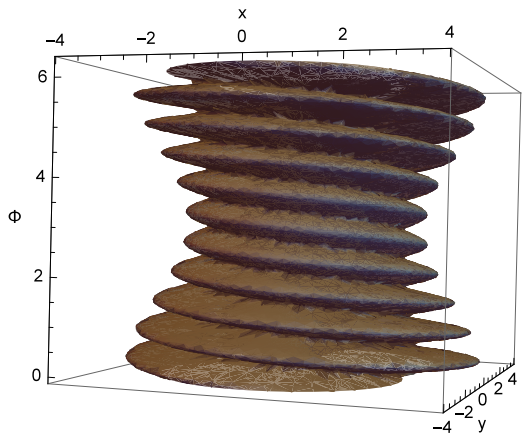

FIG. 1. Outer separatrix sheet $Z = A$ as a function of x, y and Φ, $m = 2$, $\epsilon = 10^{-1}$, $\varpi = 1$, $r_c = 2$, $\tau_3 = 0$, and $A(\Phi) = [1 + \cos(\Phi)/2]^2$.

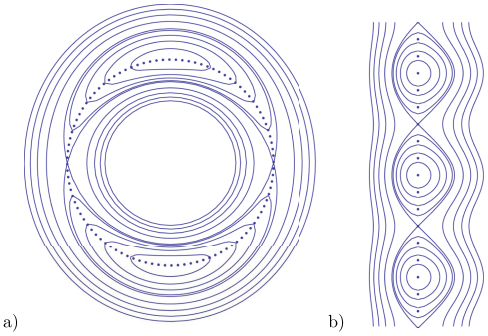

FIG. 2. Wave packet $m = 2$, $\varpi = 1$, $r_c = 2$, $\epsilon = 0.0075$, $\zeta = -0.1$, $\zeta' = 0$, $a = -0.5$, $s_i = 1$, $\beta_{l,1}^{+} = 0$, $\tau_3 = 0$, $A(\Phi) = [1 + \cos(\Phi)/2]^2$, $\mathcal{V}_1 = \mathcal{W}_1 = \sqrt{A}$, $\{\Lambda_1\}_-^+ = 1/2\sqrt{A}$, $\{\mathfrak{T}_1\}_-^+ = 0.1\sqrt{A}$, and $\{\zeta_{z,1}\}_-^+ = 0$. (a) view at $\Phi = 0$, (b) vertical cross section at $\theta = 0$ between $\Phi = 0$ and $\Phi = 0.14$. The dotted line represents the critical radius.

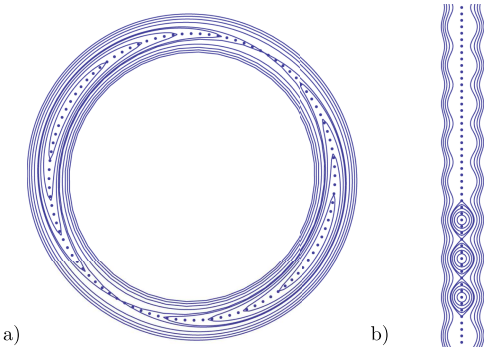

FIG. 3. Wave packet $m = 2$, $\varpi = 1$, $r_c = 2$, $\epsilon = 0.0075$, $\zeta = -0.1$, $\zeta' = 0$, $a = -0.5$, $s_i = 1$, $\beta_{l,1}^{+} = 0$, $\tau_3 = 0$, $A(\Phi) = [1 + \cos(\Phi)/2]^2$, $\mathcal{V}_1 = \mathcal{W}_1 = \sqrt{A}$, $\{\Lambda_1\}_-^+ = 1/2\sqrt{A}$, $\{\mathfrak{T}_1\}_-^+ = 0.1\sqrt{A}$, and $\{\zeta_{z,1}\}_-^+ = 0$. (a) view at $\Phi = \pi$, (b) vertical cross section at $\theta = 0$ between $\Phi = \pi - 0.21$ and $\Phi = \pi + 0.21$, only three representative cat's eyes have been drawn. The dotted line represents the critical radius.

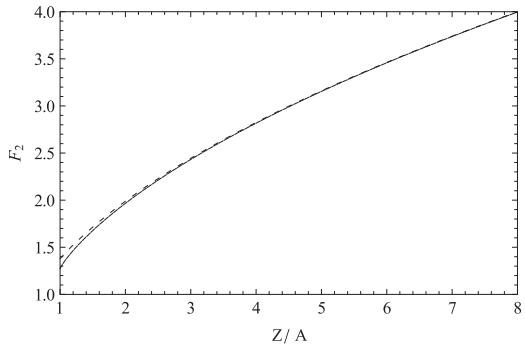

FIG. 4. Inner axial vorticity profile outside the separatrices $|(\mathcal{F}_2 - s_i\mathcal{Q}_{z,1})/(\zeta A^{1/2})|$ as a function of Z/A: wave packet profile in solid line and single mode profile in dashed line.

the mean radial velocity $u = \epsilon^{3/2}\overline{U}_{3,c}$. In earth's referential, these surfaces lose their 2π-periodicity owing to the presence of the mean radial velocity.

To find the function $\mathcal{F}_2$, we apply the secularity condition[39] on the fifth-order inviscid axial vorticity $\psi^{(5)}_{i,\mathcal{R}\mathcal{R}}$, which comes down to a PDE in $\mathcal{F}_2$,

$$\langle\psi^{(5)}_{i,\mathcal{R}\mathcal{R}x}\rangle = 0 \equiv \mathcal{U}_3\mathcal{F}_{2,Z}(Z,\tau_2)+s_i\mathcal{F}_{2,\tau_2}(Z,\tau_2)\langle Z_{\mathcal{R}}^{-1}\rangle = 0, \quad (29)$$

where $\langle\ \rangle$ is an average over x at constant Z. By matching the axial vorticity of the CL flow with the outer flow for $Z \to \infty$, we deduce the asymptotic expression for $\mathcal{F}_2$, $\mathcal{F}_2(Z) \to \zeta Z_{\mathcal{R}} + s_i\mathcal{Q}^s_{z,1}$, then by using (20), $\mathcal{F}_2(Z)$ is straightforwardly determined

$$\mathcal{F}_2(Z,\Phi,\tau_2,\tau_3) = \zeta\langle Z_{\mathcal{R}}\rangle + s_i\mathcal{Q}^s_{z,1},$$

where

$$\langle Z_{\mathcal{R}}\rangle = s\sqrt{2A}\,\mathrm{SE}[Z/A]. \quad (30)$$

All mathematical functions used in this paper are defined in Appendix H. This expression is slightly distinct from this used while describing a nonlinear CL, location of the interaction between a single mode and a swirling sheared flow,[15,16,40,41] and where the secularity condition was applied to the viscous flow; a small departure only exists near the separatrices as we can see in Figure 4. Both streamline charts are identical but depart with time. The stringent feature of the function SE that characterizes the profile of the inner axial vorticity is the unboundedness of its derivative at $Z = A$, which means that the radial gradient of the axial vorticity is infinite on the separatrix. This logarithmic singularity also appears in the viscous component of the inner azimuthal velocity $\psi^{(2)}_{v,\mathcal{R}}$, see C14. The viscous flow is crucial for the WMFI analysis since it is involved in the computation of the leading-order mean radial eddy fluxes. This singularity can be in fact smoothed out by two different ways when one examines the CL flow around the separatrices. In the viscous-CL assumption, one must consider the thin viscous boundary layers along the separatrices. In the high-Reynolds number assumption, one must consider the thin nonlinear boundary layers along the separatrices where a new relevant stressed variable $\hat{Z}$ must be employed. The singularity is then removed by deforming the CL streamlines a little more with respect to the deformations generated by the use of the stressed variable $\tilde{Z}$. We shall prefer this method since we assume $\lambda \ll 1$, that is, the nonlinear boundary layer results larger than the viscous one. A similar problem occurred in the solitary Rossby elevation wave CL modeling,[27] where the second-order vorticity had an infinite slope on the separatrices. The new cross-stream variable around the separatrices is thus defined by the expansion

$$\hat{Z} = \frac{\tilde{Z}-A}{\delta} + \frac{\mathcal{Z}^{(2)}(\tilde{Z})}{\ln\epsilon} + \epsilon^{\frac{1}{2}}\,\mathcal{Z}^{(4)}(\tilde{Z}) + \epsilon^{\frac{1}{2}}\,\frac{\mathcal{Z}^{(5)}(\tilde{Z})}{\ln\epsilon} + \cdots,$$
$$\delta = \epsilon^{\frac{1}{2}}\,\ln\epsilon.$$

As the separatrix is slightly deformed, its position is no longer defined by $\tilde{Z} = A$, but by $\hat{Z} = 0$, that is,

$$\tilde{Z} = A - \epsilon^{\frac{1}{2}}\,\mathcal{Z}^{(2)}(A) - \epsilon\ln\epsilon\,\mathcal{Z}^{(4)}(A) + \epsilon\,[\mathcal{Z}^{(2)}(A)\,\mathcal{Z}^{(2)}_{\tilde{Z}}(A) - \mathcal{Z}^{(5)}(A)] + \cdots.$$

The functions $\mathcal{Z}$ characterize the CL deformation, they are defined while matching this boundary layer flow with the CL flow as $\hat{Z} \to \infty$. A stronger computed mean radial eddy flux of angular momentum is expected whatever the way we may use to remove the singularity, which leads to a stronger WMFI in the quasi-steady state, compared to the steady case where the WMFI was negligible. This WMFI is indeed stronger as is numerically checked in Section VII. This wave/vortex interaction nevertheless causes a vortex deceleration in the opposite way to the transition stage.

Integrating $\psi^{(2)}_{i,\mathcal{R}\mathcal{R}}$ over $\mathcal{R}$ yields the second-order azimuthal velocity

$$\psi^{(2)}_{i,\mathcal{R}} = \zeta\left(AK_a[Z/Ax] + [Z(Z-A\cos x)]^{\frac{1}{2}} + A\cos x\ln[\Lambda(Z,x)]\right) + s_i\mathcal{Q}_{z,1}Z_{\mathcal{R}} + V_2(x)$$

with

$$\Lambda(Z,x) = \sqrt{Z} + \sqrt{Z - A\cos x} \quad \text{and} \quad V_2(x) = -[a + 1 - \frac{\zeta}{2}(1+3\varpi^2)]\frac{A\,\cos x}{1+\varpi^2}. \quad (31)$$

A general solution of (25) is $W^{(2)}_i = \psi^{(2)}_{\mathcal{R}} + \mathcal{G}_2(Z,\Phi,\tau_2,\tau_3) + \mathcal{W}_2(\Phi,\tau_2,\tau_3)$. The secularity condition applied to the fifth-order inviscid flow $W^{(5)}_i - \psi^{(5)}_{i,\mathcal{R}}$ yields the following PDE in $\mathcal{G}_2$:

$$\langle[W^{(5)}_i - \psi^{(5)}_{i,\mathcal{R}}]_x\rangle = 0 \equiv \mathcal{U}_3[\mathcal{G}_{2,Z}(Z,\tau_2) + s_i\frac{J_{1,c}}{\varpi^2}\langle Z_{\mathcal{R}}^{-1}\rangle] + s_i\mathcal{G}_{2,\tau_2}(Z,\tau_2)\langle Z_{\mathcal{R}}^{-1}\rangle = -\mathcal{V}_{1,\Phi}/\varpi.$$

The matching at the CL edges as $Z \to \infty$ gives $\mathcal{G}_2(Z) \to -\zeta Z - s_iJ_{1,c}\mathcal{R}/\varpi^2$. Since $J_{1,c,\tau_2} = 0$ according to (20), the solution is then straightforwardly determined

$$\mathcal{G}_2(Z,\Phi,\tau_3) = -\frac{\mathcal{V}_{1,\Phi}}{\varpi\mathcal{U}_3}Z - s_i\frac{J_{1,c}}{\varpi^2}\langle Z_{\mathcal{R}}\rangle.$$

We therefore deduce that the mean radial and azimuthal velocities are linked at r_c through

$$\mathcal{U}_3 = \frac{\mathcal{V}_{1,\Phi}}{\zeta\varpi}(\Phi,\tau_3),$$

so

$$\mathcal{G}_2(Z,\Phi,\tau_3) = -\zeta Z - s_i\frac{J_{1,c}}{\varpi^2}\langle Z_{\mathcal{R}}\rangle. \tag{32}$$

The mean velocity $\mathcal{U}_3$ is not a function of τ_2, so Equation (20) shows a secular τ_2-evolution of the induced mean vorticities.

2. Within the separatrices

We here match the inner flows inside and outside the separatrices and jointly with the extended Prandtl-Batchelor theorem and we find a unique solution inside the cat's eye. First, we match the three components of the leading-order vorticity. After the Prandtl-Batchelor theorem in Appendix F, the axial vorticity inside the separatrices is uniform at that order on any horizontal planes; it is simply a function of the slow variables

$$\psi^{(2,\odot)}_{\mathcal{RR}} = Q^{(2,\odot)}(\Phi,\tau_2,\tau_3). \tag{33}$$

Matching (33) with (30) on the separatrices yields $Q^{(2,\odot)}$ and the mean-vorticity jumps

$$Q^{(2,\odot)} = s_i\{\mathcal{Q}_{z,1}\}^+_-,\quad [\mathcal{Q}_{z,1}]^+_- = -2\zeta\sqrt{2A}\,SE[1] = -\frac{8}{\pi}\zeta A^{\frac{1}{2}}, \tag{34}$$
$$[\mathcal{Q}_{\theta,1}]^+_- = \frac{8}{\pi}\zeta\varpi A^{\frac{1}{2}}.$$

These jumps show the dynamical coupling between the wave packet and the induced mean vorticities, coupling that has been omitted until now in wave packet studies in the presence of a critical layer.[33] After C14, we can express the mean-vorticity jumps as functions of the logarithmic phase shift ϕ, the latter is proportional to λ' in this way

$$\frac{\phi(\lambda')}{\lambda'} \to -s_i\frac{16}{\pi}A^{-\frac{1}{2}},\qquad \lambda' \to 0.$$

The mean-vorticity jumps and the logarithmic phase shift are of weaker intensity when they are compared with the jumps and phase shift computed with the secularity condition applied to the viscous component of the flow in C14, for instance, $[\mathcal{Q}_{z,1}]^+_- = -2\mathcal{C}\zeta A^{1/2}$, where $\mathcal{C} \simeq 1.379$, indeed $8/\pi \simeq 2.547$. This discrepancy goes into the way of a slight increase of the vortex intensification in the transition stage according to the WMFI amounts displayed in Equation (59) of C14, although those formulae are not strictly right in the present study because of the new derived function *SE* to account for the leading-order CL axial vorticity. This change is small because we are in the nonlinear régime, where the wave packet is close to a monochromatic wave. Choosing the wave packet régime would increase the intensification even more.[31,32] Finally, the axial vorticity within the separatrices is modulated by the presence of the wave train and furthermore, varies linearly with τ_2

$$Q^{(2,\odot)}(\Phi,\tau_2,\tau_3) = s_i\{\Lambda_1(\Phi,\tau_3)\}^+_- - s_i\mathcal{V}_{1,\Phi}(\Phi,\tau_3)\frac{\tau_2}{\varpi}.$$

Through the jumps of the mean vorticities (34) applied to Eq. (20), we get the jumps of $\mathcal{V}_{1,\Phi}$ and $\mathcal{U}_3$: $[\mathcal{V}_{1,\Phi}]^+_- = 4/\pi\varpi\zeta A_{\tau_2}A^{-1/2}$, $[\mathcal{U}_3]^+_- = 4/\pi A_{\tau_2}A^{-1/2}$. From the continuity of the normal velocity on the separatrices, $[\mathcal{U}_3]^+_- = 0$, $\mathcal{U}_3$ and $\mathcal{V}_1$ are then undistorted, and we thus show that the wave packet amplitude evolves over the time τ_3 like $\mathcal{U}_3$ and $\mathcal{V}_1$,

$$A_{\tau_2} = 0. \tag{35}$$

After Eq. (25), the inviscid axial velocity is written, in a general way, within the separatrices

$$W^{(2,\odot)}_i = \psi^{(2,\odot)}_{i,\mathcal{R}} - \zeta Z + \{\mathcal{W}_2\}^+_-, \tag{36}$$

while the azimuthal velocity is given by

$$V^{(2,\odot)}_i = \frac{1}{2}\mathcal{R}^2 - s_i\mathcal{S}_1\mathcal{R} + \{\mathcal{V}_2\}^+_- + \psi^{(2,\odot)}_{i,\mathcal{R}}$$

with

$$\psi^{(2,\odot)}_{i,\mathcal{R}} = Q^{(2,\odot)}Z_{\mathcal{R}} + V^{\odot}_2(x). \tag{37}$$

The matching of the azimuthal or radial vorticity while considering (18) implies

$$J_{1,c} = 0,\quad \mathcal{Q}_{\theta,1} = -\varpi\mathcal{Q}_{z,1}. \tag{38}$$

The local equivalent Richardson number is therefore of order $O(\epsilon)$. Next, we match the pressure on the separatrix, which determines $V^{\odot}_2(x)$ and $[\mathfrak{P}_3]^+_-$ (see C14). Second, the normal-velocity continuity on the separatrix yields the leading-order nontrivial relation

$$\mathcal{R}^X[\tilde{U}^{(2)} - \tilde{U}^{(2,\odot)}] = s[\varpi^2(\tilde{W}^{(2)} - \tilde{W}^{(2,\odot)}) + \tilde{V}^{(2)} - \tilde{V}^{(2,\odot)}]A\sin x, \tag{39}$$

where the velocities are evaluated on the separatrix as $\tilde{Z} = A$. Equations (27), (36), and (37) give the radial velocity outside and within the cat's eye

$$U^{(2)}_i(Z,x) = (1+\varpi^2)\zeta A\,\sin x\left(\frac{1}{2}Z_{\mathcal{R}}\int_\infty^{Z/A}\frac{\mathrm{SE}[Z_1] - \sqrt{Z_1}}{\sqrt{Z_1 - \cos x}^3}\,dZ_1 + \{\ln[\Lambda(Z,x)] + \frac{1}{2}\}Z\mathcal{R} - s\sqrt{2Z}\right)$$
$$+(1-\varpi^2\zeta)A\,\sin x - (1+\varpi^2)V_2'(x)Z_{\mathcal{R}} + \Upsilon_2(x) \tag{40}$$

and

$$U^{(2,\odot)}_i(Z,x) = \Upsilon^{\odot}_2(x) + [(1-\zeta\varpi^2)A\sin x - (1+\varpi^2)V^{\odot'}_2(x)]Z_{\mathcal{R}}. \tag{41}$$

The matching of $U^{(2)}$ with the outer flow gives $\Upsilon_2(x) = -s_i\,\Upsilon_{2,0}A\sin x$, with

$$\Upsilon_{2,0} = \beta_{l,1} + \mathcal{S}_1 - \frac{\zeta_{z,1}}{\zeta} - \frac{3\varpi^2+1}{1+\varpi^2}\mathcal{Q}_{z,1} + \frac{2\varpi^3}{1+\varpi^2}\mathcal{Q}_{\theta,1}. \tag{42}$$

Knowing both radial velocities (40) and (41) and applying $\{$Eq. (39)$\}^+_-$ give $\Upsilon^{\odot}_2$,

$$\Upsilon_2^{\odot}(x) = \{\Upsilon_2(x)\}_-^+ - \frac{3}{4}s_i[a]_-^+ A\mathcal{R}^X \sin x - \frac{1}{2}s_i A\{[\mathcal{V}_2 + \varpi^2\mathcal{W}_2]_-^+ - [a]_-^+ A\}\frac{\sin x}{\mathcal{R}^X},$$

so that $\Upsilon_2^{\odot}(x)$ may be a continuous 2π-periodic function; the constants of integration a^s in Eq. (11) must be distinct such as

$$[a]_-^+ = \frac{1}{A}[\mathcal{V}_2 + \varpi^2\mathcal{W}_2]_-^+. \tag{43}$$

In the presence of second-order mean velocity jumps, a discontinuity appears in the azimuthal and axial velocity profiles of the inviscid nonlinear neutral VR mode. Sec. V will prove that these mean velocities are indeed distorted, see Eq. (49). Besides, these distortions have a secular term proportional to the velocity shear $\mathcal{V}_{1,\Phi}$. The phase jump (43) across the CL is not constant but evolves with Φ, τ_2, and τ_3. In the steady-state approximation in C14, no such discontinuity is assumed. The steady state is given by the second-order inner flow; proving that $\mathcal{V}_2$ and $\mathcal{W}_2$ are distorted in the absence of a vertical shear implies us to carry on the inner-flow analysis to a much higher order. This result is important because, until now, inviscid nonlinear neutral modes were considered undistorted in studies where the induced mean flow was omitted,[9,33,39,42] or in studies where only the first-order mean flow was taken into account,[43,44] contrary to viscous nonlinear neutral modes where the phase jump was found λ-dependent.[24,25] The velocities $V^{(2)}$ and $W^{(2)}$ are not then continuous through the separatrix for the second-order mean velocities are distorted. At last, the $O(\epsilon^2)$ outer flow contains an additional term in Subsection III C owing to the τ_2 dependency of the neutral mode and in phase quadrature with this mode. This contribution does not however appear in the fourth and fifth orders of the inner flow.

Next, applying $[(39)]_-^+$ imposes the condition $[\Upsilon_{20}]_-^+ = (1+\varpi^2)[\mathcal{Q}_{z,1}]_-^+$; this jointly with Eqs. (42) and (34) yields the relationship between the jumps of the first-order outer radial velocity $\beta_{l,1}{}_-^+$ and the radial gradient of the first-order mean axial vorticity at r_c, $\zeta_{z,1}$

$$[\beta_{l,1}]_-^+ = \frac{[\zeta_{z,1}]_-^+}{\zeta} - \frac{8}{\pi}\zeta(2+3\varpi^2)A^{\frac{1}{2}}. \tag{44}$$

The quasi-steady régime assumption imposes a weak equivalent Richardson number at the critical radius, which leads to the fact that leading-order induced mean azimuthal and axial vorticities are strongly coupled there. The slow time variation here does not therefore alter the relationship between both mean vorticities.[40] Assuming a small induced vertical shear of order ϵ yields a secular evolution over time τ_2 for these vorticities. Due to the mean-vorticity coupling, the induced $O(\epsilon^{3/2})$ mean radial velocity evolves like the vertical shear of the mean rotational velocity. The mean axial vorticity can then be expressed by

$$\mathcal{Q}_{z,1}^s(\Phi,\tau_2,\tau_3) = \Lambda_1^s(\Phi,\tau_3) - \mathcal{V}_{1,\Phi}(\Phi,\tau_3)\frac{\tau_2}{\varpi},$$

with

$$[\Lambda_1]_-^+ = -\frac{8}{\pi}\zeta A^{\frac{1}{2}}. \tag{45}$$

Note that the leading-order mean radial vorticity is $O(\epsilon^{3/2})$, namely, $\mathcal{Q}_{r,3} = -m\mathcal{V}_{1,\Phi}$. The leading-order CL induced mean axial vorticity has two contributions: one distorted that varies slowly with τ_3, $\Lambda_1(\Phi,\tau_3)$, and one undistorted that varies faster with τ_2 in a secular way but still more slowly than the nonlinear CL development time τ_1 of the transition stage. The steady-state assumption in C14 has led to find a unique solution of the Euler equation through the viscous secularity condition. The steady and nonlinear CL theory implies a Haberman parameter bounded between $\epsilon^{1/2} \ll \lambda' \ll 1$. The quasi-steady régime assumption now allows us to release the condition $\lambda' \gg \epsilon^{1/2}$ since the secularity condition is inviscid. As a result, we can assume a much smaller λ' so that the wave packet time scale be faster than the slow viscous homogenization time scale: $\tau_3 \gg \tau$, which is the WMFI time of the steady régime. The mean-flow and wave packet evolutions can be then computed by neglecting the viscous flow and are over the time scales τ_2 and τ_3. From now on, we will qualify as "slow," the flow only evolving over τ_3, and as "fast" the flow evolving over τ_2.

V. $O(\epsilon^2)$ MEAN FLOW EQUATIONS

We here examine the $O(\epsilon^2)$ evolution equations of the leading-order inviscid mean flow at the critical radius. We will deduce the system of τ_3-evolution equations for $A(\Phi,\tau_3)$, $\mathcal{V}_1(\Phi,\tau_3)$, $\mathcal{W}_1(\Phi,\tau_3)$, and $\Lambda_1(\Phi,\tau_3)$.

We first determine the evolution equations of $\mathcal{V}_1$ and $\mathcal{W}_1$, knowing that these velocities are inviscidly undistorted and that they are slow. The rescaled $O(\epsilon^2)$ momentum Equations (5b) and (5c) evaluated at r_c are, namely,

$$\mathcal{V}_{1,\tau_3} + \mathcal{V}_{2,\tau_2} + \varpi\mathcal{W}_1\mathcal{V}_{1,\Phi} = -\mathcal{Q}_{z,1}\frac{\mathcal{V}_{1,\Phi}}{\zeta\varpi} - s_i\lambda'\zeta_{z,1}A, \tag{46}$$

$$\mathcal{W}_{1,\tau_3} + \mathcal{W}_{2,\tau_2} + \varpi\mathcal{W}_1\mathcal{W}_{1,\Phi} = \mathcal{Q}_{\theta,1}\frac{\mathcal{V}_{1,\Phi}}{\zeta\varpi^2} + s_i\lambda'\frac{\zeta_{\theta,1}}{\varpi}A. \tag{47}$$

The divergence of the leading-order mean radial eddy fluxes that should be present in both equations and that involve the product of the viscous and inviscid components, $\lambda r_c^{-2}D[r^2\overline{U_{r,i}^{(0)}U_{\theta,v}^{(0)}}] + \lambda r_c^{-2}D[r^2\overline{U_{r,v}^{(0)}U_{\theta,i}^{(0)}}]$ for the azimuthal momentum equation and a similar expression for the vertical momentum equation, are regular and zero at r_c. However, higher-order flows bring about a $O(\lambda\,\epsilon^2)$ contribution in Equation (5b) like $-\lambda r_c^{-2}D[r^2\overline{U_{r,i}^{(1)}U_{\theta,v}^{(3)}}]$ in the CL neighborhood because they are singular at r_c. The same remark can be done for Equation (5c). Assuming $\lambda \ll 1$, we will only study the evolutions of the inviscid parts of the mean flow and neglect their evolution over $\tau = \lambda\tau_2$ and $\lambda\tau_3$.

Let us first decompose Λ_1 in an undistorted term and another distorted so that one may separate first and second-order velocity evolutions in (46) and (47); next, let us decompose $\mathcal{U}_4$ in slow and fast motions

$$\Lambda_1 = \{\Lambda_1\}_-^+ + \Lambda_{1,d}, \quad \mathcal{U}_4 = \mathfrak{u}_4(\Phi,\tau_2,\tau_3) + \mathfrak{U}_4(\Phi,\tau_3).$$

The second-order velocities are thus written

$$\begin{aligned}\mathcal{V}_2(\Phi,\tau_2,\tau_3) &= \Big(\frac{\mathcal{V}_{1,\Phi}}{2\varpi}\tau_2^2 - \Lambda_{1,d}\,\tau_2\Big)\frac{\mathcal{V}_{1,\Phi}}{\zeta\varpi} + \mathfrak{V}_2(\Phi,\tau_3),\\ \mathcal{W}_2(\Phi,\tau_2,\tau_3) &= \Big(\frac{\mathcal{V}_{1,\Phi}}{2\varpi}\tau_2^2 - \Lambda_{1,d}\,\tau_2\Big)\frac{\mathcal{V}_{1,\Phi}}{\zeta\varpi} + \mathfrak{W}_2(\Phi,\tau_3).\end{aligned} \tag{48}$$

We deduce the related jumps

$$[\mathcal{V}_2]^+_- = \frac{8}{\pi}\frac{\mathcal{V}_{1,\Phi}}{\varpi}A^{\frac{1}{2}}\tau_2 + [\mathfrak{V}_2(\Phi,\tau_3)]^+_-,$$

and

$$[\mathcal{W}_2]^+_- = \frac{8}{\pi}\frac{\mathcal{V}_{1,\Phi}}{\varpi}A^{\frac{1}{2}}\tau_2 + [\mathfrak{W}_2(\Phi,\tau_3)]^+_-. \tag{49}$$

The distortions of $\mathcal{V}_2$ and $\mathcal{W}_2$ fast evolve over τ_2 and lead to the fast distortion of the phase jump a in (11)–(43). The derivations of the evolution equations of vorticities and radial vorticity gradients are detailed in Appendix B. The outcome is the following leading-order equations of an infinite system. The velocities $\mathcal{V}_1$ and $\mathcal{W}_1$, the slow averaged vorticity $\{\Lambda_1\}^+_-$, the slow averaged azimuthal vorticity radial gradient $\{\mathfrak{T}_1\}^+_-$, the slow averaged radial velocity $\{\mathfrak{U}_4\}^+_-$, and the wave packet amplitude A satisfy the following equations:

$$\mathcal{V}_{1,\tau_3} + \varpi\mathcal{W}_1\mathcal{V}_{1,\Phi} = -\{\Lambda_1\}^+_-\frac{\mathcal{V}_{1,\Phi}}{\zeta\varpi}, \tag{50}$$

$$\mathcal{W}_{1,\tau_3} + \varpi\mathcal{W}_1\mathcal{W}_{1,\Phi} = -\{\Lambda_1\}^+_-\frac{\mathcal{V}_{1,\Phi}}{\zeta\varpi}, \tag{51}$$

$$A_{\tau_3} + \varpi\mathcal{W}_1A_\Phi = 2\varpi A(\mathcal{W}_{1,\Phi} - \mathcal{V}_{1,\Phi}) + \frac{\pi}{4}[\mathfrak{Z}_1]^+_-\frac{\mathcal{V}_{1,\Phi}}{\zeta^2\varpi}A^{\frac{1}{2}} + \frac{\pi}{4}[\mathfrak{U}_4]^+_-A^{\frac{1}{2}}, \tag{52}$$

$$\{\Lambda_{1,\tau_3}\}^+_- + \varpi\mathcal{W}_1\{\Lambda_{1,\Phi}\}^+_- = \{\mathfrak{T}_1 + \varpi\Lambda_1 - \zeta\varpi\mathcal{S}_1\}^+_-\frac{\mathcal{V}_{1,\Phi}}{\zeta\varpi^2} - \frac{\{\mathfrak{V}_{2,\Phi}\}^+_-}{\varpi}, \tag{53}$$

$$\{\mathfrak{T}_{1,\tau_3}\}^+_- + \varpi\mathcal{W}_1\{\mathfrak{T}_{1,\Phi}\}^+_- = (\frac{2}{\zeta}\mathcal{V}_{1,\Phi} + \varpi^2\mathcal{W}_{1,\Phi})\{\Lambda_1 + \frac{\mathfrak{T}_1}{\varpi}\}^+_- + \frac{8}{\pi^2}\zeta^2\varpi^2A_\Phi + \Big(2\{\Lambda_1\}^+_- - 3\mathcal{S}_1 - \frac{\{\mathfrak{T}_1^{'}\}^+_-}{\zeta\varpi}\Big)\mathcal{V}_{1,\Phi} + (\mathcal{S}_1 + \varpi^2\{\Lambda_1\}^+_-)\{\Lambda_{1,\Phi}\}^+_- - 3\{\mathfrak{V}_{2,\Phi}\}^+_- + \{\Lambda_{2,\Phi}\}^+_-, \tag{54}$$

$$\{\mathfrak{U}_4\}^+_- = \frac{\varpi}{\zeta}\{\Lambda_1\}^+_-(\mathcal{W}_{1,\Phi} - \mathcal{V}_{1,\Phi}) - \varpi\mathcal{W}_1\{\Lambda_{1,\Phi}\}^+_- - \{\mathfrak{T}_1 + \varpi(\Lambda_1 + \mathfrak{Z}_1 - \zeta\mathcal{S}_1)\}^+_-\frac{\mathcal{V}_{1,\Phi}}{\zeta^2\varpi^2} + \frac{\{\mathfrak{V}_{2,\Phi}\}^+_-}{\zeta\varpi}. \tag{55}$$

Equations (50)–(54) couple the first-order variables $\mathcal{V}_1$, $\mathcal{W}_1$, $\{\Lambda_1\}^+_-$, $\{\mathfrak{T}_1\}^+_-$, $\{\mathfrak{T}_1^{'}\}^+_-$, and A as well as the second-order variables $\mathfrak{V}_2$ and Λ_2. The wave parameter ϖ and the basic-vorticity parameter ζ are crucial as for the wave packet/mean flow dynamics since they appear in each equation. Equation (54) is the result from the slow average of (B12). The action of the wave packet on the mean flow appears through the distortions: $[\Lambda_1]^+_-$, $[\zeta_{z,1}]^+_-\ldots$ We note that the first action appears at the r.h.s of Eq. (54) in the second term proportional to A_Φ and comes from the product $[\Lambda_1]^+_-[\Lambda_{1,\Phi}]^+_-$. The first-order rescaled inviscid azimuthal and axial velocity Equations (50) and (51) are identical: the evolution of $\mathcal{V}_1$ is driven by the slow averaged divergence of the radial flux of the mean azimuthal velocity at r_c that comes down to $\equiv -\mathcal{U}_3\{\Lambda_1\}^+_-$, which is also the slow averaged divergence of the radial flux of the mean axial velocity. A trivial solution is $\mathcal{W}_1 = \mathcal{V}_1 + Cst$ or equivalently $\overline{W}_1(r_c) = \varpi(\overline{V}_1(r_c) + Cst\,\varrho_{0,c}r_c)$, which orientates the CL induced mean-flow solution toward a helical motion perpendicular to the isophase lines, since on a line $\xi = Cst$, axial and azimuthal velocities are linked by $v = -\varpi w$. The sixth Equation (55), second-order analogous to (32), gives the slow second-order mean radial velocity $\mathfrak{U}_4$. We will indeed show that the jump of $\mathfrak{U}_4$, determined through the fifth-order inner flow analysis in Subsection IV B, is zero, i.e., $\mathfrak{U}_4 = \{\mathfrak{U}_4\}^+_-$. The jump of the slow radial gradient of the axial vorticity $\zeta_{z,1}$, $[\mathfrak{Z}_1]^+_-$ in (52) is calculated through the study of the fourth-order inner flow. The second-order velocity and vorticity $\mathfrak{V}_2$ and Λ_2 and the second-order radial derivative of the first-order azimuthal vorticity $\{\mathfrak{T}_1^{'}\}^+_-$ can be only determined by their τ_3-evolution equations that may intervene new higher-order variables as well as higher-order radial derivatives through the radial fluxes. This system is thus not closed and is very complex since higher-order evolution equations are singular at r_c with the singularity increasing with the order. The subsystem ((50)–(54)) is the simplest if we wish to study the coupled evolution of $\mathcal{V}_1$, $\mathcal{W}_1$, Λ_1, $\{\mathfrak{T}_1\}^+_-$, and A as we close it by neglecting second-order variables and third-order radial derivatives of the velocity field. The first-order system cannot be studied through the weakly nonlinear hypothesis. Indeed in the steady approximation, $\mathcal{V}_1$ and $\mathcal{W}_1$ scaling like $A^{1/2}$, these equations are close to the inviscid Burgers equation, i.e., a first-order quasilinear hyperbolic equation. The latter admits typical solutions characterizing breaking waves in fluid dynamics or shock waves in gas dynamics.[45] This system is therefore ideal for modeling the onset of VR wave breaking in the spiral bands of a rapidly rotating vortex. Unfortunately, this system ceases to be valid as a description of the physical problem as soon as breaking occurs. Dissipation is required to complete the breaking modeling. Technically speaking, as yet mentioned, the problem becomes more complex to handle, integral-averaged inner variable evolutions must be studied. Moreover, those perturbation expansions may not survive to the secular motion. So that asymptotic expansions may be well posed in the presence of this τ_2-evolution, the following restrictive conditions emerge from the various leading-order expressions derived in this section and in Appendix B, but note that more restrictive conditions may occur to higher orders. Passing to dimensional quantities, denoted by an asterisk, the conditions are

$$\overline{V}^*_{z^*},\ \overline{W}^*_{z^*},\ Q^*_z \ll t^{*-1}, \quad \overline{V}^*_{z^*z^*} \ll t^{*-2}, \quad \frac{\overline{V}^*_{t^*}}{\overline{V}^*} \ll t^{*-1}.$$

The slow (Φ,τ_3) modulation must therefore vanish at large time whatever the breaking model we may use. Finally, the breaking outcome is a wave packet + mean flow system evolving more slowly than over the variables Φ and τ_3.

VI. HIGHER-ORDER INNER FLOW

We resolve in this section the fourth and fifth-order inner flows. Their solutions will enable us to complete the study of the system of Sec. V.

A. Fourth order

1. Outside the separatrices

The azimuthal and axial velocities $V^{(4)}$ and $W^{(4)}$ are defined via the functions $\psi^{(4)}$ and $\Psi^{(4)}$ in this way

$$\begin{aligned} V^{(4)} &= \psi^{(4)}_{\mathcal{R}} + \frac{s_i}{2}\zeta(\zeta\varpi^2 - 1)A\mathcal{R}\cos X, \\ W^{(4)} &= \Psi^{(4)} + \frac{s_i}{2}\zeta^2(1+2\varpi^2)A\mathcal{R}\cos X. \end{aligned} \tag{56}$$

These functions are solutions of the azimuthal and axial momentum equations (57) and (58)

$$\begin{aligned} \sin X\psi^{(4)}_{\mathcal{R}\mathcal{R}} + \frac{1}{A}(\mathcal{R}\,\psi^{(4)}_{\mathcal{R}X} - \psi^{(4)}_{X}) &= \frac{s_i}{2}\zeta(1+\varpi^2)\{\mathcal{R}\sin X\,\psi^{(2)}_{\mathcal{R}\mathcal{R}} + [\cos X\,\psi_{\mathcal{R}}{}^{(2)}]_X\} \\ &+ \frac{s_i}{2}\zeta(\zeta\varpi^2 Z^2_{\mathcal{R}} + \hat{\mathfrak{V}}^D_2)\sin X + \lambda'\psi^{(4)}_{i,\mathcal{R}\mathcal{R}\mathcal{R}} + \frac{\Pi_{4,X}}{A}(X), \end{aligned} \tag{57}$$

$$\begin{aligned} \sin X\Psi^{(4)}_{\mathcal{R}} + \frac{1}{A}(\mathcal{R}\,\Psi^{(4)}_{X} - \psi^{(4)}_{X}) &= \frac{s_i}{2}\zeta(1+\varpi^2)\{\mathcal{R}\sin X\,\psi^{(2)}_{\mathcal{R}\mathcal{R}} + [\cos X\psi^{(2)}_{\mathcal{R}}]_X\} \\ &+ \frac{s_i}{2}\zeta(\zeta\varpi^2 Z^2_{\mathcal{R}} + \hat{\mathfrak{V}}^D_2)\sin X + \lambda'\Psi^{(4)}_{i,\mathcal{R}\mathcal{R}} + \frac{\Pi_{4,X}}{A}(X). \end{aligned} \tag{58}$$

The integrations of (57) and (58) give the inviscid parts of the axial vorticity and velocity

$$\psi^{(4)}_{i,\mathcal{R}\mathcal{R}}(Z,x) = \mathcal{F}_4(Z,\Phi,\tau_2,\tau_3) - \frac{s_i}{2}\zeta^2(1+\varpi^2)Z_{\mathcal{R}} < Z^{-1}_{\mathcal{R}} > A\cos x - s_i\zeta^2\varpi^2 A\cos x,$$

and

$$\Psi^{(4)}_i(Z,x) = \psi^{(4)}_{i,\mathcal{R}} + \mathcal{G}_4(Z,\Phi,\tau_2,\tau_3).$$

The secularity condition applied, respectively, to the inviscid components of the eighth-order axial vorticity $\equiv V^{(8)}_{\mathcal{R},i}$ and the velocity $W^{(8)}_i - V^{(8)}_i$ yields again the PDE (29), which gives the trivial solutions $\mathcal{F}_4 = \mathcal{G}_4 = 0$ while matching on the edges of the CL. Finally, the $\mathcal{R}$-integration of $\psi^{(4)}_{i,\mathcal{R}\mathcal{R}}$ gives the inviscid rotational and axial velocities

$$V^{(4)}_i(Z,x) = -\frac{s_i}{2}\zeta^2(1+\varpi^2)A < Z_{\mathcal{R}} > \cos x - \frac{s_i}{2}\zeta(1+\zeta\varpi^2)AZ_{\mathcal{R}}\cos x + V_4(x), \tag{59}$$

$$W^{(4)}_i(Z,x) = -\frac{s_i}{2}\zeta^2(1+\varpi^2)A < Z_{\mathcal{R}} > \cos x + \frac{s_i}{2}\zeta^2 AZ_{\mathcal{R}}\cos x + V_4(x). \tag{60}$$

The radial-momentum equation yields the $\tilde{Z}$-pressure and the $\mathcal{R}$-integration of the mass conservation equation gives the radial $\tilde{Z}$-velocity

$$\begin{aligned} \tilde{\mathcal{P}}^{(4)}_i(Z,x) &= \frac{\zeta}{2}[-\frac{s_i}{2}(\zeta\varpi^2+3)Z_{\mathcal{R}} + \mathcal{S}_1]AZ_{\mathcal{R}}\cos x + V_4(x)Z_{\mathcal{R}} + \Pi_4(x) + \varphi^{(2)}\mathcal{P}^{(1)}_Z + \varphi^{(1)}\varphi^{(2)}\mathcal{P}^{(0)}_{ZZ} \\ &+ \varphi^{(4)}\mathcal{P}^{(0)}_Z + \varphi^{(1)}\{\frac{3}{2}Z_{\mathcal{R}} - \frac{1}{2}s_i(3\mathcal{S}_1 + \mathcal{C}_0\mathcal{C}_1) + [\mathcal{V}_2 + \frac{1}{4}(\mathcal{S}_1^2 - \mathcal{C}_1^2) + V_2(x)]Z^{-1}_{\mathcal{R}} + s_i\mathcal{Q}_{z,1}\}, \\ \tilde{U}^{(4)}_i(Z,x) &= \Upsilon_4(x) - (1+\varpi^2)V_4'(x)Z_{\mathcal{R}} - \frac{s_i}{4}\zeta(3+\varpi^2)AZ^2_{\mathcal{R}}\sin x - \frac{s_i}{2}\zeta(1+\varpi^2)^2 V_2'(x)A\cos x \\ &+ \varphi^{(2)}U^{(1)}_Z - \frac{s_i}{2}\zeta(1+\varpi^2)\Big[\zeta(1+\varpi^2)\Big(K_a[Z/A,x] + \left[\frac{Z}{A}\left(\frac{Z}{A} - \cos x\right)\right]^{\frac{1}{2}} \\ &+ \{\ln[\Lambda(Z,x)] - 1\}\cos x\Big) - (1-\zeta\varpi^2)\cos x\Big]A^2\sin x. \end{aligned}$$

2. Inside the separatrices

The integration of the analogous equation to (57) jointly with the Prandtl-Batchelor theorem (cf. Appendix F) gives the inviscid axial vorticity

$$\psi^{(4,\odot)}_{i,\mathcal{R}\mathcal{R}}(Z,x) = \mathcal{Q}^{(4,\odot)}(\Phi,\tau_2,\tau_3) - s_i\zeta^2\varpi^2 A\cos x. \tag{61}$$

The axial-vorticity matching must be done on the $\tilde{Z}$-deformed separatrix (cf. Appendix E)

$$\tilde{\psi}^{(4)}_{\mathcal{R}\mathcal{R}}(\tilde{Z},x) = \psi^{(4)}_{\mathcal{R}\mathcal{R}}(\tilde{Z},x) + \psi^{(4)}_{\mathcal{R}\mathcal{R}\tilde{Z}}(\tilde{Z},x)\varphi^{(1)}(\tilde{Z},x).$$

It results in $\mathcal{Q}^{(4,\odot)} = 0$. We deduce the inviscid azimuthal and axial velocities

$$\begin{aligned} V^{(4,\odot)}_i &= -\frac{s_i}{2}\zeta(1+\zeta\varpi^2)AZ_{\mathcal{R}}\cos x + V^{\odot}_4(x), \\ W^{(4,\odot)}_i &= \frac{s_i}{2}\zeta^2 AZ_{\mathcal{R}}\cos x + V^{\odot}_4(x) + \mathcal{G}^{\odot}_4(Z,\Phi,\tau_2,\tau_3). \end{aligned} \tag{62}$$

The $\tilde{Z}$-pressure and the radial $\tilde{Z}$-velocity are

$$\tilde{\mathcal{P}}_i^{(4,\odot)}(Z,x) = \psi^{(4,\odot)} + \frac{\zeta}{2}[\frac{s_i}{2}\zeta(\zeta\varpi^2-3)Z_{\mathcal{R}}+\mathcal{S}_1]AZ_{\mathcal{R}}\cos x + \Pi_4^{(\odot)}(x) + \varphi^{(1)}\mathcal{P}_Z^{(2,\odot)} + \varphi^{(2,\odot)}\mathcal{P}_Z^{(1)} + \varphi^{(1)}\varphi^{(2,\odot)}\mathcal{P}_{ZZ}^{(0)} + \varphi^{(4,\odot)}\mathcal{P}_Z^{(0)},$$

$$\tilde{U}_i^{(4,\odot)}(Z,x) = \Upsilon_4^{\odot}(x) - (1+\varpi^2)[V_4^{\odot'}(x)Z_{\mathcal{R}} - \frac{s_i}{2}\zeta(1-\zeta\varpi^2)A^2\sin x\cos x] - \frac{s_i}{4}\zeta(3+\varpi^2)AZ_{\mathcal{R}}^2\sin x + \varphi^{(2,\odot)}U_Z^{(1,\odot)} - \frac{s_i}{2}\zeta(1+\varpi^2)^2V_2^{\odot'}(x)A\cos x + \varpi^2 A\sin x\int_{A\cos x}^{Z}\frac{\mathcal{G}_4^{\odot'}(Z)}{Z_{\mathcal{R}}}dZ.$$

The matching of the deformed normal velocity on the separatrix enables us to determine the jump $[\mathfrak{Z}_1]_-^+$ of the slow radial gradient of the first-order mean axial vorticity. The latter appears in the A-evolution, Equation (52). The details of the matching are explained in Appendix C. The jump $[\zeta_{z,1}]_-^+$ is linked to the jump $[\beta_{l,1}]_-^+$ in Eq. (44); from Equations (45), (B3), and (C2), we then deduce

$$[\mathfrak{Z}_1]_-^+ = [\zeta_{z,1}]_-^+ = \frac{8}{\pi}\zeta^2(3+4\varpi^2)A^{\frac{1}{2}}. \tag{63}$$

The calculation of the jump $[\mathfrak{U}_4]_-^+$ at Subsection VI B will then complete the determination of Equation (52).

B. Fifth-order inner flow

This order involves the handling of several tens of terms only to express the axial vorticity, which results in a hundred of terms for the expression of the azimuthal velocity. So, we will only sketch the solution. The azimuthal velocity is defined through the function $\psi^{(5)}$ in this way

$$V^{(5)} = \frac{s_i}{6}(m^2-3)\mathcal{R}^3 + \frac{1}{2}\mathcal{S}_1\mathcal{R}^2 - s_i\mathcal{V}_2\mathcal{R} + \mathcal{V}_3(\Phi,\tau_2,\tau_3) + \psi_{\mathcal{R}}^{(5)}.$$

After eliminating the secular terms through the mean-flow Equations (46) and (47), the angular and vertical momentum equations become

$$\sin X\psi_{\mathcal{R}\mathcal{R}}^{(5)} + \frac{1}{A}(\mathcal{R}\,\psi_{\mathcal{R}X}^{(5)} - \psi_X^{(5)}) = \frac{s_i}{A}(V^{(2)} + \varpi^2W^{(2)} + s_i\mathcal{S}_1\mathcal{R} - \hat{\mathfrak{V}}_2)\psi_{\mathcal{R}X}^{(2)} + \frac{s_i}{A}\{[U^{(2)} + (s_i\mathcal{S}_1 - \mathcal{R})A\sin X]\psi_{\mathcal{R}\mathcal{R}}^{(2)} - \mathcal{R}\psi_X^{(2)}\} + \frac{\mathcal{U}_3}{A}(\psi_{\mathcal{R}\mathcal{R}}^{(2)} - s_i\mathcal{Q}_{z,1}) + \frac{s_i}{A}\psi_{\mathcal{R}\tau_2}^{(2)} + \lambda'\left(\psi_{\mathcal{R}\mathcal{R}\mathcal{R},i}^{(5)} + s_i\psi_{\mathcal{R}\mathcal{R},i}^{(2)} + s_i(m^2-\zeta')\mathcal{R} - \zeta_{z,1}\right) + \frac{\Pi_{5,X}}{A}(X), \tag{64}$$

$$\sin XW_{\mathcal{R}}^{(5)} + \frac{1}{A}(\mathcal{R}\,W_X^{(5)} - \psi_X^{(5)}) = \frac{s_i}{A}U^{(2)}W_{\mathcal{R}}^{(2)} + \frac{s_i}{A}[V^{(2)} + \varpi^2W^{(2)} + s_i\mathcal{S}_1\mathcal{R} - \hat{\mathfrak{V}}_2]W_X^{(2)} + s_i[\psi_{\mathcal{R}}^{(2)} + (s_i\mathcal{S}_1 - \mathcal{R})\psi_{\mathcal{R}\mathcal{R}}^{(2)} + \frac{1}{2}s_im^2\mathcal{R}^2 - s_i\zeta(s_i\mathcal{S}_1 - \mathcal{R})\mathcal{R}]\sin X + \frac{\mathcal{U}_3}{A}(W_{\mathcal{R}}^{(2)} + s_i\frac{\mathcal{Q}_{\theta,1}}{\varpi}) + \frac{s_i}{A}[\psi_{\mathcal{R}\tau_2}^{(2)} + \mathcal{G}_{2,\tau_2}] + \frac{\mathcal{V}_{1,\Phi}}{A\varpi}\mathcal{R} + \lambda'\left(W_{\mathcal{R}\mathcal{R},i}^{(5)} + s_iW_{\mathcal{R},i}^{(2)} + \frac{\zeta_{\theta,1}}{\varpi} + \frac{\mathcal{Q}_{\theta,1}}{\varpi}\right) + \frac{\Pi_{5,X}}{A}(X) \tag{65}$$

with $\hat{\mathfrak{V}}_2 = \mathfrak{V}_2 + (\mathfrak{V}_{1,\tau_3} + \mathfrak{V}_{2\tau_2})\tau_2$. The inviscid axial vorticity, solution of (64), and the inviscid axial velocity are given by

$$\psi_{i,\mathcal{R}\mathcal{R}}^{(5)}(Z,x) = \mathcal{F}_5(Z,\Phi,\tau_2,\tau_3) - s_i\zeta\varpi^2\psi_{\mathcal{R}}^{(2)} - s_i\int_0^x\frac{\psi_X^{(2)}(Z,x_1)}{Z_{\mathcal{R}}(Z,x_1)}dx_1 - \frac{\mathcal{V}_{1,\Phi}}{\varpi}\Pi[Z,x] + s_i\zeta\langle Z_{\mathcal{R}^{-1}}\rangle\Big[(\zeta\varpi^2Z + \hat{\mathfrak{V}}_2^D)\mathcal{R} - \frac{1}{6}(1+2\varpi^2\zeta)\mathcal{R}^3 - (1+\varpi^2)(\psi^{(2)} - \psi^{(0)}) + s_i(\Upsilon_{2,0} - \mathcal{S}_1)A\cos x\Big], \tag{66}$$

$$W_i^{(5)}(Z,x) = \psi_{\mathcal{R}}^{(5)} + \frac{s_i}{6}[m^2 + \zeta(1+2\zeta\varpi^2)]\mathcal{R}^3 - s_i\zeta(\zeta\varpi^2Z + \hat{\mathfrak{V}}_2^D)\mathcal{R} - \zeta(\Upsilon_{2,0} - \mathcal{S}_1)A\cos x + s_i[1+\zeta(1+\varpi^2)]\psi^{(2)} + \zeta(1+\varpi^2)\mathcal{Q}_{z,1}^sA\cos x + \mathcal{G}_5(Z,\Phi,\tau_2,\tau_3) + \mathcal{W}_3(\Phi,\tau_2,\tau_3). \tag{67}$$

The integration functions $\mathcal{F}_5$ and $\mathcal{G}_5$ are determined through the secularity condition applied to the inviscid ninth-order inner flow: $\langle\psi_{i,\mathcal{R}\mathcal{R}x}^{(9)}\rangle = \langle[W_i^{(9)} - V_i^{(9)}]_x\rangle = 0$. $\mathcal{F}_5$ satisfies a PDE of the following form:

$$\mathcal{F}_5(Z,\tau_2) + \frac{s_i}{\mathcal{U}_3}\mathcal{F}_{5,\tau_2}(Z,\tau_2)\langle Z_{\mathcal{R}}^{-1}\rangle = B(Z,\tau_2). \tag{68}$$

Finally, the integration of the mass conservation equation yields the radial velocity

$$U_i^{(5)}(Z,x) = \Upsilon_5(x) + \mathcal{U}_3'\mathcal{R} - \frac{s_i}{2}A\mathcal{R}^2\sin x - \psi_X^{(5)} - \varpi^2\int^{\mathcal{R}}W_X^{(5)}\,d\mathcal{R} + s_i\int^{\mathcal{R}}\mathcal{R}\psi_{\mathcal{R}X}^{(2)} - U^{(2)}\,d\mathcal{R} + s_i\mathcal{U}_4. \tag{69}$$

The functions $\Pi[Z,x]$ and $\langle Z_{\mathcal{R}}^{-1}\rangle$ in (66) are logarithmically divergent on the separatrix at $Z = A$, singularity that comes from the wave packet assumption. The matching of the axial and azimuthal vorticities on the separatrices can be however carried out by considering the nonlinear boundary $\hat{Z}$-layer (see, for instance, in the case of a planar CL[27]). The matching of the deformed normal velocity on the separatrix enables us to show that the slow second-order mean radial velocity is undistorted, so $[\mathfrak{U}_4]_-^+ = 0$. The details of the matching are explained in Appendix D. The amplitude Equation (52) is thus completely determined. Unfortunately, the fifth-order inner flow matching conditions do not permit to close the system to first-order variables.

VII. NUMERICAL RESOLUTION OF THE TRUNCATED SYSTEM

In this section, we compute the evolutions of the wave packet amplitude A and the first-order mean velocities and vorticities at r_c by numerically integrating the subsystem ((51)–(54)). The latter is solved by the pseudo-spectral method implemented in the software *Mathematica* through the command NDSolve. We eliminate the azimuthal velocity $\mathcal{V}_1$ from the system by choosing the helical solution $\mathcal{V}_1 = \mathcal{W}_1 + Cst$ so that the first-order inertia becomes $\mathcal{S}_1 = 2\mathcal{W}_1 + C_1$; the parameter C_1 is arbitrarily fixed to 0.1. Next, we take closing assumptions: $\{\mathfrak{T}_1'\}_-^+ = \{\Lambda_{2,\Phi}\}_-^+ = \{\mathfrak{V}_{2,\Phi}\}_-^+ = 0$. The computational domain is taken as a 2π-height interval with periodic boundary conditions, the envelope period L_z being much larger than the vertical wavelength, $L_z = \lambda_z\varpi/\epsilon$ with $\lambda_z = 2\pi/k$. The initial time $\tau_2 = \tau_3 = 0$ is associated with the end of the rapid and unsteady WMFI and with the beginning of the quasi-steady stage. As a result, the velocity $\mathcal{W}_1$ is initially positive (outcome of the intensification), and A is positive by definition and must remain positive all along the simulation. For stability reason, the radial vorticity gradient ζ is negative. In order to save computation time, the WMFI induced amounts of slow mean vorticity and velocity as well as the partially absorbed wave packet amplitude, that are used as initial conditions, are chosen so that they may be trivially decomposed in the basis of Fourier modes. We will take, namely, $A(\Phi,0) = [1+\cos(\Phi)/2]^2$, $\mathcal{W}_1(\Phi,0) = S\sqrt{A(\Phi,0)}$, $\{\Lambda_1\}_-^+(\Phi,0) = Y\sqrt{A(\Phi,0)}$, and $\{\mathfrak{T}_1\}_-^+(\Phi,0) = 0.1\sqrt{A(\Phi,0)}$, introducing two amplitude parameters S and Y. We start the simulations from the steady-state scaling: $\mathcal{W}_1 \equiv \{\Lambda_1\}_-^+ \equiv A^{1/2}$. We restrict ourselves to positive phase tilts. Changing ϖ in $-\varpi$ gives a symmetric motion with respect to $\Phi = \pi$, while the breaking time is the same. We limit our study to a moderate phase tilt, we hence basically examine two values $\varpi = 0.1$ and $\varpi = 1$. We have some doubts on the results at large ϖ because as we have mentioned it in C14, the perturbation approach fails when the phase tilt ϖ becomes large as expansions become divergent. This divergence is also likely to occur in this infinite system. We study the case of a weak basic-vorticity radial gradient $\zeta = -0.1$. Increasing $|\zeta|$ leads to the damping of the coupling between $\mathcal{W}_1$, $\{\Lambda_1\}_-^+$, $\{\mathfrak{T}_1\}_-^+$, and A in Equations (51)–(54) with the exception of the coupling between $\{\mathfrak{T}_1\}_-^+$ and A in (54), so breaking takes place later.

Numerical runs show that a breaking always appears for all the values of the parameters we have chosen. This breaking occurs as the profiles of $\mathcal{W}_1$, $\{\Lambda_1\}_-^+$, $\{\mathfrak{T}_1\}_-^+$, and A develop an infinite slope (see Figures 5 and 6). Next, in the presence of a small dissipation, the motion should gradually become steady. But after the discontinuity formation, we here observe, as time proceeds, oscillations that keep on amplifying. The small oscillations that occur when the infinite slope is about to form in Figures 7–10 are due to numerical scattering in the absence (or weakness) of viscosity. We note that a shock-like solution is not particular to a wave breaking in a swirling flow; the induced mean wind that appears in the numerical simulations of a gravity wave packet interacting with a critical layer[46] at the base of a convectively unstable CL is also shock-shaped. The breaking appears all the earlier since the phase

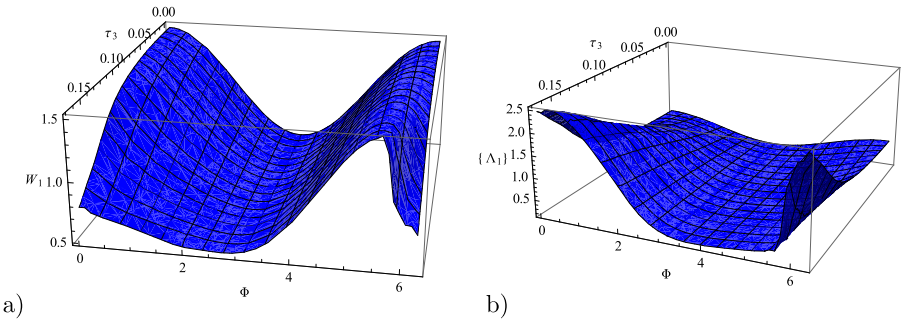

FIG. 5. (a) Velocity $\mathcal{W}_1$ and (b) vorticity $\{\Lambda_1\}_-^+$ as functions of τ_3 and Φ, $\varpi = 1$, $\zeta = -0.1$, $S = 1$, and $Y = 0.5$, breaking at $\tau_3 \simeq 0.18$ and $\Phi \simeq 5.6$.

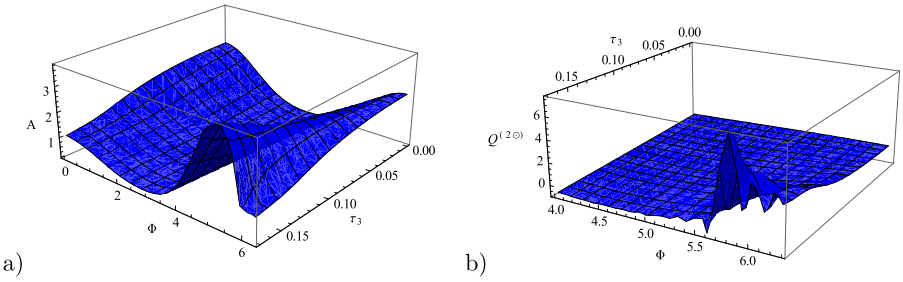

FIG. 6. (a) Amplitude A and (b) axial vorticity inside the cat's eye $\mathcal{Q}^{(2,\odot)}$ as functions of τ_3 and Φ, $\epsilon = 10^{-2}$, $\varpi = 1$, $\zeta = -0.1$, $S = 1$, $Y = 0.5$, breaking at $\tau_3 \simeq 0.18$ $\Phi \simeq 5.6$.

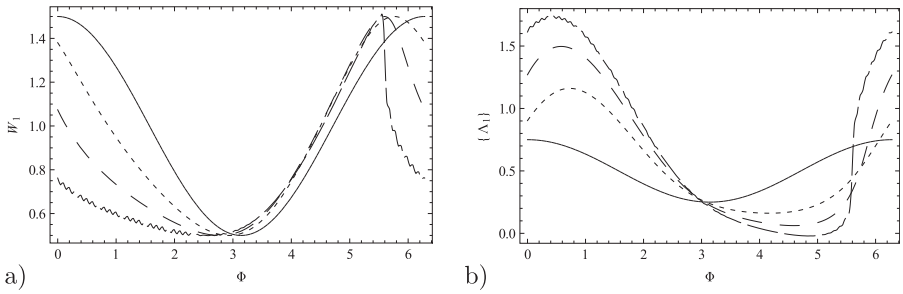

FIG. 7. (a) Velocity $\mathcal{W}_1$ and (b) Vorticity $\{\Lambda_1\}^+_-$ as functions of Φ at various times, $\varpi = 1, S = 1, Y = 0.5$, breaking at $\tau_3 \simeq 0.18$ and $\Phi \simeq 5.6$. The legend is as follows: solid line $\tau_3 = 0$, short-dashed line $\tau_3 = 0.06$, dashed line $\tau_3 = 0.12$, long-dashed line $\tau_3 = 0.17$.

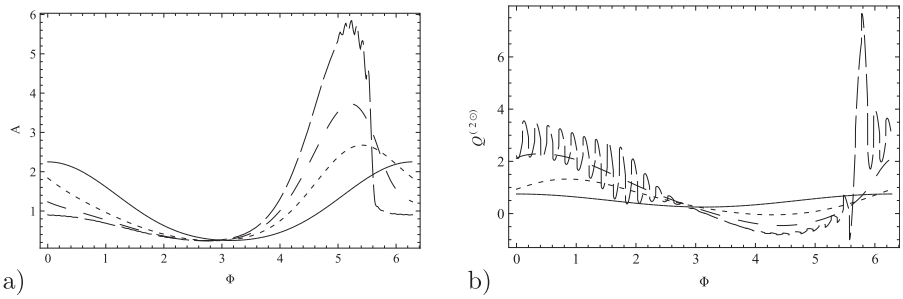

FIG. 8. (a) Amplitude A and (b) axial vorticity inside the cat's eye $\mathcal{Q}^{(2,\odot)}$ as functions of Φ at various times, $\epsilon = 10^{-2}, \varpi = 1, S = 1, Y = 0.5$, breaking at $\tau_3 \simeq 0.18$ and $\Phi \simeq 5.6$. The legend is as follows: solid line $\tau_3 = 0$, short-dashed line $\tau_3 = 0.06$, dashed line $\tau_3 = 0.12$, long-dashed line $\tau_3 = 0.17$.

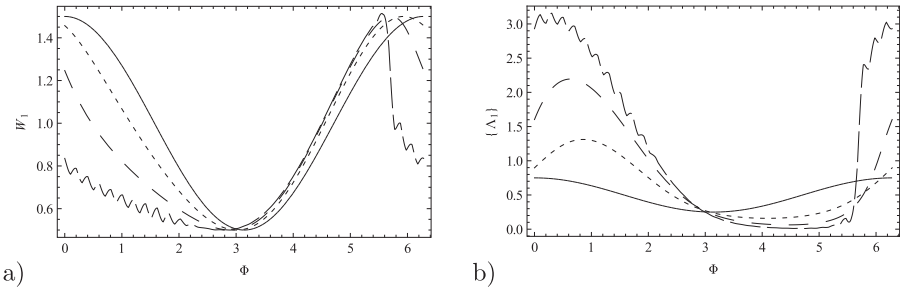

FIG. 9. (a) Velocity $\mathcal{W}_1$ and (b) vorticity $\{\Lambda_1\}^+_-$ as functions of Φ at various times, $\varpi = 0.1, S = 1, Y = 0.5$, breaking at $\tau_3 \simeq 0.014$ and $\Phi \simeq 5.7$. The legend is: solid line $\tau_3 = 0$, short-dashed line $\tau_3 = 0.005$, dashed line $\tau_3 = 0.009$, long-dashed line $\tau_3 = 0.013$.

tilt ϖ is small. A weak ϖ generally corresponds to VR waves that propagate inside thin vortices, like tornadoes or compact hurricanes, i.e., violent vortices. The maximum amplitude of $\mathcal{W}_1$ is not altered by the values of ζ or ϖ, it is a quasi-constant in Figures 7(a) and 9(a). The maximum of $\{\Lambda_1\}^+_-$, as the discontinuity forms, is more than twice larger in Figure 7(b) and four times larger in Fig. 9(b) with respect to the maximum of $\{\Lambda_1\}^+_-$ at $\tau_3 = 0$. The profile of the wave packet amplitude is all the more altered since ϖ is large, and the maximum amplitude is always larger at the discontinuity formation than at the initial time. For instance, at $\varpi = 1$ in Figure 8(a), the maximum is nearly three times larger, but at $\varpi = 0.1$ in Figure 10(a), it is nearly identical at the breaking onset. The amplitude of the oscillations of the axial vorticity inside the cat's eye $Q^{(2,\odot)}$ becomes so large as time proceeds in Figs. 8(b) and 10(b) that this vorticity can become negative in a Φ-range whereas $Q^{(2,\odot)}$ is chosen positive in all the 2π range at $\tau_3 = 0$. The secular motion is particularly high where vertical shear is strong around the discontinuity that appears during the breaking development, as the fast evolution of the axial vorticity inside the cat's eye is shown in Figures 6(b), 8(b), and 10(b). The profile of $Q^{(2,\odot)}$ suddenly peaks at the breaking height.

The Φ-integral average gives us valuable information about the conservation of $\mathcal{W}_1$, $\{\Lambda_1\}^+_-$ and A over time. As a result, we have plotted the relative variations of such an average between the beginning of the simulation up to the breaking onset for the velocity $\mathcal{W}_1$ in Figure 11 and for the amplitude A in Figure 12 as a function of the magnitude Y of the induced slow vorticity $\{\Lambda_1\}^+_-(0, \Phi)$ for $\varpi = 0.1$ and 1, and for a magnitude S of the velocity $\mathcal{W}_1$, $S = 0.5$, 1 and 2. The variations of averaged $\mathcal{W}_1$ weakly depend on S in Fig. 11(a) but depend on ϖ and ζ in Fig. 11(b). The averaged velocity is generally decreasing except in a small zone of negative induced slow vorticity around $Y \lesssim -1$ for $S = 2$. For $Y > 0$, the decay spans the range 15%–30% except in the case where ϖ is small. For $Y < 0$, the decay is weaker, between 0% and 15%

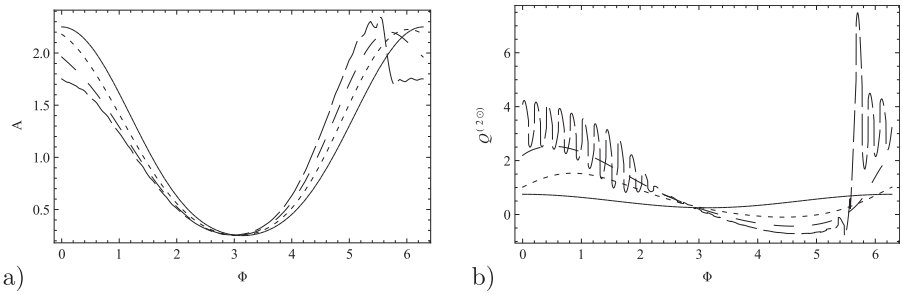

FIG. 10. (a) Amplitude A and (b) axial vorticity inside the cat's eye $\mathcal{Q}^{(2,\odot)}$ as functions of Φ at various times, $\epsilon = 10^{-2}, \varpi = 0.1, S = 1, Y = 0.5$, breaking at $\tau_3 \simeq 0.014$ and $\Phi \simeq 5.7$. The legend is as follows: solid line $\tau_3 = 0$, short-dashed line $\tau_3 = 0.005$, dashed line $\tau_3 = 0.009$, long-dashed line $\tau_3 = 0.013$.

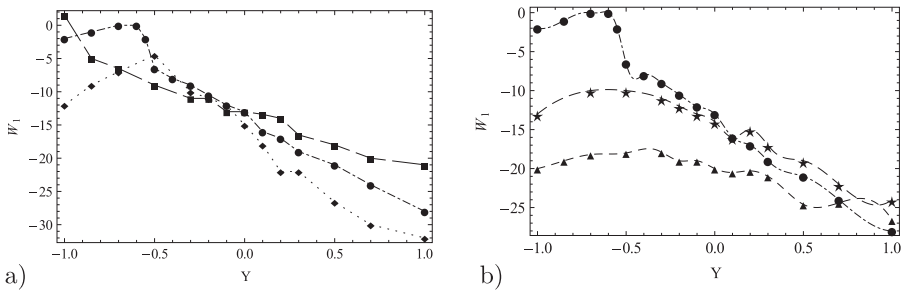

FIG. 11. Variations of the integral averaged $\mathcal{W}_1$ in percent between $\tau_3 = 0$ and the breaking point: (a) $\varpi = 1$, $S = 0.5$, 1, 2 and (b) $S = 1$:$\varpi = 0.1$; $\varpi = 1$ and $\varpi = 1$, $\zeta = -0.2$. The legend is as follows: $\varpi = 1$, $S = 1$ ● — · —; $\varpi = 1$, $S = 0.5$ ♦ . . .; $\varpi = 1$, $S = 2$ ■ — —; $\varpi = 0.1$, $S = 1$ ▲ – – –; $\varpi = 1$, $S = 1$, $\zeta = -0.2$ ★ — —.

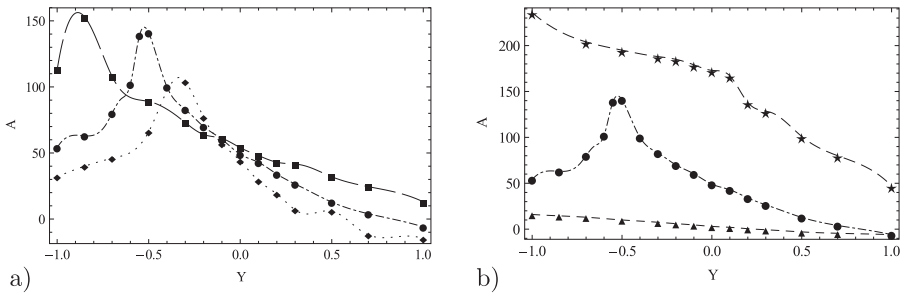

FIG. 12. Variations of the integral averaged A in percents between $\tau_3 = 0$ and the breaking point: (a) $\varpi = 1$, $S = 0.5$, 1, 2, (b) $S = 1$: $\varpi = 0.1$; $\varpi = 1$; and $\varpi = 1$, $\zeta = -0.2$. The legend is as follows: $\varpi = 1$, $S = 1$ ● — · —; $\varpi = 1$, $S = 0.5$ ♦ . . .; $\varpi = 1$, $S = 2$ ■ — —; $\varpi = 0.1$, $S = 1$ ▲ – – –; $\varpi = 1$, $S = 1$, $\zeta = -0.2$ ★ — — ($\zeta = -0.1$ when it is not indicated).

for $\varpi = 1$, but for $\varpi = 0.1$, the decay is around 18%–20%. The averaged velocity gets strongly reduced as the induced slow vorticity $\{\Lambda_1\}^+_-(0,\Phi)$ is large and of the same sign as the basic-vortex vorticity. The averaged amplitude A is generally increasing inside the studied Y-range but is decreasing as $\varpi = 1$, at $S = 0.5$ for $Y \gtrsim 0.5$, at $S = 1$ for $Y \geq 0.8$, and at $S = 2$ for $Y \gg 1$. At $\varpi = 0.1$ and $S = 1$, A is slightly decreasing for $Y \geq 0.25$. At $\zeta = -0.2$, $\varpi = 1$, $S = 1$ in Figure 12(b), A is always increasing for $|Y| \leq 1$, more strongly than in the case $\zeta = -0.1$, $\varpi = 1$, and $S = 1$. The peak of averaged A occurs at a negative induced slow vorticity and is all the higher since ϖ, $|\zeta|$, and S are large. The averaged vorticity $\{\Lambda_1\}^+_-$ is generally increasing according to Figure 13(a) but is decreasing when averaged $\mathcal{W}_1$ is increasing. The variation is all the stronger since S is large and ϖ small. The variables $\mathcal{W}_1$ and $\{\Lambda_1\}^+_-$ are not therefore any longer scaling like $A^{1/2}$ at the breaking point. The kinetic energy spectrum analysis shows a direct cascade whereas the quadratic amplitude spectrum shows a cascade toward both small and large scales.

The breaking time is displayed in Fig. 13(b); it increases with $|\zeta|$ and ϖ but decays with the induced velocity S. In our simulations, it is always small: $\tau_3 < 0.5$. For instance, for $\varpi = 0.1$, $S = 1$, and $Y = 0.5$, we get $\tau_3 \simeq 0.014$; then choosing $\epsilon = 10^{-2}$, $m = 2$, and parameter values corresponding to a compact hurricane[16] $V_{mw} = 62$ m/s, $R_{mw} = 13$ km, $r_c = 2$, $f = 5\times10^{-5}$ s^{-1}, we obtain a dimensional time $t^* \simeq 32$ mn, which is not really a long time when compared to the intensification period of a few hours usually encountered in a hurricane.[47,48] Intensification can last from a few minutes for a violently rotating vortex like a tornado, to a few hours for a mesocyclone or a TC, up to a few days for a TC.[8,16,49,50] For a nearly complete absorption of the wave packet by the WMFI, A tends to 0 at $\tau_3 = 0$, so $S \gg 1$ and $|Y| \gg 1$. As a result, the breaking time should be very short since it decreases with S and $|Y|$. Figures 12 and 13 show that the longest breaking time corresponds to the maximum increase of the averaged amplitude A. For instance, for $\varpi = 1$ and $S = 1$, the maximum breaking time is at $Y = -0.5$ as the packet amplitude has reached a 140% growth, and is equal to $\tau_3 \simeq 0.29$; with the same parameters, we get a dimensional time $t^* \simeq 11$ h, which corresponds to a long time in a VR wave life if we compare with a 2 h common wave period.[47]

From Figure 2 at $\tau_3 = 0$, we can follow up the evolution of the streamline chart inside the $m = 2$ CL characterized by $\epsilon = 7.5\times10^{-3}$, $\varpi = 1$, $r_c = 2$, $S = 1$, and $Y = 1/2$. The evolution of the cat's eye width as a function of the height follows the evolution of $A(\Phi,\tau_3)$. Figure 14 at $\tau_3 = 0.11$, for instance, shows that the CL has swollen around the height $\Phi = 5.4$; both satellites have grown up and the vortex core has shrunk, while Figure 15 shows the height $\Phi = \pi$ at the same time, where the CL has not really changed and is still the thinnest. These charts can give a more accurate prediction of the onset of the wave packet breaking: the time when the streamlines start to tangle up. Here, this time is $\tau_3 = 0.12$ as we can see in Figure 16: the streamlines that are outside and on the edge of the separatrix enter the cat's eyes. This is here a shorter time than that is inaccurately given by the infinite

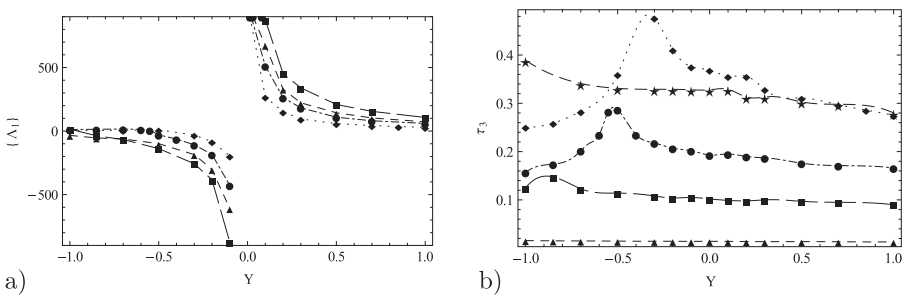

FIG. 13. (a) Variations of the integral averaged $\{\Lambda_1\}^+_-$ in percent between $\tau_3 = 0$ and the breaking point. (b) Breaking time τ_3 as the infinite slope appears. The legend is as follows: $\varpi = 1$, $S = 1$ ● — · —; $\varpi = 1$, $S = 0.5$ ♦ . . .; $\varpi = 1$, $S = 2$ ■ — —; $\varpi = 0.1$, $S = 1$ ▲ – – –; $\varpi = 1$, $S = 1$, $\zeta = -0.2$ ★ — — ($\zeta = -0.1$ when it is not indicated).

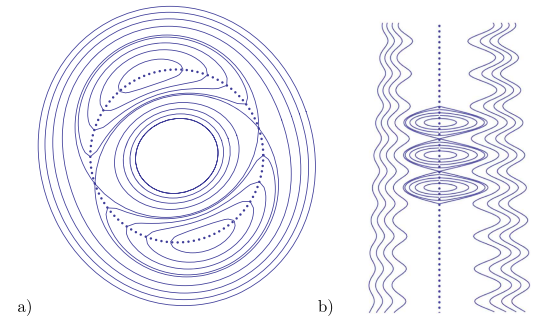

FIG. 14. Wave packet $m = 2$ at $\tau_3 = 0.11$: $\varpi = 1$, $r_c = 2$, $\epsilon = 0.0075$, $\zeta = -0.1$, $\zeta' = 0$, $\mho_0 = 0.1$, $a = -0.5$, $s_i = 1$, $\beta^+_{l,1} = 0$. (a) View at $\Phi = 5.4$ where $A = 2.77$, (b) vertical cross section at $\theta = 0$ between $\Phi = 5.2$ and $\Phi = 5.62$. The dotted line represents the critical radius.

slope of the mean flow and wave packet amplitude ($\tau_3 \simeq 0.18$), but choosing a smaller amplitude ϵ puts off the breaking onset.

Comparing these results with observational data is not easy because in nature, first, vortex intensification can be caused by various physical processes. Second, numerous VR wave packets can coexist and interact. Moreover, wave packets can be continually generated for a long time if they are forced, for instance, by diabatic heating.[34] Third, the lack of continued coverage in time makes difficult to fully follow the intensification process.[8] Fourth, the lack of resolution prevents from detecting VR wave overturning and critical layers. At last, intensification and VR wave breaking processes cannot be always distinguished. Breaking and mixing may occur before intensification has ended.[49] However, observations show that VR wave breaking is often associated with a vortex weakening.[8,47,49] Numerical simulations show the same tendency.[34] In the case of a forced internal wave[31] or Rossby wave[32] packet, breaking occurs at large time as WMFI is decaying; mean-flow weakenings are observed among long-extent wave packets and are due to over-reflections. Numerical-code resolution can be however weaker than radar resolution;[8] the nonlinear CL is usually not resolved properly by the numerical scheme[5,13] within an appropriate subgrid that would consume less memory. Let us take the example of the numerical simulation of an idealized TC at a latitude 20 N by the mesoscale model MM5[13] where the radial resolution is $\delta r^* = 2.36$ km. (The

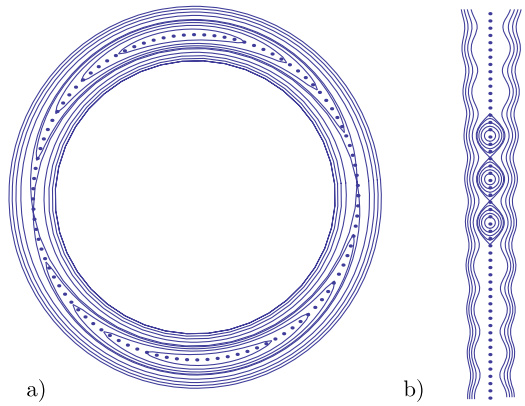

FIG. 15. Wave packet $m = 2$ at $\tau_3 = 0.11$: $\varpi = 1$, $r_c = 2$, $\epsilon = 0.0075$, $\zeta = -0.1$, $\zeta' = 0$, $\mho_0 = 0.1$, $a = -0.5$, $s_i = 1$, $\beta^+_{l,1} = 0$. (a) View at $\Phi = \pi$ where $A = 0.266$, (b) vertical cross section at $\theta = 0$ between $\Phi = \pi - 0.21$ and $\Phi = \pi + 0.21$. The dotted line represents the critical radius.

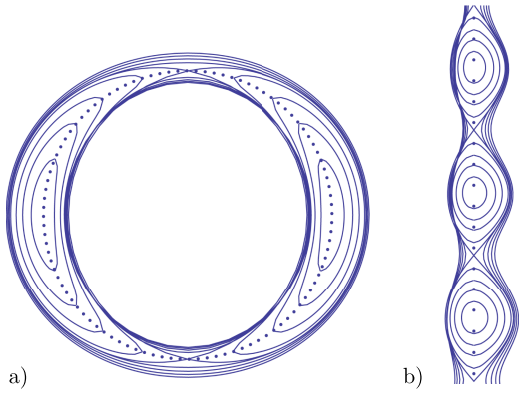

FIG. 16. Wave packet $m = 2$ at $\tau_3 = 0.12$: $\varpi = 1$, $r_c = 2$, $\epsilon = 0.0075$, $\zeta = -0.1$, $\zeta' = 0$, $\mho_0 = 0.1$, $a = -0.5$, $s_i = 1$. (a) View at $\Phi = 6.1$ where $A = 1.84$, (b) vertical cross section between $\Phi = 6.03$ and $\Phi = 6.17$. The dotted line represents the critical radius.

asterisk $*$ means a dimensional quantity.) The critical radius is located at $r_c^* \simeq 60$ km for a height $h = 1$ km and from time $t^* = 112$ h up to 124 h. The mean tangential velocity at this radius is $\overline{V}_0^*(r_c) \simeq 24$ m/s, the overall Reynolds number is $Re \simeq 8 \times 10^{10}$ for an air kinematic viscosity $\nu = 17 \times 10^{-6}$ m^2/s. The mean eddy kinetic energy is less than 2 m^2/s^2 (1 m^2/s^2) for $m = 2$ ($m = 3$). The wave packet dimensionless amplitude is then $\epsilon A < 0.016$ for $m = 2$, and $\epsilon A < 0.0076$ for $m = 3$. The unstratified and zero-vorticity CL cat's eye thickness $4 r_c^* \sqrt{\epsilon A}$ is less than 30 km for $m = 2$ and 21 km for $m = 3$. For a density-stratified TC and for a non zero vorticity $Q_{z,0}(r_c)$, the thickness should be even smaller.[15] The CL modeling is thus given by less than ten points. Let us take another example, a 2D TC model at the same latitude[51] where the radial resolution is $\delta r^* = 2.5$ km. The critical radius is $r_c^* \simeq 90$ km. The mean rotation velocity is $\overline{V}_0^*(r_c) \simeq 37.9$ m/s, and $Re \simeq 15 \times 10^{10}$. The $m = 2$ PV perturbation has an amplitude of order 10^{-11} s/m^2 at r_c and at $t^* = 20$ h and scales like $\mathrm{PV}' = O(\epsilon A/(\varrho^*_{0,c} r_c^{*2}))$. It results an amplitude $\epsilon A \simeq 7.2 \times 10^{-5}$ and a cat's eye width $\simeq 3.1$ km nearly equal to the resolution. Accurate numerical simulations require a better resolution. Indeed, the intense atmospheric vortex CL is the location of steep gradients and very large Reynolds numbers. In the modeling of a Kelvin-Helmholtz instability generating a cat's eye flow in a stably stratified medium and at lower Reynolds numbers, for instance,[52] the cat's eye thickness was of the same order as the most unstable wavelength L_x and the vertical resolution was $\delta_z = L_x/1536$ at $Re = 2600$.

Though the WMFI is only slowly evolving in the asymptotic quasi-steady régime, it can result in an important mean-flow change. This secondary motion opposes the primary caused by the intensification stage. The latter is characterized by a momentum exchange between the wave packet and the vortex, i.e., an increase of the mean velocities $\mathcal{V}_1$ and $\mathcal{W}_1$ and a partial wave packet absorption inside the CL (a decrease of A), accompanied by a vortex erosion with $Q_{z,0}(r_c)$ decreasing up to zero. In most of runs, the CL induced mean angular momentum is decreasing in the quasi-steady stage whereas the wave packet amplitude and the induced slow mean vorticities are increasing. In C14, we had also obtained such a mean-flow evolution but over the slower viscous time scale $\tau \equiv \lambda\, \epsilon\, t$. The changes in the asymptotic steady stage resulted negligible.[16] In the case

of vortex/unstable VR wave interaction, the mean rotational flow decrease in the eyewall after intensification is caused by the transfer of mean vorticity and angular momentum from the eyewall to the wave packet, then from the wave packet to the eye through unstable VR wave propagation and breaking.[34] Here, the numerical integration of the present system yields a local angular-momentum transfer from the CL induced mean flow to the wave packet and a slow-vorticity transfer from the packet to the mean flow, while the resonant-wave packet growth is restricted to the CL neighborhood. In the numerical simulations[6,7] of a wave packet/3D vortex interaction, a secondary circulation characterized by an intensification-induced mean radial flow can be observed that always acts to oppose the basic-vortex primary changes and tends to resist the spin-up. The quasi-steady stage assumption of our study involves the presence of a small secondary circulation provided by the $O(\epsilon^{3/2})$ mean radial velocity and does enhance the WMFI attempt to damp its own changes compared to the steady stage study.

The numerical solution obtained here shows a mean-flow decay and a second wave-packet breaking, since the first breaking during the unsteady WMFI is assumed saturated by the nonlinear CL. As the quasi-steady stage generated a fast secular motion, the second breaking must proceed until the latter be eliminated, which implies a vertical homogenization around r_c at the end of the breaking and subsequently the disappearance of the small mean radial circulation. In summary, if a neutral VR wave packet propagates within a vortex and encounters a CL, if it resists to the strong WMFI of the unsteady stage and conserves its modulation, then the weak vertical shear of the CL induced mean-flow leads the wave packet to break. This shear vanishes during the breaking and the wave packet turns into either a damped and plain wave or vanishes as well. The angular-momentum gain for the basic vortex during the unsteady stage is anyway substantially damped by the quasi-steady stage. Note that a vertical shear negatively impacts TC intensification;[8,47,53] vertical advection of momentum indeed acts to decrease intensification.[54] Including the viscous flow would permit to proceed the breaking up to its end. If small viscosity is insufficient to damp all vertical shear then turbulence should emerge but the Prandtl-Batchelor theorem would not be then valid.

We now compare the above wave packet evolution with these given by a nonlinear Schrödinger (NLS) or a Ginzburg-Landau equation. The NLS equation describes the evolution of wave envelopes, characterized by a competition between a weak linear dispersion that tends to break up the wave packet and a focusing effect of the cubic nonlinearity, provided by the interaction of the wave packet with itself. The inverse scattering transform theory shows that, for an initial finite-extent disturbance, the solution is obtained from a discrete set of eigenvalues, each of them corresponding to a soliton, and from a continuous spectrum, corresponding to an oscillatory dispersive wave. The oscillatory part of the solution is found to decay with time and the solitons thus dominate the asymptotic large-time solution.[55] The NLS equation hence yields a long-time solution that is a localized and saturated wave packet, a balance solution between both effects mentioned above. It has an exact solution that is an unchanged-in-shape solitary wave propagating with a constant velocity.[45] The NLS equation therefore appears as a crude model to represent the coherent structures generated by VR wave breaking that are the inner spiral rainbands.[4] The Ginzburg-Landau equation has unsteady solutions that take the form of fronts or kinks. It can be the outcome of a weakly nonlinear viscous critical layer that forms in a weakly supercritical flow where the induced mean flow has been omitted. If supercriticality is small enough, the envelope motion can be described by a cubic or quintic-cubic Ginzburg-Landau equation.[19]

VIII. DIFFUSION BOUNDARY LAYERS

The vorticity diffusion from the nonlinear CL by a very small viscosity creates at either side of the CL two diffusion boundary layers. These layers are entrained by the differential rotation of the wind and take the form of spiral bands. The vorticity filaments visible during VR wave breaking are located in the DBLs where effective flow diffusivity is high.[11] The spiral rainbands observed in TCs or tornadoes are also embedded in DBLs. The system CL + DBLs evolves with time in a complex way, in a decelerated process in the transition stage.[29] Here, we will use a quasi-steady theory of the diffusion boundary layer developed by Troitskaya and Reznik (1996)[29] for internal waves and applied to Rossby solitary waves[26] to describe the DBL dynamics in the quasi-steady stage. The present difficulty lies in the multiple time scales.

In the quasi-steady régime, the DBLs are mainly expanding through the viscous-diffusion process: $Q_{z,\tau_1} \equiv \lambda Q_{z,\mathcal{R}\mathcal{R}}$ over the time scale τ_1. A long time after the nonlinear CL formation such as $\tau_1 \gg 1$, one assumes that the DBL extents L_{DBL} are very large: $L_{DBL} \equiv \sqrt{\lambda\tau_1} \gg 1$. To describe the motion inside the DBLs, we use two new independent variables: a time variable ν that is in fact the diffusive wavenumber $\nu \equiv (\lambda\tau_1)^{-1/2}$, and a cross-stream variable $H = \nu\mathcal{R}$ that is $O(1)$ in the DBLs. At the DBL scale, the CL is seen as a thin helix. The outer and inner CL edges are then, respectively, considered to be the limits $H \to 0^{\pm}$. The critical radius is also assumed slowly moving in this way

$$r_c = r_0 + s_i r_0 \frac{\epsilon^{\frac{1}{2}}}{\nu}\kappa(\epsilon, \nu, \Phi, \tau_2, \tau_3), \tag{70}$$

where r_c tending to the constant value r_0 as $\lambda\tau_1 \to 0$. The departure from r_0 is given by the unknown function κ, which tends to a constant in the limit $\epsilon^{\frac{1}{2}}/\nu \to 0$. As one considers a slow motion of the critical radius, we use r_0 as a reference critical radius, for example,

$$\mathcal{Q}_{z,1} = Q_{z,1}(r_c)/\varrho_0(r_0), \quad \zeta_{z,1} = r_0 Q'_{z,1}(r_c)/\varrho_0(r_0),$$
$$\nu = 1/2\left(\lambda^*\tau_1\right)^{-\frac{1}{2}}, \quad \lambda^* = \lambda/(m\, r_0^2\, \sigma(r_0)).$$

A. Axial vorticity in the DBLs

The induced $O(\epsilon^{1/2})$ mean axial vorticity satisfies this rescaled equation inside the DBLs

$$4Q^{(2)}_{DB,z,\tau_2}\tau_2 - Q^{(2)}_{DB,z,HH} - 2\nu Q^{(2)}_{DB,z,\nu} - 2(H + \kappa - \nu\frac{d\kappa}{d\nu})\, Q^{(2)}_{DB,z,H} \equiv \tau_2\, \frac{\epsilon}{r^2}\partial_r[r^2\mathcal{F}_q], \tag{71}$$

where the r.h.s. term is the divergence of the mean axial vorticity flux $\mathcal{F}_q$. Outside the CL, this flux is considered as decaying as $1/r^2$, so this term is zero in the DBLs. Equation (71) is solved perturbatively and the mean vorticity and κ being expanded following $\epsilon^{\frac{1}{2}}/\nu$

$$Q^{(2)}_{DB,z}(H,\nu) = \sum_{k=0}\left(\frac{\epsilon^{\frac{1}{2}}}{\nu}\right)^k Q^{(2)}_{z,k}(H), \qquad \kappa = \sum_{k=0}\left(\frac{\epsilon^{\frac{1}{2}}}{\nu}\right)^k \kappa_k\,. \tag{72}$$

This expansion is valid provided $\epsilon^{1/2}/\nu \ll 1$ or $\lambda\tau_3 \ll 1 \ll \lambda\tau_1$. Each $Q^{(2)}_{z,k}$ then satisfies Eq. (73) that is solved in Appendix G to the first order in $\epsilon^{1/2}/\nu$:

$$Q^{(2)}_{z,k,HH} - 2kQ^{(2)}_{z,k} + 2HQ^{(2)}_{z,k,H} + 2\sum_{j=0}^{k}(1+j)k_jQ^{(2)}_{z,k,-j,H} = 4Q^{(2)}_{z,k,\tau_2}\tau_2. \tag{73}$$

The boundary conditions at infinity are $Q_{DB,z}(H,\nu) \to Q_0(r)$, $H \to \infty$, whereas on the CL edges

$$Q_{DB,z}(H,\nu) \to Q_z(r) = Q_0(r) + \epsilon^{\frac{1}{2}}\,Q_{z,1}(r) + \epsilon\,Q_{z,2}(r) + \ldots, \quad H \to 0.$$

The boundary conditions on the CL edges are derived by using the induced mean-flow expansions around r_c of Section II expressed via the DBL inner variable H, so when $H \to 0$

$$Q^{(2)}_{DB,z,H} \to s_i\frac{\epsilon^{\frac{1}{2}}}{\nu}\zeta_{z,1} + O(\frac{\epsilon}{\nu^2}) \qquad Q^{(2)}_{DB,z} \to \mathcal{Q}_{z,1} + \frac{\epsilon^{\frac{1}{2}}}{\nu}[\sum_{j=0}^{\infty}\mu_{1j}\,\tau_2^j + s_i\zeta_{z,1}H] + O(\frac{\epsilon}{\nu^2})\,,$$

and

$$V^{(2)}_{DB} \to \sum_{j=0}^{\infty}\frac{v_{0j}}{\nu}\,\tau_2^j + \mathcal{Q}_{z,1}\frac{H}{\nu} + \frac{\epsilon^{\frac{1}{2}}}{\nu^2}\Big(\sum_{j=0}^{\infty}[v_{1j}+\mu_{1j}H]\,\tau_2^j + \frac{1}{2}s_i\zeta_{z,1}H^2\Big) + O(\frac{\epsilon}{\nu^3})\,. \tag{74}$$

We will justify the presence of the additional velocities v_{0j} and v_{1j} and vorticities μ_{1j} later on. The induced mean flow has a simple power law τ_2-dependency as we have noticed in Section VI. This dependency is conserved inside the DBLs at $H = O(1)$. Through nonlinear coupling, the DBL mean motion is described by integer series in τ_2,

As a result, it is necessary to expand $\kappa_i, i = 0, 1\ldots$ in this way

$$\kappa_i = \sum_{j=0}\kappa_{ij}\,\tau_2^j. \tag{75}$$

The expansion of the mean rotational flow $\overline{V}$ around r_c is therefore more complex than this displayed in Eq. (7b),

$$\overline{V} = \overline{V}_0 + \epsilon^{1/2}\overline{V}_1 + \frac{\epsilon}{\nu}\Big[s_i\sum_{j=0}^{\infty}v_{0j}\,\tau_2^j + \sum_{j=0}^{\infty}\mu_{1j}\,\tau_2^j(r-r_c) + s_i\frac{\epsilon^{\frac{1}{2}}}{\nu}\sum_{j=0}^{\infty}v_{1j}\,\tau_2^j + \ldots\Big] + \epsilon\overline{V}_2 + \ldots.$$

In addition to the classic CL expansion following $\epsilon^{1/2}$, we observe a second expansion in $\epsilon^{1/2}/\nu$ showing the mixing around $H = 0$ between the mean flows generated by both the DBLs and the CL. The critical radius is finally moving in the following way at the leading order:

$$r_c = r_0 + 2s_ir_0\sqrt{\lambda^*\tau_3}\,[\kappa_{00}(\Phi,\tau_3) + \tau_2\,\kappa_{01}(\Phi,\tau_3) + \cdots].$$

As $\lambda^*\tau_3 \ll 1$, the zeroth-order term induces a motion slower than τ_3, whereas the first-order term induces a motion slower than τ_2 but faster than τ_3. This displacement is described by a τ_2-integer series. The DBL motion therefore evolves in a more complex way than the CL flow since it is necessary to use infinite series in τ_2 to mathematically describe it. The question of the series convergence cannot be unfortunately issued. The explicit solution of the DBL mean flow in Appendix G shows that the leading-order motion is a 3D helical spiral, but this coherent structure rapidly collapses when the higher-order τ_2-terms get large. We also notice the strong coupling that exists between both CL and DBL motions and that affects the system of Section V. The expelling of the quasi-steady stage induced secondary vorticity into the spiral DBLs during the wave packet breaking and could explain the formation of an inner spiral rainband transporting a local vorticity maximum. The rainbands conserving the dispersive properties of the VR waves indicates that the breaking wave packet does not collapse but saturates.

IX. CONCLUSIONS

The extension of the theory of the stationary nonlinear critical layer to a quasi-steady state has permitted to study a vortex Rossby wave packet a long time after the beginning of its interaction with a linearly stable, columnar, dry, and rapidly rotating vortex. The wave packet is a 3D weakly singular, helical, and amplitude-modulated mode slowly evolving in height and time and slowly interacting with the vortex. The resulting helical CL motion is however complex, evolving with the same modulation but also over a faster and secular time. As soon as the CL forms, it induces a mean flow of higher amplitude than the wave packet that has generated it and whose evolution is strongly coupled with the wave dynamics. The matching conditions of the CL flow on the separatrices show that the induced mean flow is modulated in the same way as the wave packet. However, the interplay of this 3D mean flow, and in particular the formation of a small secondary mean radial circulation,

leads to a time $\tau_2 \equiv \epsilon t$ driven secular motion that may make asymptotic expansions divergent.

The matched asymptotic method has been carried out up to the third nontrivial order of the inner expansion, which allowed us to relate the second-order mean-flow distortions with the nonlinear mode phase jump. Until now, this phase jump was considered zero in the inviscid nonlinear continuous mode assumption. This jump is associated with discontinuities in the axial and azimuthal modal velocities across the critical radius and evolves over τ_2 and with the modulation. The streamlines within the wave packet CL are more distorted than within a steady CL, since in addition to a stressed cross-stream variable to describe the deformed streamlines,[15] an inner nonlinear boundary layer with its own scaling must be inserted along the separatrices in order to avoid a singularity there. It results in stronger mean radial eddy fluxes of axial and angular momenta in the quasi-steady stage compared to the steady case, and subsequently a larger WMFI, but the outcome is a local deceleration of the vortex in this stage.

The wave packet amplitude equation is derived from the leading-order CL induced mean axial vorticity distortion equation. Its evolution is driven by the jump of the radial gradient of the leading-order induced mean axial vorticity at r_c, jump that can be deduced from the study of the low-order inner flow.

The CL induced mean flow at r_c however obeys an infinite system. The mean radial velocity $\mathcal{U}_3$ couples all successive radial derivatives of a mean quantity and leads to a kinetic energy cascade toward small scales. As a result, all radial scales are concerned including the small viscous scale. The viscous phase-averaged outer equations are, however, singular as soon as the first order at r_c while the inviscid phase-averaged outer equations become singular to higher orders. The CL dynamics coupled with the surrounding mean flow is thus a very complex problem.

The numerical resolution of the leading-order equations of the system shows that the wave packet always breaks at a certain height of the vortex (cf. Figs. 5 and 6). This breaking is accompanied by a substantial tendency of the mean flow to oppose the basic-vortex intensification. The mean flow generally loses angular and vertical momenta, while it gains azimuthal and axial vorticities (cf. Figs. 11 and 13(a)). The wave packet amplitude that has decreased during the intensification stage increases again and its change can be strong (cf. Fig. 12). The secular motion acquires a large amplitude during the breaking development, which imposes a vertically homogenized CL flow as well as the end of the τ_2 and $\tau_3 \equiv \epsilon^{3/2} t$ evolutions as breaking ceases. The breaking process cannot be wholly simulated since viscous diffusion and probably eddy-viscous diffusion should be taken into account in order to eliminate the secular motion. As a result, we cannot evaluate the remaining amounts of the induced mean flow and wave packet amplitude when the motion has lost its dependency on the slow variables (Φ, τ_2, τ_3). We can only expect diffusion to damp the wave packet amplitude as well as the CL induced mean velocities and vorticities.

The diffusion boundary layers and the critical radius slowly evolve in height and in time in the quasi-steady régime in a more complex way than the CL flow since τ_2-integer series are involved in their description. The presence of the DBLs alters the infinite system to higher orders as DBL and CL dynamics are coupled. The DBLs initially evolve like helical spirals that are disrupted by the breaking. The CL theory could then explain the formation of inner spiral rainbands by the expelling into the spiral DBLs of the CL induced secondary vorticity as the breaking wave packet has saturated in a monochromatic wave.

For simplicity sake, we have omitted the axial group velocity of the wave packet. A group velocity resonance appears in our system at a certain height and at a certain time, as the mean velocity $\overline{W}_1(r_c, \Phi, \tau_3)$ is equal to the propagation velocity of the wave packet. It would be interesting to see what effect this singularity has on the WMFI.

Finally, this study has shown that if an asymptotic quasi-steady regime exists following the strong nonlinear CL interaction between the vortex and the shear wave packet, provided the wave packet survives to this interaction, i.e., if a packet of weakly singular and damped modes described by a modulated amplitude is remaining, then the coupling of the wave packet and the induced mean flow through the nonlinear CL would rapidly lead to the breaking of the wave packet and the loss of its modulation. A next WMFI step would assume a larger vertical-extent of the wave packet, which would imply the formation of a smaller radial circulation and subsequently a slower secular motion and another breaking, since the leading-order evolution equation system would be identical. The final stage would be then characterized by a steady VR wave as described in C14. This study therefore makes unlikely the presence of a quasi-steady state described by the nonlinear Schrödinger equation.[33] A future work will consist of examining a smaller-extent wave packet that would more strongly CL-interact with a rapidly rotating vortex and whose evolution equation would probably be dispersive.

At last, the author hopes that this study has highlighted the importance of the critical layer in the wave/mean flow interaction process and that further efforts will be made to model it properly in numerical schemes.

ACKNOWLEDGMENTS

The author is grateful to four anonymous reviewers for many helpful comments that greatly improved the quality and presentation of the paper. This research was supported by the Chilean funding organisation, National Fund for Scientific and Technological Development, as the project Fondecyt No. 1150600.

APPENDIX A: THE OUTER FLOW

This subsection gives the coefficients of the Frobenius series outer-flow solutions valid around the radius r_c.

1. Order $\epsilon^{\frac{3}{2}}$

The first coefficients of the Frobenius series (15) related to the inviscid radial flow $U_r^{(1)}$ are

$$c_{l,1,0} = J_{1c} = \varpi^2 \mathcal{Q}_{z,1} + \varpi \mathcal{Q}_{\theta,1} - (1+2\varpi^2)\zeta \hat{\mho}_1^D,$$
$$d_{l,1,0} = \mathcal{S}_1 - \frac{\zeta_{z,1}}{\zeta} - \frac{1+3\varpi^2}{1+\varpi^2}\mathcal{Q}_{z,1} - \frac{2+a}{\zeta(1+\varpi^2)}J_{1,c} + \frac{2\varpi^3}{1+\varpi^2}\mathcal{Q}_{\theta,1}. \quad \text{(A1)}$$

Owing to the inner-flow study, $\hat{\mho}_1^D = 0$, and $J_{1,c} = 0$.

2. Order ϵ^2

The inviscid radial flows $U_{r,l}^{(2)}$ and $U_{r,n}^{(2)}$ satisfy the following modal equations:

$$\mathcal{L}_0(U_{r,l}^{(2)}) = -\mathcal{L}_1(U_r^{(1)}) - \mathcal{L}_2(U_{r,i}^{(0)}), \quad \text{(A2)}$$

$$\mathcal{L}_0(U_{r,n}^{(2)}) = -\omega_0^{D\,-1}(r)\partial_\xi\left[NHr(U_i^{(0)})\right] + \frac{m}{\omega_0^D(r)}D\left[\frac{S(r)}{r}NH\theta(U_i^{(0)})\right] + \frac{k}{\omega_0^D(r)}D\left[S(r)NHz(U_i^{(0)})\right] - mS(r)\frac{k\varrho_0(r)}{r\omega_0^{D\,2}(r)}\left[NHz(U_i^{(0)}) - \frac{kr}{m}NH\theta(U_i^{(0)})\right] \quad \text{(A3)}$$

with

$$\mathcal{L}_2(U) = \left(\frac{\omega_2^D(r)}{\omega_0^D(r)} - \frac{\omega_1^{D\,2}(r)}{\omega_0^{D\,2}(r)}\right)\{D[S(r)D^*U] + \partial_\xi^2 U\} - \frac{m\omega_1^D(r)}{\omega_0^{D\,2}(r)r^2}\left[[rD-2]\{S(r)[\mathcal{Q}_{z,1}(r) - \frac{kr}{m}\mathcal{Q}_{\theta,1}(r)]\}\right]U$$
$$+ k\frac{mS(r)\varrho_0(r)}{r\omega_0^{D\,2}(r)}\left(\frac{\varrho_1(r)}{\varrho_0(r)} - 2\frac{\omega_1^D(r)}{\omega_0^D(r)}\right)\left[\frac{kr}{m}\mathcal{Q}_{z,1}(r) + \mathcal{Q}_{\theta,1}(r)\right]U + \frac{m}{\omega_0^D(r)r^2}\left[[rD-2]\{S(r)[\mathcal{Q}_{z,2}(r) - \frac{kr}{m}\mathcal{Q}_{\theta,2}(r)]\}\right]U$$
$$+ k\varrho_0(r)\frac{mS(r)}{r\omega_0^{D\,2}(r)}\left[\frac{kr}{m}\mathcal{Q}_{z,2}(r) + \mathcal{Q}_{\theta,2}(r)\right]U + k^2\frac{\varrho_0(r)S(r)}{\omega_0^{D\,2}(r)}\mathcal{Q}_{z,0}(r)\left(\frac{\varrho_2(r)}{\varrho_0(r)} - 2\frac{\varrho_1(r)}{\varrho_0(r)}\frac{\omega_1^D(r)}{\omega_0^D(r)} + 2\frac{\omega_1^{D\,2}(r)}{\omega_0^{D\,2}(r)} - \frac{\omega_2^D(r)}{\omega_0^D(r)}\right)U$$

and with

$$NHr\left(U_i^{(0)}\right) = \mathcal{N}_i^{(0)}\left(U_{r,i}^{(0)}\right) - \frac{U_{\theta,i}^{(0)2}}{r}, \qquad NH\theta(U_i^{(0)}) = \mathcal{N}_i^{(0)}(U_{\theta,i}^{(0)}) + \frac{U_{\theta,i}^{(0)}}{r}U_{r,i}^{(0)},$$
$$NHz\left(U_i^{(0)}\right) = \mathcal{N}_i^{(0)}\left(U_{z,i}^{(0)}\right),$$

and

$$\mathcal{N}_i^{(0)}(U) = U_r^{(0)}D[U] + \left(\frac{m}{r}U_\theta^{(0)} + kU_\theta^{(0)}\right)\partial_\xi U.$$

The Frobenius series related to the inviscid radial velocity is written as

$$\phi_l^{(2)}(\eta) = \left(\sum_{n=0}^{\infty}\left[a_{l,2,n}\ln^3|\eta^*| + b_{l,2,n}\ln^2|\eta^*| + c_{l,2,n}\ln|\eta^*| + d_{l,2,n}\right]\eta^n + \alpha_{l,2}\phi_a + \beta_{l,2}\phi_b\right),$$
$$\phi_n^{(2)}(\eta) = \left(\sum_{n=0}^{\infty}\left[b_{n,2,n}\ln^2|\eta^*| + c_{n,2,n}\ln|\eta^*| + \frac{d_{n,2,n}}{\eta}\right]\eta^n + \alpha_{n,2}\phi_a + \beta_{n,2}\phi_b\right).$$

The first coefficients of the inviscid radial velocity expansion are

$$c_{d,2,0} = 0, \quad c_{l,2,0} = \varpi(\varpi\mathcal{Q}_{z,2} + \mathcal{Q}_{\theta,2}) - \zeta(1+2\varpi^2)\left[\mho_2^D + (\mho_{1,\tau_3} + \mho_{2,\tau_2})\tau_2\right],$$
$$c_{n,2,0} = -\frac{b_0 S_c^2 m^3}{2r_c^4\varrho_{0,c}}\{(6+5\varpi^2)(1+\varpi^2) + 4a(1+\varpi^2)^2 + b_0 r_c[4+5\varpi^2(2+\varpi^2)]\} - \frac{\varpi^2\zeta'}{2mr_c\varrho_{0,c}}.$$

APPENDIX B: $O(\epsilon^2)$ MEAN FLOW EQUATIONS

We here derive the inviscid $O(\epsilon^2)$ evolution equations of the leading-order mean vorticities, and the radial gradients of mean vorticities at the critical radius.

By r-derivating the inviscid azimuthal and axial momentum Equations (5b) and (5c), we find the mean-vorticity evolution equations at r_c. By using Eq. (5d), we can eliminate $\mathcal{U}_3'$ and we get finally

$$\mathcal{Q}_{z,1,\tau_3} + \mathcal{Q}_{z,2,\tau_2} + \varpi\mathcal{W}_1\mathcal{Q}_{z,1,\Phi} = \mathcal{Q}_{\theta,1}\mathcal{V}_{1,\Phi} + \varpi\mathcal{Q}_{z,1}\mathcal{W}_{1,\Phi} - \zeta_{z,1}\mathcal{U}_3 - \zeta\mathcal{U}_4, \quad \text{(B1)}$$

$$\mathcal{Q}_{\theta,1,\tau_3} + \mathcal{Q}_{\theta,2,\tau_2} + \varpi\mathcal{W}_1\mathcal{Q}_{\theta,1,\Phi} = (\mathcal{Q}_{\theta,1} - \zeta_{\theta,1})\mathcal{U}_3 + \mathcal{V}_{2,\Phi} + \mathcal{S}_1\mathcal{V}_{1,\Phi}. \quad \text{(B2)}$$

These vorticities are generated in part by the divergence of their radial flux, which is made possible by the presence of the small radial velocities $\mathcal{U}_3$ and $\mathcal{U}_4$; as a result, the radial gradients of the mean axial and azimuthal vorticities at r_c appear. The axial vorticity is also generated by tilting and by stretching (respectively, first term and second term at the r.h.s of Eq. (B1)) while some azimuthal vorticity is created by the radial gradient of the vertical pressure shear. By deriving the τ_2-evolutions of the radial mean-vorticity gradients $\zeta_{z,1}$ and $\zeta_{\theta,1}$, we find their

expressions

$$\zeta_{z,1}(\Phi,\tau_2,\tau_3)=(\zeta-\zeta')\frac{\mathcal{V}_{1,\Phi}}{\zeta\varpi}\tau_2+2\zeta\varpi\mathcal{W}_{1,\Phi}\tau_2+\mathfrak{Z}_1(\Phi,\tau_3) \tag{B3}$$

and

$$\zeta_{\theta,1}(\Phi,\tau_2,\tau_3)=-\frac{1}{2}\frac{\mathcal{V}_{1,\Phi\Phi}}{\varpi}\tau_2^2+(\Lambda_{1,\Phi}-3\mathcal{V}_{1,\Phi})\tau_2+\mathfrak{T}_1(\Phi,\tau_3). \tag{B4}$$

After introducing (B3) and (B4) in Equations (B1) and (B2), the second-order axial and azimuthal vorticity expressions follow

$$\begin{aligned}\mathcal{Q}_{z,2}(\Phi,\tau_2,\tau_3)=&\frac{1}{2}(\mathcal{V}_{1,\Phi}-3\mathcal{W}_{1,\Phi})\mathcal{V}_{1,\Phi}\tau_2^2\\&+\frac{1}{2}\left(\mathcal{V}_{1,\Phi\tau_3}+\varpi\mathcal{W}_1\mathcal{V}_{1,\Phi\Phi}\right)\frac{\tau_2^2}{\varpi}-\zeta\mathfrak{u}_{4,\tau_2^{-1}}\\&+\frac{1}{2}(\zeta'-\zeta)\frac{\mathcal{V}_{1,\Phi}^2}{(\zeta\varpi)^2}\tau_2^2+\Lambda_2(\Phi,\tau_3),\end{aligned} \tag{B5}$$

$$\begin{aligned}\mathcal{Q}_{\theta,2}(\Phi,\tau_2,\tau_3)=&\frac{1}{2}\left(\frac{\mathcal{V}_{1,\Phi\Phi}}{\varpi}\tau_2-\Lambda_{1,\Phi}-\Lambda_{1d,\Phi}+4\mathcal{V}_{1,\Phi}\right)\frac{\mathcal{V}_{1,\Phi}}{\zeta\varpi}\tau_2^2\\&-\frac{1}{2}\left(\mathcal{V}_{1,\Phi\tau_3}+\varpi\mathcal{W}_1\mathcal{V}_{1,\Phi\Phi}+\Lambda_{1d}\frac{\mathcal{V}_{1,\Phi\Phi}}{\zeta\varpi}\right)\tau_2^2\\&+\Theta_2(\Phi,\tau_3).\end{aligned} \tag{B6}$$

The equation of the slow vorticity Λ_1 is derived by eliminating the fast motion from the axial-vorticity equation (B1) and is, namely,

$$\Lambda_{1,\tau_3}+\varpi\mathcal{W}_1\Lambda_{1,\Phi}=\varpi\Lambda_1(\mathcal{W}_{1,\Phi}-\mathcal{V}_{1,\Phi})-\mathfrak{Z}_1\frac{\mathcal{V}_{1,\Phi}}{\zeta\varpi}-\zeta\mathfrak{U}_4(\Phi,\tau_3). \tag{B7}$$

From the azimuthal-vorticity equation (B2), we get a second equation

$$\Lambda_{1,\tau_3}+\varpi\mathcal{W}_1\Lambda_{1,\Phi}=(\mathfrak{T}_1+\varpi\Lambda_1-\zeta\varpi\mathcal{S}_1)\frac{\mathcal{V}_{1,\Phi}}{\zeta\varpi^2}-\frac{\mathfrak{V}_{2,\Phi}}{\varpi}(\Phi,\tau_3). \tag{B8}$$

Deducing from Equations (B7), (B8), and (45), the evolution equations of the jumps of Λ_1 at either side of r_c, we obtain two evolution equations for A. From the axial-vorticity equation, we get

$$\begin{aligned}A_{\tau_3}+\varpi\mathcal{W}_1A_\Phi=&2\varpi A(\mathcal{W}_{1,\Phi}-\mathcal{V}_{1,\Phi})+\frac{\pi}{4}[\mathfrak{Z}_1]_-^+\frac{\mathcal{V}_{1,\Phi}}{\zeta^2\varpi}A^{\frac{1}{2}}\\&+\frac{\pi}{4}[\mathfrak{U}_4]_-^+A^{\frac{1}{2}}.\end{aligned} \tag{B9}$$

The evolution of A is driven, in addition to the vertical shear of the induced mean flow, by the jump of $\mathfrak{Z}_1$, the slow radial gradient of the first-order mean axial vorticity, and the jump of $\mathfrak{U}_4$, the slow second-order mean radial velocity. From the azimuthal-vorticity equation, we get

$$A_{\tau_3}+\varpi\mathcal{W}_1A_\Phi=2\frac{\mathcal{V}_{1,\Phi}}{\zeta\varpi}A-\frac{\pi}{4}[\mathfrak{T}_1]_-^+\frac{\mathcal{V}_{1,\Phi}}{\zeta^2\varpi^2}A^{\frac{1}{2}}+\frac{\pi}{4}\frac{[\mathfrak{V}_{2,\Phi}]_-^+}{\zeta\varpi}A^{\frac{1}{2}}. \tag{B10}$$

The evolution of A is driven this time by the jump of $\mathfrak{T}_1$, the slow radial gradient of the first-order mean azimuthal vorticity, and the jump of $\mathfrak{V}_{2,\Phi}$, the slow vertical shear of the second-order mean azimuthal velocity (i.e., the jump of the crossed derivatives of pressure $\overline{\Gamma}'_{2,\Phi}(r_c)$). The existence of two evolution equations for the same amplitude is not surprising because the leading-order CL flow is not really three-dimensional but keeps much of the helical structure of the normal modes. Equation (B10) loses its interest as an evolution equation; it links the jumps of $\mathfrak{T}_1$, $\mathfrak{V}_{2,\Phi}$, $\mathfrak{Z}_1$, and $\mathfrak{U}_4$. By equating and averaging (B7) and (B8), we obtain the expression of $\{\mathfrak{U}_4\}_-^+$. The evolution equations of the mean axial and azimuthal vorticity radial gradients are

$$\begin{aligned}\zeta_{z,1,\tau_3}+\zeta_{z,2,\tau_2}+\varpi\mathcal{W}_1\zeta_{z,1,\Phi}=&2\varpi\zeta_{z,1}\mathcal{W}_{1,\Phi}-\varpi\mathcal{Q}_{z,1}(\mathcal{Q}_{z,1,\Phi}-\mathcal{V}_{1,\Phi})\\&+\zeta_{\theta,1}\mathcal{V}_{1,\Phi}+2\zeta\mathcal{W}_{2,\Phi}+(\zeta_{z,1}-\zeta'_{z,1})\mathcal{U}_3+(2\zeta-\zeta')\mathcal{U}_4,\end{aligned} \tag{B11}$$

$$\begin{aligned}\zeta_{\theta,1,\tau_3}+\zeta_{\theta,2,\tau_2}+\varpi\mathcal{W}_1\zeta_{\theta,1,\Phi}=&\mathcal{Q}_{\theta,1}\mathcal{Q}_{\theta,1,\Phi}+\varpi(\zeta_{\theta,1}-\mathcal{Q}_{\theta,1})\mathcal{W}_{1,\Phi}+(2\mathcal{Q}_{z,1}-3\mathcal{S}_1)\mathcal{V}_{1,\Phi}\\&+\mathcal{S}_1\mathcal{Q}_{z,1,\Phi}-3\mathcal{V}_{2,\Phi}+\mathcal{Q}_{z,2,\Phi}+(2\zeta_{\theta,1}-2\mathcal{Q}_{\theta,1}-\zeta'_{\theta,1})\mathcal{U}_3.\end{aligned} \tag{B12}$$

Here again, the divergences of the radial fluxes of the radial mean vorticity gradients let appear the second-order radial derivatives of the mean axial and azimuthal vorticities at r_c. The slow average of (B11) allows us to determine $\zeta_{z,1}$; we will then use this equation to evaluate $\Upsilon^s_{2,0}$ while plotting the streamlines in the CL.

APPENDIX C: FOURTH-ORDER INNER FLOW MATCHINGS

In this section, we match the fourth-order inner flow with the outer flow and with itself on the separatrices, which enables us to determine $[\zeta_{z,1}]_-^+$ through $[\beta_{l,1}]_-^+$ according to Eq. (44).

The matching with the outer flow as $Z\to\infty$ yields the following functions:

$$V_4(x)=\frac{\beta_{l,1}}{2}\zeta A\cos x,\qquad \Pi_4(x)=\frac{s_i}{4}\zeta[1+a-\zeta(1+\varpi^2)]A^2\cos(2x)+\frac{s_i}{2}\zeta\hat{\mathfrak{V}}_2^DA\cos x+s_i\pi_4,$$

and

$$\Upsilon_4(x)=-s_i(\beta_{l,2a}+\frac{1}{2}c_{l,2,0})A\sin x-\frac{1}{4}c_{n,2,0}U_0\,A\sin(2x). \tag{C1}$$

The matching of the $\tilde{Z}$-pressure on the separatrices yields

$$\Pi_4^{\odot}(x) = \frac{s_i}{2}\zeta(1+\varpi^2)\Big(\{V_2(x)\}_-^+ - V_2^{\odot}(x)\Big)A\cos x + \{\Pi_4(x)\}_-^+,$$

and

$$V_4^{\odot}(x) = \{V_4(x)\}_-^+ + \frac{\zeta}{8}\frac{A}{\mathcal{R}^X}\{2(1+\varpi^2)[\mathcal{V}_2]_-^+ - 3[a]_-^+A\} + \frac{\zeta}{4}\{(1+\varpi^2)[\mathcal{V}_2]_-^+ - [a]_-^+A\}A\frac{\cos x - 1}{\mathcal{R}^X} + \frac{s_i}{2}\frac{[\pi_4]_-^+}{\mathcal{R}^X}.$$

In order to guarantee the continuity of $V_4^{\odot}(x)$, a condition on π_4 appears

$$[\pi_4]_-^+ = \frac{\zeta}{4}\{3[a]_-^+A - 2(1+\varpi^2)[\mathcal{V}_2]_-^+\}A.$$

The matching of the normal velocity on the separatrices makes necessary the presence of the logarithmic order in the outer flow expansion (6). Indeed, it imposes the relationship

$$\int_{A\cos x}^{A}\frac{\mathcal{G}_4^{\odot'}(Z)}{|Z_{\mathcal{R}}|}dZ = \frac{\mathcal{G}_4^{\odot}(A)}{\mathcal{R}^X} + \frac{s_i[\Upsilon_4(x)]_-^+}{2\varpi^2 A\sin x} + \frac{\zeta}{8}\frac{1+\varpi^2}{\varpi^2}[a]_-^+(\mathcal{R}^{X2} - 4A) - \frac{\zeta}{4\varpi^2}(1+\varpi^2)^2[\mathcal{V}_2]_-^+,$$

which comes down to $\mathcal{G}_4^{\odot}(A) = 0$, while $\mathcal{G}_4^{\odot'}(Z)$ has the following expression:

$$\mathcal{G}_4^{\odot'}(Z) = -\frac{[c_{l,2,0}]_-^+ + [\beta_{l,2a}]_-^+ + \zeta(1+\varpi^2)\{2[a]_-^+A + (1+\varpi^2)[\mathcal{V}_2]_-^+\}}{2\pi\varpi^2\sqrt{2(A-Z)}} + \frac{\zeta}{2\pi}\frac{1+\varpi^2}{\varpi^2}[a]_-^+\sqrt{2(A-Z)}. \tag{C2}$$

Moreover, after the matching of the azimuthal $\tilde{Z}$-vorticity (or the radial vorticity) on the separatrices,

$$\tilde{W}_{i,\mathcal{R}}^{(4)} = -\frac{s_i}{2}\zeta^2\varpi^2 A\cos x, \qquad \tilde{W}_{i,\mathcal{R}}^{(4,\odot)} = Z_{\mathcal{R}}\,\mathcal{G}_4^{\odot'}(Z) - \frac{s_i}{2}\zeta^2\varpi^2 A\cos x,$$

we get $\mathcal{G}_4^{\odot'}(A) = 0$. We remove the singularity in Eq. (C1); according to the definition of $c_{l,2,0}$ in Appendix A 2, and after Equations (B5) and (B6) in Appendix B, we obtain the jump of the logarithmic-order radial velocity

$$\begin{aligned}[\beta_{l,2a}]_-^+ = &-\frac{4}{\pi}\varpi[\mathcal{V}_{1,\Phi}A]_{\Phi}A^{-\frac{1}{2}}\tau_2^2 - \frac{8}{\pi}\zeta(1+\varpi^2)(4+5\varpi^2)\frac{\mathcal{V}_{1,\Phi}}{\varpi}A^{\frac{1}{2}}\tau_2\\ &- \varpi[\varpi\Lambda_2 + \Theta_2]_-^+ - \zeta(1+\varpi^2)^2[\mathfrak{V}_2]_-^+ - \zeta(3+4\varpi^2)[\mathfrak{V}_2 + \varpi^2\mathfrak{W}_2]_-^+.\end{aligned}$$

The $O(\epsilon^2\ln\epsilon)$ distorted outer flow is thus created as a CL feedback flow. Finally from (C1), the expression of the integration function $\mathcal{G}_4^{\odot}$ is

$$\mathcal{G}_4^{\odot}(Z,\Phi,\tau_2,\tau_3) = -\frac{\zeta}{6\pi}\frac{1+\varpi^2}{\varpi^2}[a]_-^+\sqrt{2(A-Z)}^3.$$

We also get the integration function $\Upsilon_4^{\odot}$,

$$\begin{aligned}\Upsilon_4^{\odot}(x) = &\{\Upsilon_4(x)\}_-^+ - \frac{s_i}{2}(1+\varpi^2)[V_4'(x)]_-^+\mathcal{R}^X + \frac{s_i}{2}\zeta(1+\varpi^2)^2[V_2^{\odot'}(x) - \{V_2'(x)\}_-^+]A\cos x\\ &- \frac{s_i}{2}\zeta^2(1+\varpi^2)^2\Big[K_a[1,x] + [1-\cos x]^{\frac{1}{2}} + \cos x\{\ln[\Lambda(A,x)] - 1\}\Big]A^2\sin x\\ &- \frac{s_i}{4}(1+\varpi^2)\{2[V_4(x)]_-^+ + \zeta(1+\varpi^2)[\mathcal{Q}_{z,1}]_-^+A\cos x\}A\frac{\sin x}{\mathcal{R}^X}.\end{aligned}$$

The continuity of $\Upsilon_4^{\odot}(x)$ and its 2π periodicity implies that $2[V_4(x)]_-^+ = -\zeta(1+\varpi^2)[\mathcal{Q}_{z,1}]_-^+A\cos x$, which comes down, using (C1), to another relationship

$$[\beta_{l,1}]_-^+ = -(1+\varpi^2)[\mathcal{Q}_{z,1}]_-^+. \tag{C3}$$

APPENDIX D: FIFTH-ORDER INNER FLOW MATCHINGS

The asymptotic expression of $\mathcal{F}_5$ as $Z\to\infty$ is

$$\begin{aligned}\mathcal{F}_5(Z,\Phi,\tau_2,\tau_3) = &\,s_i(\zeta^2\varpi^2 + \zeta' - \frac{2}{3}\zeta + \frac{1}{3}\zeta^2 - m^2)Z\\ &+ [\zeta_{z,1} + \frac{1}{2}(3\zeta\varpi^2 + \zeta - 2)\mathcal{Q}_{z,1}]\langle Z_{\mathcal{R}}\rangle\\ &+ s_i(\mathcal{Q}_{z,2} - \zeta\hat{\mathfrak{V}}_2^D) + O(\langle Z_{\mathcal{R}}^{-1}\rangle).\end{aligned}$$

We deduce from it that the vorticity jump $[\mathcal{Q}_{z,2}]_-^+$ determination follows from the matching of the axial vorticity on the separatrix. The asymptotic expression of $\mathcal{G}_5(Z)$ at $Z\to\infty$ is

$$\begin{aligned}\mathcal{G}_5(Z,\Phi,\tau_2,\tau_3) = &\,s_i(\zeta\hat{\mathfrak{V}}_2^D - \mathcal{Q}_{z,2} - \frac{\mathcal{Q}_{\theta,2}}{\varpi})\langle Z_{\mathcal{R}}\rangle\\ &- [\zeta_{z,1} + \frac{\zeta_{\theta,1}}{\varpi} + \zeta(1+\varpi^2)\mathcal{Q}_{z,1}]Z\\ &- \frac{s_i}{6}\Big(\zeta' + \zeta^2 + \zeta\Big)\langle Z_{\mathcal{R}}^3\rangle + O(\langle Z_{\mathcal{R}}\cos x\rangle).\end{aligned}$$

Matching the azimuthal vorticity on the separatrix yields a relationship between $\mathcal{Q}_{z,2}$ and $\mathcal{Q}_{\theta,2}$, as we have done in the second-order inner flow study for $\mathcal{Q}_{z,1}$ and $\mathcal{Q}_{\theta,1}$.

1. Within the separatrices

The azimuthal velocity is expressed with the function $\psi^{(5,\odot)}$,

$$V^{(5,\odot)} = \frac{s_i}{6}(m^2-3)\mathcal{R}^3 + \frac{1}{2}\mathcal{S}_1\mathcal{R}^2 - s_i\{\mathcal{V}_2\}^+_-\mathcal{R} + \{\mathcal{V}_3\}^+_-(\Phi,\tau_2,\tau_3) + \psi^{(5,\odot)}_{\mathcal{R}}.$$

The angular and vertical momentum equations are similar to Eqs. (64) and (65). The general expression of the inviscid axial vorticity is

$$\psi^{(5,\odot)}_{i,\mathcal{R}\mathcal{R}}(Z,x) = \mathcal{F}^{\odot}_5(Z,\Phi,\tau_2,\tau_3) - s_i(1+\zeta\varpi^2)V^{\odot}_2(x) - s_i\zeta\varpi^2\mathcal{Q}^{(2,\odot)}\mathcal{R} - \frac{\mathcal{V}_{1,\Phi}}{\varpi}\int_{x_0}^{x}\frac{dx_1}{Z_{\mathcal{R}}(Z,x_1)}, \quad \text{(D1)}$$

where $x_0 = \arccos(Z/A)$. The Prandtl-Batchelor theorem gives $\mathcal{F}^{\odot}_5$ (cf. Appendix F),

$$\mathcal{F}^{\odot}_5(Z,\Phi,\tau_2,\tau_3) = s_i(\zeta' + \zeta - m^2)Z + \mathcal{Q}^{(5,\odot)}(\Phi,\tau_2,\tau_3).$$

The inviscid axial and radial velocities are

$$W^{(5,\odot)}_i(Z,x) = \psi^{(5,\odot)}_{i,\mathcal{R}} + \frac{s_i}{6}[m^2+\zeta(1+2\zeta\varpi^2)]\mathcal{R}^3 - s_i\zeta(\zeta\varpi^2 Z + \mathfrak{V}^D_2)\mathcal{R} - \zeta(\{\Upsilon_{2,0}\}^+_- - \mathcal{S}_1)A\cos x + s_i[1+\zeta(1+\varpi^2)][\mathcal{Q}^{(2,\odot)}(Z - A\cos x) + V^{\odot}_2(x)\mathcal{R}] + \mathcal{G}^{\odot}_5(Z,\Phi,\tau_2,\tau_3) + \mathcal{W}^{\odot}_3(\Phi,\tau_2,\tau_3),$$

$$U^{(5,\odot)}_i(Z,x) = \Upsilon^{\odot}_5(x) + \mathcal{U}'_3\mathcal{R} + [(1-\zeta\varpi^2)\{\Upsilon_{2,0}\}^+_- + \zeta\varpi^2\mathcal{S}_1]A\mathcal{R}\sin x - s_i[1-\frac{1}{2}\zeta\varpi^2(1-\zeta\varpi^2)]A\mathcal{R}^2\sin x - (1+\varpi^2)\psi^{(5,\odot)}_X + s_i[1-\frac{1}{2}\zeta\varpi^2(1+\varpi^2)]V^{\odot\prime}_2(x)\mathcal{R}^2 + \varpi^2 A\sin x\int_{A\cos x}^{Z}\frac{\mathcal{G}^{\odot\prime}_5(Z_1)}{Z_{\mathcal{R}}(Z_1,x)}dZ_1 + s_i\mathcal{U}^{\odot}_4(\Phi,\tau_2,\tau_3). \quad \text{(D2)}$$

The normal-velocity continuity on the separatrix imposes the following relation:

$$\mathcal{R}^X(\hat{U}^{(5)} - \hat{U}^{(5,\odot)}) = sA\sin x\,[\hat{V}^{(5)} - \hat{V}^{(5,\odot)} + \varpi^2(\hat{W}^{(5)} - \hat{W}^{(5,\odot)})] \quad \text{(D3)}$$

evaluated at $\hat{Z} = 0$, where $\hat{U}^{(5)}(\hat{Z}=0) = \tilde{U}^{(5)}(\tilde{Z}=A)$, $\hat{V}^{(5)}(\hat{Z}=0) = \tilde{V}^{(5)}(\tilde{Z}=A)\ldots$

The jumps of the mean axial and azimuthal vorticity radial gradients $\zeta_{z,1}$ and $\zeta_{\theta,1}$, respectively, appear in the amplitude equations (B9) and (B10). The first jump has been evaluated at Subsection VI A. The second jump $[\zeta_{\theta,1}]^+_-$ is involved in the matching condition (D3), when we take the average $\{\text{D3}\}^+_-$. The matching imposes a condition on this jump jointly with the jump of the third-order mean velocities

$$[\zeta_{z,1} + \frac{\zeta_{\theta,1}}{\varpi}]^+_- A - [\mathcal{V}_3 + \varpi^2\mathcal{W}_3]^+_- - 2\{\zeta\mathfrak{V}^D_2 - \mathcal{Q}_{z,2} - \frac{\mathcal{Q}_{\theta,2}}{\varpi}\}^+_-\sqrt{2A}\,\text{SE}[1].$$

The radial vorticity gradient jump $[\zeta_{\theta,1}]^+_-$ is thus constrained by the CL inner study but it is related to higher-order mean velocity distortions. So we cannot close the system of Sec. V to the first-order mean flow. All orders are in fact coupled. The jump of $\mathcal{U}_4$ is calculated while matching the normal velocity along the separatrices as well, when applying $[\text{D3}]^+_-$, then x-averaging. A lot of cancellations occur and only the term involving $\mathcal{V}_{1,\Phi}/\varpi$ in $\langle\psi^{(5)}_X\rangle$ remains but is cancelled by $\langle\psi^{(5)}_{\mathcal{R}}\sin x/\mathcal{R}\rangle$ in this way

$$[\mathcal{U}_4]^+_- = (1+\varpi^2)\Big\{\langle[\psi^{(5)}_X - \psi^{(5,\odot)}_X]^+_-\rangle + 2s_iA\langle\frac{\sin x}{\mathcal{R}^X}\{\psi^{(5)}_{\mathcal{R}} - \psi^{(5,\odot)}_{\mathcal{R}}\}^+_-\rangle\Big\} = 0.$$

The functions $\psi^{(5)}_{\mathcal{R}}$ and $\psi^{(5)}_X$ are evaluated at $Z = A$. The second-order mean radial velocity is therefore undistorted.

APPENDIX E: NEW PARAMETRIZATION OF THE STREAMLINES

Each streamline is defined in the CL by a unique value of Z. The meeting points MP of the separatrices and the centre points CP (the core of the cat's eye) are located on specific isophases: evolving helices as time proceeds. The velocity field at these points must then satisfy certain relationships. We express this field with the strained coordinates $\tilde{Z}$ so that the latter may be satisfied, for the velocities defined with the independent variable Z does not generally satisfy them. The variable Z is thus expanded as follows:

$$Z = \tilde{Z} + \epsilon^{\frac{1}{2}}\ln\epsilon\,\varphi^{(1)}(\tilde{Z},x) + \epsilon^{\frac{1}{2}}\varphi^{(2)}(\tilde{Z},x) + \epsilon\ln^2\epsilon\,\varphi^{(3)}(\tilde{Z},x) + \epsilon\ln\epsilon\,\varphi^{(4)}(\tilde{Z},x) + \cdots, \quad \text{(E1)}$$

The deformation functions $\varphi^{(i)}$ describe how high the streamlines are deformed inside the CL. We can then define by analogy a new radius $\tilde{\mathcal{R}}$ such as $\tilde{Z} = 1/2\tilde{\mathcal{R}}^2 + A\cos x$. In the distorted frame $(x,\tilde{\mathcal{R}})$ moving with the angular velocity $\Omega_{0,c} + \epsilon^{1/2}\Omega_{1,c}$, vertical speed $\epsilon^{1/2}\overline{W}_{1,c}$, and mean radial velocity $\epsilon^{3/2}\overline{U}_{3,c}$, the MPs are defined by $x = 0\,[2\pi]$ and $\tilde{\mathcal{R}} = 0$, which according to (E1) yields values for Z close to A. From the expression of the height, we deduce the axial velocity after time-derivating

$$z = \frac{\xi - m\theta + \omega t}{k}, \qquad w = \frac{\omega}{k} - \frac{m}{k}\dot{\theta}.$$

Here the angular time-derivative $\dot{\theta}$ is linked to the azimuthal relative velocity v_r at MP in this way $v_r(MP) = r(MP)(\dot{\theta} - \Omega)$. So, the velocities are constrained at MP by the following

relationships:

$$w_r(MP) = -\frac{m}{k}\Big(\frac{v_r(MP)}{r(MP)} - \frac{\omega^D}{m}\Big) = \epsilon \ln \epsilon\, W^{(1)}(MP) + \epsilon\,[W^{(2)}(MP) - \overline{W}_{2,c}] + \cdots . \tag{E2}$$

At CP defined by $x = \pi\,[2\pi]$ and $\tilde{\mathcal{R}} = 0$, both velocities satisfy the same relationships (E2). The deformation functions are defined by

$$\varphi^{(1)}(Z,x) = \varphi^{(1,\odot)}(Z,x) = \frac{s_i}{2}\zeta(1+\varpi^2)AZ_{\mathcal{R}}\cos x,$$
$$\varphi^{(2)}(Z,x) = s_i Z_{\mathcal{R}}\Big(V^{(2)}(MP) + \varpi^2 W^{(2)}(MP) - \mho_2\Big),$$
$$\varphi^{(2,\odot)}(Z,x) = s_i Z_{\mathcal{R}}\Big(V^{(2,\odot)}(Z,x_0) + \varpi^2 W^{(2,\odot)}(Z,x_0) - \mho_2\Big),$$
$$\varphi^{(4)}(Z,x) = s_i Z_{\mathcal{R}}(1+\varpi^2)\Big(\frac{\zeta}{2}[(1+\varpi^2)\mathcal{Q}_{z,1} - \mathcal{S}_1]\,A\cos x + V_4(x)\Big) + \frac{\varphi^{(1)}}{Z_{\mathcal{R}}^2}\varphi^{(2)},$$
$$\varphi^{(4,\odot)}(Z,x) = s_i(1+\varpi^2)Z_{\mathcal{R}}\Big(\frac{\zeta}{2}[s_i(1+\varpi^2)\mathcal{Q}^{(2,\odot)} - \mathcal{S}_1]\,A\cos x_0 + V_4^{\odot}(x_0)\Big) + \frac{\varphi^{(1)}}{Z_{\mathcal{R}}^2}\varphi^{(2,\odot)}.$$

The contour Z crosses the streamwise axis of the cat's eye at the location $x_0 = \arccos[Z/A]$.

APPENDIX F: PRANDTL-BATCHELOR EXTENDED THEOREM

We here adapt Batchelor (1956) procedure[56] to determine the quasi-steady motion within a 3D bounded domain by finding closure equations. The vortex momentum equations are in the frame moving with the angular rotation $\Omega_c = \Omega_{c,0} + \epsilon^{1/2}\Omega_{c,1}$,

$$\partial_T \overline{\mathbf{W}}_{\mathbf{c}} + \partial_T \mathbf{u} + \partial_T \mathbf{\Omega_c} \times \mathbf{r} + \mathbf{Q}\times\mathbf{u} + \boldsymbol{\nabla} H = \frac{1}{Re}\Delta\mathbf{u} + \mathbf{F} \tag{F1}$$

with $H = P/\rho + 1/2|\mathbf{u}|^2 - (\varrho_{0,c} + \epsilon^{1/2}\varrho_{1,c})^2 r^2/8$ and $Q = \nabla\times\mathbf{u} + (\varrho_{0,c} + \epsilon^{1/2}\varrho_{1,c})\,\mathbf{e}_z$ is the absolute vorticity of the flow. Decomposing the motion into inviscid and viscous components, we perform a curvilinear integral on a surface $\tilde{Z} = Cst$ either in the plane $z = cst$, in which case θ varies over a bounded range smaller than $2\pi/m$, or in the plane $\theta = cst$, in which case z varies over a range smaller than $2\pi/k$. From the $O(\lambda)$ flow, we then obtain two conditions on the cat's eye inviscid flow. The surface $\tilde{Z} = Cst$ is a cylinder which spirals, at a distance roughly equal to r_c, with respect to the axis of the vortex (see Fig. 1),

$$\oint [\mathbf{Q}_i\times\mathbf{u}_v]\cdot d\mathbf{l} + \oint [\mathbf{Q}_v\times\mathbf{u}_i]\cdot d\mathbf{l} + \epsilon^{\frac{3}{2}}\oint [\boldsymbol{\nabla}\times\mathbf{Q}_i + \Delta_r \bar{V}_0\mathbf{e}_\theta]\cdot d\mathbf{l} = -\oint \partial t\mathbf{u}_v\cdot d\mathbf{l}. \tag{F2}$$

Both first integrands do not vanish like in Batchelor (1956) because $\mathbf{l}$ is not a tangent to a streamline. The computation of the integral equation (F2) at the first nontrivial order inner flow in C14 yields that the axial vorticity $Q^{(2,\odot)}$ in (33) is uniform.

1. Fourth order

Condition (F2) at $z = const$ jointly with (61) yields

$$\int_{x_0}^{2\pi-x_0} |Z_{\mathcal{R}}(Z,x)|\psi^{(4,\odot)}_{\mathcal{R}\mathcal{R}Z}\,dx = \mathcal{F}^{\odot}_{4,Z}(Z,\Phi,\tau_2,\tau_6)\int_{x_0}^{2\pi-x_0}|Z_{\mathcal{R}}(Z,x)|\,dx = 0 \tag{F3}$$

so that $\mathcal{F}^{\odot}_4 = \mathcal{Q}^{(4,\odot)}(\Phi,\tau_2,\tau_3)$ is a function of the slow variables only. Condition (F2) with (62) at $\theta = const$ yields

$$\int_{x_0}^{2\pi-x_0}|Z_{\mathcal{R}}(Z,x)|\mathcal{G}^{\odot}_{4,\mathcal{R}Z}\,dx = \int_{x_0}^{2\pi-x_0}|Z_{\mathcal{R}}|\sin x(W_v^{(4,\odot)} - V_v^{(4,\odot)})\,dx = 0. \tag{F4}$$

2. Fifth order

Condition (F2) with (D1) at $z = const$: From the viscous model in C14, the viscous contributions cancel out and it only remains

$$\int_{x_0}^{2\pi-x_0}|Z_{\mathcal{R}}(Z,x)|\psi^{(5,\odot)}_{\mathcal{R}\mathcal{R}Z}\,dx = s_i(\zeta' + \zeta - m^2)\int_{x_0}^{2\pi-x_0}|Z_{\mathcal{R}}|\,dx,$$

which comes down to

$$\mathcal{F}^{\odot}_5(Z) = s_i(\zeta' + \zeta - m^2)Z + Q^{(5,\odot)}(\Phi,\tau_2,\tau_3). \tag{F5}$$

Condition (F2) with (D2) at $\theta = const$: Assuming that the viscous flow vanishes within the separatrices, we get

$$\int_{x_0}^{2\pi-x_0}|Z_{\mathcal{R}}(Z,x)|\mathcal{G}^{\odot}_{5,\mathcal{R}Z}\,dx = s_i[\zeta' + \zeta(1-\zeta\varpi^2)]\int_{x_0}^{2\pi-x_0}|Z_{\mathcal{R}}|\,dx.$$

APPENDIX G: DIFFUSION BOUNDARY LAYERS

1. Order $k = 0$

a. Induced mean axial vorticity

The general solution for $Q^{(2)}_{z,0}$ that asymptotes zero at $H \to \infty$ is

$$Q^{(2)}_{z,0} = q^s_{00}\int_{s\infty}^{\hat{H}} e^{-u^2}\,du + \frac{1}{3}\kappa_{01}\,q^s_{00}\,\tau_2\,e^{-\hat{H}^2} + q^s_{01}\,\tau_2\,\mathrm{He}[-3,s\hat{H}]\times e^{-\hat{H}^2} + q^s_{02}\,\tau_2^2\,\mathrm{He}[-5,s\hat{H}]\,e^{-\hat{H}^2} + \cdots, \tag{G1}$$

where $\hat{H} = H + \kappa_{00}$ and He is a function of Hermite. Note that the negative index implies that it is not a polynomial. The expression of $Q^{(2)}_{z,0}$ involves the classic error-function encountered in the evolution of a laminar boundary layer. The final dots ... mean that the expression is uncomplete, $Q^{(2)}_{z,0}$ is a τ_2-integer series, and higher τ_2-powers are missing. We will restrict ourselves to the first two terms in the τ_2-integer series. We express the boundary conditions with the dependent variables of our system ((50)–(54)), $\{\Lambda_1\}^+_-$ and $[\Lambda_1]^+_-$ ($\equiv A$) and $\{\mathfrak{T}_1\}^+_-$. On the CL edges, the boundary conditions yield the following relations:

$$q_{00}^{+}\int_{+\infty}^{\kappa_{00}} e^{-u^2}\,du - q_{00}^{-}\int_{-\infty}^{\kappa_{00}} e^{-u^2}\,du = [\mathcal{Q}_{z,1}]_{-}^{+} = [\Lambda_1]_{-}^{+}, \quad \frac{1}{2}q_{00}^{+}\int_{+\infty}^{\kappa_{00}} e^{-u^2}\,du + \frac{1}{2}q_{00}^{-}\int_{-\infty}^{\kappa_{00}} e^{-u^2}\,du = \{\Lambda_1\}_{-}^{+},$$

and

$$q_{01}^{s}\mathrm{He}[-3, s\kappa_{00}] + \frac{1}{3}\kappa_{01}q_{00}^{s} = -\frac{\mathcal{V}_{1,\Phi}}{\varpi}e^{\kappa_{00}^2}.$$

The leading-order streamwise velocity is obtained after H-integrating (G1),

$$V_0^{(2)} = \frac{q_{00}^{s}}{\nu}\Big(\hat{H}\int_{s\infty}^{\hat{H}} e^{-u^2}\,du + \frac{1}{2}e^{-\hat{H}^2}\Big) - s\frac{q_{01}^{s}}{12\nu}\,\tau_2\Big((3\hat{H}+2\hat{H}^3)\int_{s\infty}^{\hat{H}} e^{-u^2}\,du + (1+\hat{H}^2)e^{-\hat{H}^2}\Big)$$
$$+ \frac{1}{3}\frac{\kappa_{01}}{\nu}\,q_{00}^{s}\,\tau_2\int_{s\infty}^{\hat{H}} e^{-u^2}\,du\ldots. \tag{G2}$$

If we assume a jump $\delta v_0 = [v_0]_{-}^{+}$ of the rotational velocity (74) at either side of the CL, we have another condition that allows us to determine κ_0. For the two first terms in the τ_2-expansion (75) of κ_0, we have the related conditions

$$q_{00}^{+}[e^{-\kappa_{00}^2} - \kappa_{00}\sqrt{\pi}E_0] - q_{00}^{-}[e^{-\kappa_{00}^2} + \kappa_{00}\sqrt{\pi}(2-E_0)] = 2\delta v_{00}$$

and

$$-\frac{q_{01}^{+}}{12}[2(1+\kappa_{00}^2)e^{-\kappa_{00}^2} - \sqrt{\pi}\kappa_{00}(3+2\kappa_{00}^2)E_0] - \frac{1}{3}\sqrt{\pi}\kappa_{01}q_{00}^{+}E_0$$
$$-\frac{q_{01}^{-}}{12}[2(1+\kappa_{00}^2)e^{-\kappa_{00}^2} + \sqrt{\pi}\kappa_{00}(3+2\kappa_{00}^2)(2-E_0)] - \frac{1}{3}\sqrt{\pi}\kappa_{01}q_{00}^{-}(2-E_0) = 2\delta v_{01},$$

with $E_0 = \mathrm{Erfc}[\kappa_{00}] = 2/\sqrt{\pi}\int_{\kappa_{00}}^{\infty} e^{-u^2}\,du$. Finally, q_{00}^{s} are defined by

$$q_{00}^{+} = -\frac{2\{\Lambda_1\}_{-}^{+} + [\Lambda_1]_{-}^{+}}{\sqrt{\pi}\,E_0}, \qquad q_{00}^{-} = \frac{2\{\Lambda_1\}_{-}^{+} - [\Lambda_1]_{-}^{+}}{\sqrt{\pi}\,(2-E_0)},$$

while κ_{00} satisfies the relation

$$\frac{D^{-}E_0 - D^{+}(2-E_0)}{D^{-}E_0 + D^{+}(2-E_0)} = 2\frac{\{\Lambda_1\}_{-}^{+}}{[\Lambda_1]_{-}^{+}} + \sqrt{\pi}\frac{\delta v_{00}}{[\Lambda_1]_{-}^{+}}E_0(2-E_0)e^{\kappa_{00}^2}, \tag{G3}$$

with $D^{+} = e^{-\kappa_{00}^2}/\sqrt{\pi} - \kappa_{00}E_0$ and $D^{-} = D^{+} + 2\kappa_{00}$. To the next order, the departures κ_{01} and q_{01} are defined by

$$\kappa_{01} = \frac{72\delta v_{01}He[-3,\kappa_{00}]He[-3,-\kappa_{00}] - 3\{He[-3,-\kappa_{00}]S^{+} + He[-3,\kappa_{00}]S^{-}\}\,e^{\kappa_{00}^2}\frac{\mathcal{V}_{1,\Phi}}{\varpi}}{q_{00}^{+}S^{+}He[-3,-\kappa_{00}] + q_{00}^{-}S^{-}He[-3,\kappa_{00}] + 24He[-3,-\kappa_{00}]He[-3,\kappa_{00}][\Lambda_1]_{-}^{+}},$$
$$q_{01}^{s} = -\frac{\mathcal{V}_{1,\Phi}e^{\kappa_{00}^2} + \frac{1}{3}\varpi\kappa_{01}q_{00}^{s}}{\varpi\mathrm{He}[-3,s\kappa_{00}]},$$

where

$$S^{+} = 2(1+\kappa_{00}^2)D^{+} - \kappa_{00}E_0, \quad S^{-} = 2(1+\kappa_{00}^2)D^{-} + \kappa_{00}(2-E_0).$$

The departures κ_{00} and κ_{01} are functions of Φ and τ_3 via Λ_1, $\mathcal{V}_1$, and v_0. The calculation of the other coefficients q_{0i} and κ_{0i}, $i>1$, can be made in the same way. In spite of the simple τ_2 dependency inside the CL, the DBLs have a more complex τ_2-evolution since the leading-order terms in the expansions (72) are expressed as τ_2-integer series. The convergence of those series is not insured. The mean-flow solution of the system in Section V constraints the DBL motion.

b. Induced mean azimuthal vorticity

The leading-order mean azimuthal vorticity satisfies the same Equation (71) with similar boundary conditions. The expansion of the distorted mean flow $\overline{W}$ around the CL therefore takes the following form:

$$\overline{W} = \epsilon^{\frac{1}{2}}\overline{W}_1 + \frac{\epsilon}{\nu}\Big[s_i\sum_{j=0} w_{0j}\tau_2^{j} - \sum_{j=0}\pi_{1j}\tau_2^{j}(r-r_c) + \frac{\epsilon^{\frac{1}{2}}}{\nu}s_i\sum_{j=0} w_{1j}\tau_2^{j} + \cdots\Big] + \epsilon\overline{W}_2 + \cdots.$$

The expressions of the zeroth-order solution, $Q_{\theta,0}^{(2)}$ and $W_0^{(2)}$ are similar to (G1) and (G2). The matching at $H\to 0$ gives $w_{01}^{s} = \varpi v_{01}^{s}$. At the order $k=0$ of (72), the azimuthal vorticity and the axial velocity are, respectively, proportional to the axial vorticity and the azimuthal velocity, which suggests that the leading-order mean motion inside the DBLs is a helical spiral.

2. Order $\epsilon^{\frac{1}{2}}/\nu$

a. Induced mean axial vorticity

The first-order vorticity $Q^{(2)}_{z,1}$ satisfies the equation

$$Q^{(2)}_{z,1,HH} - 2Q^{(2)}_{z,1} + 2(H+\kappa_0)Q^{(2)}_{z,1,H} = 4(Q^{(2)}_{z,1,\tau_2}\tau_2 - \kappa_1 Q^{(2)}_{z,0,H})\,. \tag{G4}$$

We find the general solution as

$$\begin{aligned} Q^{(2)}_{z,1} = {} & q^s_{10}\Big(\hat{H}\int_{s\infty}^{\hat{H}} e^{-u^2}\,du + \frac{1}{2}e^{-\hat{H}^2}\Big) - 2\kappa_{10}\Big(q^s_{00}\hat{H}\int_{s\infty}^{\hat{H}} e^{-u^2}\,du + 2q^s_{01}\tau_2\,Fq^s[\hat{H}] + \frac{1}{3}\kappa_{01}\,q^s_{00}\,\tau_2\,\hat{H}e^{-\hat{H}^2}\Big) \\ & + 2q^s_{11}\,\tau_2\Big((1+\hat{H}^2)e^{-\hat{H}^2} + (3\hat{H}+2\hat{H}^3)\int_{s\infty}^{\hat{H}} e^{-u^2}\,du\Big) + \frac{1}{3}\kappa_{01}\,(q^s_{10} - 2\kappa_{10}q^s_{00})\,\tau_2\int_{s\infty}^{\hat{H}} e^{-u^2}\,du \\ & + \frac{1}{6}\kappa_{11}q^s_{00}\,\tau_2\,e^{-\hat{H}^2} + \cdots\,. \end{aligned} \tag{G5}$$

The function Fq appears owing to the forcing $-4\kappa_1 Q^{(2)}_{z,0,H}$ in Eq. (G4) and is generated by the third term of $Q^{(2)}_{z,0}$ in (G1), it cannot be reduced to a simple analytical expression. The first-order radius departure κ_{10} and the integration constants q^s_{10} and q^s_{11} are determined by the following relations. The radial axial-vorticity gradient satisfies four boundary conditions as $H \to 0$. They are, namely,

$$\begin{aligned} & \frac{1}{2}q^+_{10}\sqrt{\pi}E_0 + \frac{1}{2}q^-_{10}\sqrt{\pi}(2-E_0) + \kappa_{10}q^+_{00}(2\kappa_{00}e^{-\kappa^2_{00}} - \sqrt{\pi}E_0) \\ & \quad - \kappa_{10}q^-_{00}[2\kappa_{00}e^{-\kappa^2_{00}} + \sqrt{\pi}(2-E_0)] = -s_i[\zeta_{z,1}]^+_- = -s_i[\mathfrak{Z}_1]^+_-\,, \end{aligned} \tag{G6}$$

$$\begin{aligned} & \frac{1}{4}q^+_{10}\sqrt{\pi}E_0 - \frac{1}{4}q^-_{10}\sqrt{\pi}(2-E_0) + \frac{1}{2}\kappa_{10}q^+_{00}(2\kappa_{00}e^{-\kappa^2_{00}} - \sqrt{\pi}E_0) \\ & \quad + \frac{1}{2}\kappa_{10}q^-_{00}[2\kappa_{00}e^{-\kappa^2_{00}} + \sqrt{\pi}(2-E_0)] = -s_i\{\zeta_{z,1}\}^+_- = -s_i\{\mathfrak{Z}_1\}^+_-\,, \end{aligned} \tag{G7}$$

and

$$\begin{aligned} & 3q^+_{11}\,[2\kappa_{00}e^{-\kappa^2_{00}} - (1+2\kappa^2_{00})\sqrt{\pi}E_0] - 4\kappa_{10}q^+_{01}\,Fq^+_H[\kappa_{00}] - \frac{2}{3}\kappa_{10}\kappa_{01}q^+_{00}(1-2\kappa^2_{00})e^{-\kappa^2_{00}} \\ & \quad + \frac{1}{3}\kappa_{01}\,(q^+_{10} - 2\kappa_{10}q^+_{00})\,e^{-\kappa^2_{00}} - \frac{1}{3}\kappa_{00}\kappa_{11}q^+_{00}e^{-\kappa^2_{00}} \\ & = 3q^-_{11}\,[2\kappa_{00}e^{-\kappa^2_{00}} + (1+2\kappa^2_{00})\sqrt{\pi}(2-E_0)] - 4\kappa_{10}q^-_{01}\,Fq^-_H[\kappa_{00}] - \frac{2}{3}\kappa_{10}\kappa_{01}q^-_{00}(1-2\kappa^2_{00})e^{-\kappa^2_{00}} \\ & \quad + \frac{1}{3}\kappa_{01}\,(q^-_{10} - 2\kappa_{10}q^-_{00})\,e^{-\kappa^2_{00}} - \frac{1}{3}\kappa_{00}\kappa_{11}q^-_{00}e^{-\kappa^2_{00}} = s_i(\zeta-\zeta')\frac{\mathcal{V}_{1,\Phi}}{\zeta\varpi} + 2s_i\zeta\varpi\mathcal{W}_{1,\Phi}. \end{aligned} \tag{G8}$$

The vorticity matching does not introduce any new conditions; it enables us to determine the additional vorticities μ^s_{10} and μ^s_{11}. The related velocity is obtained after integration over H of (G5)

$$\begin{aligned} V^{(2)}_1 = {} & \frac{1}{4}\frac{q^s_{10}}{\nu}\Big((2\hat{H}^2+1)\int_{s\infty}^{\hat{H}} e^{-u^2}\,du + \hat{H}e^{-\hat{H}^2}\Big) \\ & + \kappa_{10}\Big(\frac{q^s_{00}}{4\nu}[(2\hat{H}^2-1)\int_{s\infty}^{\hat{H}} e^{-u^2}\,du + \hat{H}e^{-\hat{H}^2}] - 4\frac{q^s_{01}}{\nu}\tau_2\int_{s\infty}^{\hat{H}} Fq^s(u)\,du + \frac{1}{3}\kappa_{01}\,q^s_{00}\,\tau_2\,e^{-\hat{H}^2}\Big) \\ & + \frac{q^s_{11}}{4\nu}\,\tau_2\Big((3+12\hat{H}^2+4\hat{H}^4)\int_{s\infty}^{\hat{H}} e^{-u^2}\,du + (5\hat{H}+2\hat{H}^3)e^{-\hat{H}^2}\Big) \\ & + \frac{1}{6}\frac{\kappa_{01}}{\nu}\,(q^s_{10} - 2\kappa_{10}q^s_{00})\,\tau_2\,\Big(2\hat{H}\int_{s\infty}^{\hat{H}} e^{-u^2}\,du + e^{-\hat{H}^2}\Big) + \frac{1}{6}\kappa_{11}\frac{q^s_{00}}{\nu}\,\tau_2\int_{s\infty}^{\hat{H}} e^{-u^2}\,du + \cdots\,. \end{aligned} \tag{G9}$$

Assuming a jump of the streamwise velocity $\delta v_1 = [v_1]^+_-$ in (74) yields

$$\begin{aligned} & q^+_{10}\Big(2\kappa_{00}e^{-\kappa^2_{00}} - (1+2\kappa^2_{00})\sqrt{\pi}E_0\Big) + \kappa_{10}q^+_{00}\Big(2\kappa_{00}e^{-\kappa^2_{00}} - (2\kappa^2_{00}-1)\sqrt{\pi}E_0\Big) \\ & \quad - q^-_{10}\Big(2\kappa_{00}e^{-\kappa^2_{00}} + (1+2\kappa^2_{00})\sqrt{\pi}(2-E_0)\Big) - \kappa_{10}q^-_{00}\Big(2\kappa_{00}e^{-\kappa^2_{00}} + (2\kappa^2_{00}-1)\sqrt{\pi}(2-E_0)\Big) = 8\delta v_{10}. \end{aligned} \tag{G10}$$

We express κ_{10} with the help of (G10) and inject it into the system ((G6) and (G7)). The resolution of the latter gives q^s_{10} and finally κ_{10}. The departure κ_{11} is calculated in the same way with the analogous of (G10) by assuming a jump of the velocity v^s_{11} between both DBLs. Then, we can solve Equation (G8), which gives q^s_{11}.

b. Azimuthal vorticity

The first-order vorticity $Q^{(2)}_{\theta,1}$ satisfies an analogous equation to (G4); its general solution is

$$Q^{(2)}_{\theta,1} = r^s_{10}\Big(\hat{H}\int_{s\infty}^{\hat{H}} e^{-u^2}\,du + \frac{1}{2}e^{-\hat{H}^2}\Big) + 2\varpi\kappa_{10}\Big(q^s_{00}\hat{H}\int_{s\infty}^{\hat{H}} e^{-u^2}\,du + 2q^s_{01}\tau_2 Fq^s[\hat{H}] + \frac{1}{3}\kappa_{01}\,q^s_{00}\,\tau_2\,\hat{H}e^{-\hat{H}^2}\Big)$$
$$+ 2r^s_{11}\,\tau_2\Big((1+\hat{H}^2)e^{-\hat{H}^2} + (3\hat{H}+2\hat{H}^3)\int_{s\infty}^{\hat{H}} e^{-u^2}\,du\Big) + \frac{1}{3}\kappa_{01}\,(r^s_{10} + 2\varpi\kappa_{10}q^s_{00})\,\tau_2\int_{s\infty}^{\hat{H}} e^{-u^2}\,du - \frac{1}{6}\varpi\kappa_{11}q^s_{00}\,\tau_2\,e^{-\hat{H}^2} + \cdots.$$

The computations of the radius departure κ_{10} and the integration constants r^s_{10} and r^s_{11} are carried out in the same way as Appendix G 2 a. As a result, we get another expression of κ_{10}. From the equality between both obtained values of κ_{10}, we deduce a relationship between δv_{10}, δw_{10}, $\{\mathfrak{T}_1\}^+_-$, $\{\mathfrak{Z}_1\}^+_-$, $[\mathfrak{T}_1]^+_-$, and $[\mathfrak{Z}_1]^+_-$. At this order, the mean axial and azimuthal velocities are not proportional inside the DBLs, neither are the mean axial and azimuthal vorticities. We note that the departure from a helical motion increases with τ_2. The DBL motion constraints the system of Section V. The CL and DBLs are strongly coupled.

APPENDIX H: SPECIAL FUNCTIONS

Here we define the functions that we have used in the study:

- $SE[Z] = \frac{1}{2\pi}\int_0^{2\pi}[Z-\cos x]^{\frac{1}{2}}\,dx,$
- $\Pi[Z,x] = \int_0^x \frac{1}{Z_{\mathcal{R}}(Z,x)} - \langle\frac{1}{Z_{\mathcal{R}}(Z)}\rangle\,dx,$
- $K_a[Z,x] = \int_\infty^Z \frac{1}{\sqrt{Z_1-\cos x}}\Big[SE[Z_1] - Z_1^{\frac{1}{2}}\Big]\,dZ_1.$

[1] R. A. Houze, Jr., S. S. Chen, W. Lee, R. F. Rogers, J. A. Moore, G. J. Stossmeister, M. M. Bell, J. Cetrone, W. Zhao, and S. R. Brodzik, "The hurricane and intensity change experiment: Observations and modeling of Hurricanes Katrina, Ophelia, and Rita," Bull. Am. Meteorol. Soc. **87**, 1503–1521 (2006).

[2] Y. Chen, G. Brunet, and M. K. Yau, "Spiral bands in a simulated hurricane. Part II: Wave activity diagnostics," J. Atmos. Sci. **60**, 1239–1256 (2003).

[3] M. T. Montgomery and C. Lu, "Free waves on vortices. Part I: Eigenmode structure," J. Atmos. Sci. **54**, 1868–1885 (1997).

[4] Y. Chen and M. K. Yau, "Spiral bands in a simulated hurricane. Part I: Vortex Rossby wave verification," J. Atmos. Sci. **58**, 2128–2145 (2001).

[5] M. T. Montgomery and R. J. Kallenbach, "A theory for vortex Rossby-waves and its application to spiral bands and intensity changes in hurricanes," Q. J. R. Meteorol. Soc. **123**, 435–465 (1997).

[6] J. D. Moller and M. T. Montgomery, "Tropical cyclone evolution via potential vorticity anomalies in a three-dimensional balance model," J. Atmos. Sci. **57**, 3366–3387 (2000).

[7] M. T. Montgomery and J. Enagonio, "Tropical cyclogenesis via forced vortex Rossby waves in a three-dimensional quasigeostrophic model," J. Atmos. Sci. **55**, 3176–3206 (1998).

[8] F. Judt and S. S. Chen, "Convectively generated potential vorticity in rainbands and formation of the secondary eyewall in Hurricane Rita of 2005," J. Atmos. Sci. **129**, 3581–3599 (2010).

[9] D. J. Benney and R. F. Bergeron, "A new class of nonlinear waves in parallel flows," Stud. Appl. Math. **48**, 181–204 (1969).

[10] S. A. Maslowe, "Critical layers in shear flows," Annu. Rev. Fluid Mech. **18**, 405–432 (1986).

[11] E. A. Hendricks and W. H. Schubert, "Transport and mixing in idealized hurricane-like vortices," Q. J. R. Meteorol. Soc. **135**, 1456–1470 (2009).

[12] Y. Troitskaya, "The viscous-diffusion nonlinear critical layer in a stratified shear flow," J. Fluid Mech. **233**, 25–48 (1991).

[13] X. Qiu, Z. M. Tan, and Q. Xiao, "The roles of vortex Rossby waves in hurricane secondary formation," Mon. Weather Rev. **138**, 2092–2109 (2010).

[14] S. A. Maslowe and N. Nigam, "The nonlinear critical layer for Kelvin modes on a vortex with a continuous velocity profile," SIAM J. Appl. Math. **68**, 825–843 (2008).

[15] P. Caillol, "A steady nonlinear and singular vortex Rossby wave within a rapidly rotating vortex. Part I: Theory," Geophys. Astrophys. Fluid Dyn. **108**, 387–436 (2014).

[16] P. Caillol, "A steady nonlinear and singular vortex Rossby wave within a rapidly rotating vortex. Part II: Application to geophysical vortices," Geophys. Astrophys. Fluid Dyn. **109**, 111–144 (2015).

[17] D. S. Nolan and M. T. Montgomery, "Nonhydrostic, three-dimensional perturbations to balanced, hurricane-like vortices. Part I: Linearized formulation, stability, and evolution," J. Atmos. Sci. **59**, 2989–3020 (2002).

[18] S. M. Churilov and I. G. Shukhman, "Nonlinear stability of a stratified shear flow: A viscous critical layer," J. Fluid Mech. **180**, 1–20 (1987).

[19] S. M. Churilov, "The nonlinear stabilization of a zonal shear flow instability," Geophys. Astrophys. Fluid Dyn. **46**, 159–175 (1989).

[20] S. M. Churilov and I. G. Shukhman, "The nonlinear critical layer resulting from the spatial or temporal evolution of weakly unstable disturbances in shear flows," J. Fluid Mech. **318**, 189–221 (1996).

[21] S. V. Shagalov, V. P. Reutov, and G. V. Rybushkina, "The asymptotic theory of the generation of long-wave structures in critical layers of weakly dissipative jet flows," Izv. Atmos. Oceanic Phys. **45**, 629–645 (2009).

[22] V. P. Reutov, S. V. Shagalov, and G. V. Rybushkina, "The onset of turbulence in a shear flow on the beta-plane. An asymptotic approach based on the critical layer theory," in *Advances in Turbulence VII*, edited by U. Frisch (Kluwer, Dordrecht, 1998), pp. 483–486.

[23] S. V. Shagalov, V. P. Reutov, and G. V. Rybushkina, "Asymptotic analysis of transition to turbulence and chaotic advection in shear zonal flows on a beta plane," Izv. Atmos. Oceanic Phys. **46**, 95–108 (2010).

[24] R. Haberman, "Critical layers in parallel flows," Stud. Appl. Math. **51**, 139–161 (1972).

[25] R. Haberman, "Wave-induced distortions of a slightly stratified shear flow: A nonlinear critical-layer effect," J. Fluid Mech. **58**, 727–735 (1972).

[26] P. Caillol and R. H. J. Grimshaw, "Rossby solitary waves in the presence of a critical layer," Stud. Appl. Math. **118**, 313–364 (2007).

[27] P. Caillol and R. H. J. Grimshaw, "Rossby elevation waves in the presence of a critical layer," Stud. Appl. Math. **120**, 35–64 (2008).

[28] P. Caillol and R. H. J. Grimshaw, "Internal solitary waves with a weakly stratified critical layer," Phys. Fluids **24**, 056602 (2012).

[29] Y. Troitskaya and S. Reznik, "Quasi-steady dissipative nonlinear critical layer in a stratified shear flow," Phys. Fluids **8**, 3313–3328 (1996).

[30] K. B. Winters and E. A. D'Asaro, "Three-dimensional wave instability near a critical level," J. Fluid Mech. **272**, 255–284 (1994).

[31] L. J. Campbell and S. A. Maslowe, "Nonlinear critical-layer evolution of a forced gravity wave packet," J. Fluid Mech. **493**, 151–179 (2003).

[32] L. J. Campbell, "Wave-mean flow interactions in a forced Rossby wave packet critical layer," Stud. Appl. Math. **112**, 39–85 (2004).

[33] D. J. Benney and S. A. Maslowe, "The evolution in space and time of nonlinear waves in parallel shear flows," Stud. Appl. Math. **54**, 181–205 (1975).

[34] Y. Wang, "Vortex Rossby waves in a numerically simulated tropical cyclone. Part I: Overall structure, potential vorticity, and kinetic energy budgets," J. Atmos. Sci. **59**, 1213–1238 (2002).

[35]J. A. Zhang, R. F. Rogers, D. S. Nolan, and F. D. Marks, Jr., "On the characteristic height scales of the hurricane boundary layer," Mon. Weather Rev. **139**, 2523–2535 (2011).
[36]P. D. Reasor, M. T. Montgomery, F. D. Marks, and J. F. Gamache, "Low-wavenumber structure and evolution of the hurricane inner core observed by airborne Dual-Doppler radar," Mon. Weather Rev. **128**, 1653–1680 (2000).
[37]R. Mallier and S. A. Maslowe, "Weakly nonlinear evolution of a wave packet in a zonal mixing layer," Stud. Appl. Math. **102**, 69–85 (1999).
[38]M. L. Salby, D. O'Sullivan, R. R. Garcia, and P. Callaghan, "Air motions accompanying the development of a planetary wave critical layer," J. Atmos. Sci. **47**, 1179–1204 (1990).
[39]D. J. Benney, "Nonlinear wave packets in flows with critical layers," Stud. Appl. Math. **69**, 177–200 (1983).
[40]P. Caillol and S. A. Maslowe, "The small-vorticity nonlinear critical layer for Kelvin modes on a vortex," Stud. Appl. Math. **118**, 221–254 (2007).
[41]P. Caillol, "Multiple vortices induced by a tridimensional critical layer within a rapidly rotating vortex," IMA J. Appl. Math. **77**, 282–292 (2012).
[42]S. A. Maslowe, D. J. Benney, and D. J. Mahoney, "Wave packet critical layers in shear flows," Stud. Appl. Math. **91**, 1–16 (1994).
[43]R. Kelly and S. A. Maslowe, "The nonlinear critical layer in a slightly stratified shear flow," Stud. Appl. Math. **49**, 301–325 (1970).
[44]S. A. Maslowe, "The generation of clear air turbulence by nonlinear waves," Stud. Appl. Math. **51**, 1–16 (1972).
[45]G. B. Whitham, *Linear and Nonlinear Waves* (John Wiley & Sons, New York, 1999).
[46]T. J. Dunkerton and D. C. Fritts, "Transient gravity wave-critical layer interaction. Part I: Convective adjustment and the mean zonal acceleration," J. Atmos. Sci. **41**, 992–1007 (1984).
[47]P. D. Reasor, M. D. Eastin, and J. F. Gamache, "Rapidly intensifying Hurricane Guillermo (1997). Part I: Low-wavenumber structure and evolution," Mon. Weather Rev. **137**, 603–631 (2009).
[48]Y. Martinez, G. Brunet, M. K. Yau, and X. Wang, "On the dynamics of concentric genesis: Space-time empirical normal modes diagnosis," J. Atmos. Sci. **68**, 457–476 (2011).
[49]J. P. Kossin and M. D. Eastin, "Two distinct regimes in the kinematic and thermodynamic structure of the hurricane and eyewall," J. Atmos. Sci. **58**, 1079–1090 (2001).
[50]J. Wurman, "The multiple-vortex structure of a tornado," Weather Forecasting **17**, 473–505 (2002).
[51]J. D. Moller and M. T. Montgomery, "Vortex Rossby waves and hurricane intensification in a model," J. Atmos. Sci. **56**, 1674–1687 (1999).
[52]C. Staquet, "Two-dimensional secondary instabilities in a strongly stratified shear layer," J. Fluid Mech. **296**, 73–126 (1995).
[53]W. M. Frank and E. A. Ritchie, "Effects of vertical wind shear on the intensity and structure of numerically simulated hurricanes," Mon. Weather Rev. **129**, 2249–2269 (2001).
[54]J. C. Marín, D. J. Raymond, and G. B. Raga, "Intensification of tropical cyclones in the GFS model," Atmos. Chem. Phys. **9**, 1407–1417 (2009).
[55]D. H. Peregrine, "Water waves, nonlinear Schrödinger equations and their solutions," J. Aust. Math. Soc. Ser. B. Appl. Math. **25**, 16–43 (1983).
[56]G. K. Batchelor, "On steady laminar flow with closed streamlines at large Reynolds number," J. Fluid Mech. **1**, 177–190 (1956).